Elucidating quality control at the ribosome with the natural product ternatin

by
Keely Oltion

DISSERTATION
Submitted in partial satisfaction of the requirements for degree of
DOCTOR OF PHILOSOPHY

in

Chemistry and Chemical Biology

in the

GRADUATE DIVISION
of the
UNIVERSITY OF CALIFORNIA, SAN FRANCISCO

Approved:

DocuSigned by:
Jack Taunton
0FD9D71201FC43C...

Jack Taunton
Chair

DocuSigned by:
Martin Kampmann
DocuSigned by:
Davide Ruggero
14C3B6AD60C5446...

Martin Kampmann

Davide Ruggero

Committee Members

Acknowledgements

I first thank my advisor, Jack Taunton, for his tireless mentorship over the years. Jack has a truly impressive breadth of knowledge across chemistry and biology, and is a master at crafting a narrative. I cannot thank him enough for the amount of time he has spent providing me with detailed advice and suggestions, while providing similar focus to all other members of the lab. Jack has given me the independence to pursue my own ideas, connected me to additional mentors when I needed it, and provided me with numerous opportunities to broaden my scientific knowledge outside the lab. Jack is an excellent role model for scientific rigor, integrity, and enthusiasm. Finally, thank you for all of your encouragement over the years.

My thesis committee members, Martin Kampmann and Davide Ruggero, have likewise provided encouragement, suggestions, and excellent examples of how to think about and do science. I was lucky to get to know Martin's lab during my time with CRISPRi, and to see Martin's wit and mentorship up close. Thank you to Davide for your encouragement and reminding me to think about biology at multiple scales – talking to you is always a blast. I am also grateful to my other rotation mentors, Danica Fujimori, Jason Gestwicki, Marton Siklos, and Hao Shao, for the time they devoted early in my training.

I will be forever indebted to Jordan Carelli, who provided me with excellent mentorship in my first quarter in graduate school, and performed the pioneering work that allowed my project to be possible. Your kindness, scientific rigor, and creativity were invaluable as I tried to find my footing and figure out how to start a PhD project, and I cannot thank you enough. In Martin's lab, Steph was instrumental in guiding me through CRISPRi screens, especially at a time in graduate school when I was still very uncertain – thank you for all your help and kindness.

Thank you to my labmates, past and present, who all contributed to an excellent working environment during graduate school. Although we only overlapped briefly, Geoff was an inspirational member of the lab. Adolfo provided me with positivity, advice, a great source of puns, and early help with proteomics. Nicole and I have been partners in crime for most of

graduate school. Tangpo and Ying are some of the hardest workers I know – thank you for all your help. To all of you and the rest – Pat, Yazmin, Liye, Jackie, Haoyuan, and Greg – thank you for being such committed scientific resources, and for the countless fun times we have had.

A number of people from other labs were also very generous with their time. Thanks to Kaitlyn and Jordan in the Fujimori lab for my incessant pestering about polysome profiling, and for being fellow ribosome friends. Everyone in the Shokat lab has helped me at some point, and I've had so much fun being your neighbor. A special shoutout goes to Megan for our HEK trade and a killer Halloween costume. Finally, a huge thank you to my CCB classmates, an inspirational bunch of people who are equal parts talented, kind, and hilarious.

I would not be here without my previous mentors. My high school chemistry teacher, Rhonda Bell, gave me an extremely solid introduction to chemistry. In college, Rick Cerione and his lab welcomed me when I had no idea what scientific research looked like. A massive thank you goes to Jon and Ram for teaching me independence and how to approach science even when things aren't working out. During my internship at Seattle Genetics, Phil Moquist was the coolest mentor – thank you for providing an introduction to how science works in industry.

Finally, thank you to my friends and family. Sarah and Max – it's been a blast going on adventures with you, and thinking about something other than science. Living with the crew in all its iterations at Precita and then GGH has been a highlight of graduate school – sometimes our combined grad student stress made things get a little crazy, in the most fun way. My parents gave me a very strong academic background – thank you for encouraging learning. Thank you especially to my mom for providing such a strong example of independence. And to my brother, who I've always looked up to as the coolest person around. It's also been so much fun getting to know my aunts, uncles, and cousins as adults. A huge thank you goes to the Asarnows, who welcomed me into their lives with such kindness. Finally, to Daniel – thank you for listening to me and for all the fun adventures. I can't wait to see what the future holds.

Contributions

Chapter 1 is adapted from a manuscript that was co-written with Prof. Jack Taunton, deposited on bioRxiv, and submitted for publication:

Oltion, K., Carelli, J. D., Yang, T., See, S. K., Wang, H.-Y., Kampmann, M., and Taunton, J. (2022). An E3 ligase network engages GCN1 to promote elongation factor-1α degradation on stalled ribosomes. bioRxiv. DOI: 10.1101/2022.03.21.485216.

Chapter 2 contains experiments that were included in the final version of the above manuscript.

Elucidating quality control at the ribosome with the natural product ternatin

Keely Oltion

Abstract

Protein synthesis is fundamental to all life. The ribosome is central to this process and is aided at every stage by numerous translation factors. Innate defects within the translation apparatus, as well as external environmental stressors, may cause the ribosome to stall. This threatens to expose the cell to potentially toxic, partially synthesized protein products, while sequestering the ribosome in an unproductive state. A number of ribosome-sensing pathways have begun to be elaborated. Of these, the HBS1L/Pelota complex and the E3 ligase ZNF598 constitute the best studied initiators into ribosome quality control. HBS1L/Pelota preferentially sense ribosomes stalled with an empty A site, and ZNF598 recognizes ribosome collisions. While many quality control pathways have been studied in the context of mRNA or translation inhibitor-mediated stalls, the cellular response to ribosomes specifically stalled with an occluded A site has not been systematically studied.

In Chapter 1, we describe the use of a natural product derivative, ternatin-4, as a chemical probe to identify novel ribosome-sensing quality control pathways. Ternatin-4 traps the eEF1A/GTP/aminoacyl-tRNA ternary complex at the ribosome A site, preventing accommodation. We made the serendipitous discovery that ternatin-4 causes near complete degradation of eEF1A in a translation and ubiquitin-dependent manner. Using a fluorescent reporter-based CRISPRi screen, we identify two E3 ligases, RNF14 and RNF25, as central players in this pathway. Characterization of proteome-wide, ternatin-induced, and RNF14/25-dependent ubiquitination marks revealed eEF1A, RPS27A, and GCN1 as key targets for ubiquitination. We define a role for RNF14 in direct ubiquitination of eEF1A, whereas RNF25 directly ubiquitinates RPS27A. The ribosome collision sensor GCN1 binds RNF14, likely through the RNF14 RWD domain, and is required for eEF1A degradation. Ubiquitination of

RPS27A is also prerequisite for eEF1A degradation. Thus, two combined signaling inputs, collision sensing via GCN1 and RPS27A ubiquitination by RNF25, allow RNF14 activation and ultimately, clearance of stalled eEF1A from the ribosome.

In Chapter 2, we expand the scope of the RNF14/RNF25/GCN1 pathway to additional activators and substrates. We first examine differences in ternatin-induced eEF1A degradation which arise between the two isoforms of eEF1A, eEF1A1 and eEF1A2. Next, we expand the pathway to a poorly understood translational GTPase, DRG1, which may represent a constitutive RNF14 substrate. We show that the RNF14/RNF25 pathway recognizes not only translation elongation factors at the A site, but also the termination factor eRF1 when stalled by a small molecule, SRI-41315, or a hydrolysis-deficient AAQ mutation. We finally examine the role of environmental stresses in activating the RNF14/RNF25/GCN1 pathway and find that ultraviolet light, which likely causes decoding defects through mRNA crosslinks, stimulates ubiquitination of eEF1A, ribosomal proteins, and GCN1 in an RNF14-dependent manner. Collectively, this thesis presents a mechanism for a ribosome-sensing pathway which responds to multiple disruptions to translation factors at the A site.

Table of Contents

List of Figures

List of Tables

Chapter 1: An E3 ligase network engages GCN1 to promote elongation factor-1α degradation on stalled ribosomes

Abstract

Ribosomes frequently stall during mRNA translation, resulting in context-dependent activation of quality control pathways to maintain proteostasis. However, surveillance mechanisms that specifically respond to stalled ribosomes with an occluded A site have not been identified. We discovered that the elongation factor-1a (eEF1A) inhibitor, ternatin-4, triggers ubiquitination and degradation of eEF1A on stalled ribosomes. Using a chemical genetic approach, we unveiled a novel signaling network comprising two E3 ligases, RNF14 and RNF25, which are both required for eEF1A degradation. Quantitative proteomics revealed RNF14 and RNF25-dependent ubiquitination of eEF1A and a discrete set of ribosomal proteins. The ribosome collision sensor GCN1 plays an essential role by engaging RNF14, which directly ubiquitinates eEF1A. Site-specific, RNF25-dependent ubiquitination of the ribosomal protein RPS27A/eS31 provides a second essential signaling input. Our findings illuminate a ubiquitin signaling network that monitors the ribosomal A site and promotes eEF1A degradation on stalled ribosomes.

Introduction

Protein synthesis is essential for growth and survival in all organisms. Each stage of this process, including initiation, elongation, and termination, is choreographed by factors that interact with the central catalytic machinery – the ribosome (Dever and Green, 2012). The initiation stage, often rate limiting for protein production, is tightly regulated by cellular signaling pathways (Jackson et al., 2010; Sonenberg and Hinnebusch, 2009). We know less about how cells regulate elongation rates, which are highly variable across coding sequences. Such regulation underlies, for example, the dependence of elongation rates on peptide sequence, codon usage, tRNA expression, and post-transcriptional modifications of tRNA and mRNA (Richter and Coller, 2015; Schuller and Green, 2018). As a consequence, ribosomes may pause

or stall in a context-dependent manner, and this may be critical for optimal folding or subcellular targeting of a nascent polypeptide (Stein and Frydman, 2019).

Ribosome stalling can also result from attempted translation of a defective mRNA (Brandman and Hegde, 2016; Yip and Shao, 2021). Such pathological stalls can lead to proteotoxic stress caused by depletion of active ribosomes and accumulation of partially synthesized nascent polypeptides. Experiments monitoring translation of mRNA reporters with poly(A) and other stall-prone coding sequences have revealed surveillance pathways that recognize distinct structural features (Yip and Shao, 2021). The HBS1L/PELO complex recognizes the empty ribosomal A site at the 3' end of a truncated mRNA and promotes ribosome splitting by the recycling factor ABCE1 (Doma and Parker, 2006; Shoemaker et al., 2010). By contrast, attempted translation of poly(A) slows down a leading ribosome to the point that a trailing ribosome collides, resulting in Hel2/ZNF598-mediated ubiquitination of 40S ribosomal proteins and subunit dissociation by the ribosome-associated quality control (RQC)-triggering (RQT) complex (Ikeuchi et al., 2019; Juszkiewicz and Hegde, 2017; Juszkiewicz et al., 2018, 2020; Matsuo et al., 2017, 2020; Simms et al., 2017). An emerging view posits that ribosome collisions comprise a fundamental structural unit recognized by multiple quality control and stress response factors (Kim and Zaher, 2022; Meydan and Guydosh, 2021), including the E3 ligase, Hel2/ZNF598, and the integrated stress response coactivator, GCN1 (Pochopien et al., 2021). Although these translation surveillance pathways were identified in budding yeast more than 10 years ago, elucidation of their physiological roles in mammalian systems has only just begun. Moreover, it is currently unknown whether there are additional surveillance pathways that specifically respond to stalled ribosomes occupied by translation factors, such as elongation factor-1α (eEF1A) or termination factors (eRF1 and eRF3).

Studies of translation quality control have critically relied on the use of drugs and chemical probes to modulate protein synthesis in a graded, dose-dependent manner (Juszkiewicz et al., 2018, 2020; Simms et al., 2017; Wu et al., 2020; Yan and Zaher, 2021). We

recently described ternatin-4, a small-molecule inhibitor of translation elongation that targets the complex of eEF1A bound to aminoacyl-tRNAs (aa-tRNA) (Carelli et al., 2015). Similar to didemnin B (Shao et al., 2016), ternatin-4 stalls elongation by preventing aa-tRNA release from eEF1A on the ribosome (Juette et al., 2022; Wang et al., 2022). Based on this mechanism, we reasoned that ternatin-4 could be used as a tool to illuminate the cellular response to elongation-stalled ribosomes in which the A site is persistently occupied by eEF1A bound to aa-tRNA.

Here, we elucidate a novel surveillance pathway, which ultimately results in ubiquitination and degradation of eEF1A trapped on the ribosome by ternatin-4. A CRISPRi screen uncovered two poorly characterized E3 ligases, RNF14 and RNF25, both of which are required for ternatin-induced eEF1A degradation. In response to ternatin-induced stalls, RNF14 and RNF25 play essential roles in the ubiquitination of eEF1A, as well as multiple ribosomal proteins. Ubiquitination of the ribosomal protein RPS27A is mediated solely by RNF25 and is required for eEF1A degradation. We further show that GCN1 – whose biological roles beyond the canonical integrated stress response are poorly understood – interacts with RNF14 and is also essential for eEF1A degradation. We propose that the RNF14/RNF25 surveillance network monitors the status of elongating ribosomes and specifically responds to stalls containing an occluded A site.

Results

Ternatin-4 promotes eEF1A degradation in a manner that requires translating ribosomes

In experiments evaluating the cellular response to ternatin-induced elongation stalls, we unexpectedly observed a sharp reduction in eEF1A levels (**Figure 1.1A**). Loss of eEF1A was dependent on the concentration of ternatin-4, with an effective half-maximal concentration (EC_{50}) of ~8 nM. We noted that concentrations higher than 50 nM had progressively diminished effects on eEF1A levels, despite effectively inhibiting translation (**Figure 1.1B**). This dose-

response behavior is reminiscent of mechanistically distinct elongation inhibitors (e.g., cycloheximide, emetine, anisomycin), in which intermediate, but not high concentrations were found to activate ribosome quality control and stress kinase pathways by promoting ribosome collisions (Juszkiewicz et al., 2018; Simms et al., 2017; Wu et al., 2020). Based on these precedents and the observed 'V-shaped' dose-response curve (**Figure 1.1B**), it seemed plausible that intermediate concentrations of ternatin-4 could induce ribosome collisions, and ultimately, eEF1A degradation. Consistent with this notion, treatment with ternatin-4 for 1 h led to an increase in the proportion of nuclease-resistant disomes and trisomes (**Figure 1.2A**).

eEF1A is one of the most abundant cellular proteins (~35 μM in cells) and has been reported to turn over slowly (Zecha et al., 2018). In contrast to results obtained with ternatin-4, treatment of HeLa cells for 20 h with cycloheximide (CHX) or homoharringtonine (HHT) had no

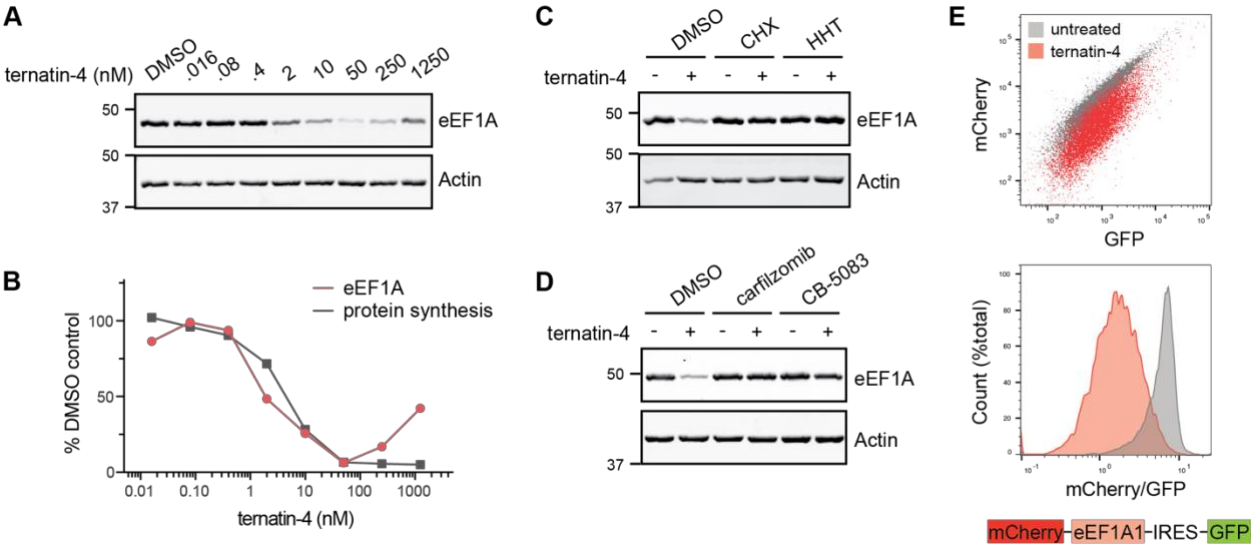

Figure 1.1: Ternatin-4 promotes eEF1A degradation in a manner that requires translating ribosomes.
(**A**) HeLa cells were treated for 20 h with the indicated concentrations of ternatin-4 and analyzed by immunoblotting. (**B**) Quantification of eEF1A levels is derived from (**A**), and protein synthesis measurements were performed on the same day with cells treated for 20 h with ternatin-4, pulsed for 1 h with O-propargyl puromycin, and analyzed by flow cytometry (see Methods). (**C**) HeLa cells were treated for 20 h with ternatin-4 (50 nM) in the presence or absence of cycloheximide (CHX, 50 ug/mL) or homoharringtonine (HHT, 2 μg/mL, 20 min pretreatment). (**D**) HeLa cells were treated for 20 h with ternatin-4 (50 nM) in the presence or absence of the proteasome inhibitor, carfilzomib (500 nM), or the p97 inhibitor, CB-5083 (2.5 μM). (**E**) Fluorescent reporter to monitor eEF1A degradation. Ternatin-resistant HCT116 cells (eEF1A1$^{A399V/A339V}$) stably expressing mCherry-eEF1A1_IRES-GFP and dCas9 were treated ± ternatin-4 (50 nM) for 8 h and analyzed by flow cytometry.

effect on eEF1A levels (**Figure 1.1C**). Hence, inhibiting translation per se is not sufficient to promote loss of eEF1A; rather, direct binding of ternatin-4 to eEF1A on the ribosome might be required. In support of this hypothesis, co-treatment with ternatin-4 and either CHX or HHT – which target the ribosomal E site and peptidyl-transferase center, respectively – completely prevented eEF1A degradation (**Figure 1.1C**). These results suggest that ternatin-induced eEF1A degradation requires actively translating ribosomes that are competent to bind eEF1A/aa-tRNA; such ribosomes would be less abundant in cells treated with cycloheximide or homoharringtonine owing to their inhibitory effects on mRNA-tRNA translocation and initiation, respectively (Budkevich et al., 2011; Fresno et al., 1977). Ternatin-induced eEF1A degradation was also prevented by co-treatment with either proteasome or p97/VCP inhibitors (**Figure 1.1D**), thus implicating the ubiquitin/proteasome system (UPS) in this process. Collectively, our findings suggest that ternatin-4, which traps eEF1A on the ribosome and prevents aa-tRNA accommodation into the A site (Juette et al., 2022; Wang et al., 2022), targets eEF1A for UPS-mediated destruction by a mechanism that requires elongation-competent ribosomes.

CRISPRi screen reveals two E3 ligases required for ternatin-induced eEF1A degradation

We sought to identify the UPS components, and in particular the E3 ligase(s) required for ternatin-induced eEF1A degradation. To do this, we performed a CRISPRi screen using an mCherry-eEF1A fusion as a fluorescent reporter, which also contains an internal ribosome entry site followed by GFP. We stably expressed this bicistronic reporter construct, along with dCas9-BFP-KRAB, in HCT116 cells that are homozygous for an A399V mutation in the didemnin/ternatin-4 binding site of eEF1A1. We previously showed that this mutation abrogates ternatin-4 binding and confers complete resistance to its cellular effects (Carelli et al., 2015). Hence this reporter cell line, which expresses mCherry-eEF1A at low levels relative to endogenous A399V eEF1A, allows us to study ternatin-induced eEF1A degradation without globally inhibiting protein synthesis. Treatment of the reporter cells with ternatin-4 resulted in a

strong reduction in mCherry-eEF1A fluorescence, whereas GFP was unaffected (**Figure 1.1E**). Loss of mCherry-eEF1A was dependent on the ternatin-4 concentration (EC_{50} ~5 nM; **Figure 1.2B**) and treatment time ($t_{1/2}$ ~5 h; **Figure 1.2C**), and it was prevented by co-treatment with either a proteasome inhibitor or ribosome-targeted translation inhibitors (**Figure 1.2D**).

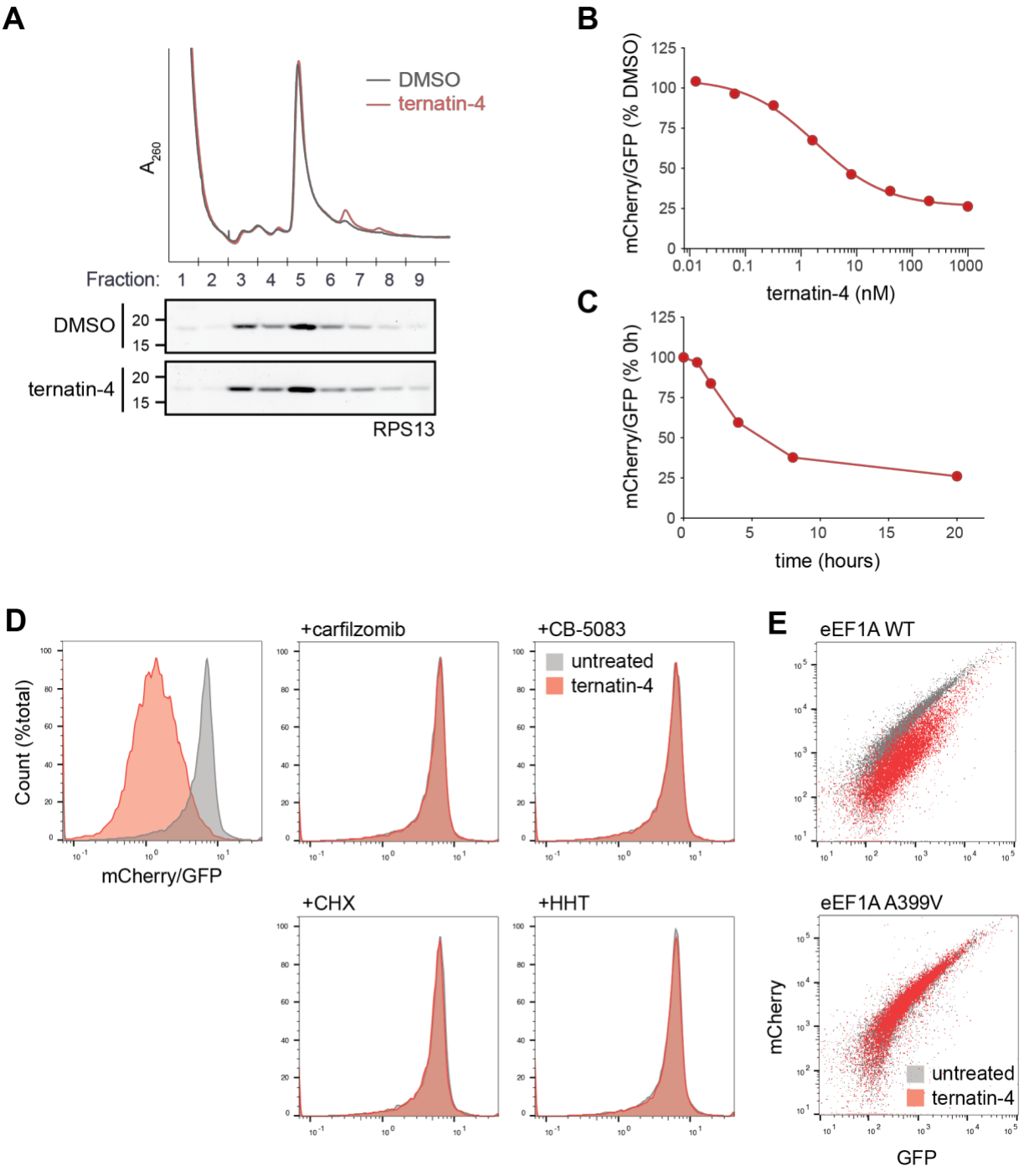

Figure 1.2: A fluorescent reporter for ternatin-induced eEF1A degradation.
(**A**) HeLa cells were treated for 1 h with ternatin-4 (50 nM). Lysates were digested with micrococcal nuclease and subjected to ultracentrifugation through 10-50% sucrose gradients. Ribosome abundance was measured by monitoring absorbance throughout the gradient at 260 nm. (**B**) Dose-dependent mCherry-eEF1A reporter degradation. Ternatin-resistant HCT116 cells stably expressing the Flag-mCherry-eEF1A1_IRES-GFP reporter and dCas9-BFP-KRAB were treated with 50 nM ternatin-4 for 8 h and analyzed by flow cytometry. (**C**) Time dependence of mCherry-eEF1A reporter degradation. Cells as in (**B**) were treated with 50 nM ternatin-4 for the indicated times and analyzed by flow cytometry. (**D**) Cells in each panel were treated for 8 h ± ternatin-4 (50 nM), along with carfilzomib (500 nM), CB-5083 (2.5 μM), CHX (50 ug/mL), or HHT (2 μg/mL, 20 min pretreatment), as indicated. (**E**) Cells expressing WT or A399V mCherry-eEF1A were treated for 8 h ± ternatin-4 (50 nM) and analyzed by flow cytometry.

Importantly, ternatin-4 had no effect on mCherry-eEF1A bearing the A399V mutation, which confirms that ternatin-4 binding is required to promote eEF1A degradation (**Figure 1.2E**).

We transduced the mCherry-eEF1A reporter cells with a focused sgRNA library targeting ~1700 genes primarily involved in ubiquitin signaling and proteostasis (5 sgRNAs/gene, see **Supplementary Table 1** for the complete list of genes), plus 250 nontargeting sgRNAs (Chen et al., 2019). Transduced cells were treated with ternatin-4 for 8 h or left untreated, followed by sorting into high and low fluorescence populations based on mCherry normalized to GFP (**Figure 1.3A**). For each population, sgRNA frequencies were quantified by Illumina sequencing and analyzed using our established bioinformatics pipeline (Kampmann et al., 2013; Tian et al., 2019). We focused on genes whose knockdown led to increased mCherry-eEF1A levels (less degradation) in ternatin-treated but not untreated cells. Two E3 ligase genes, *RNF14* and *RNF25*, emerged as the most prominent hits (**Figure 1.3B**).

Knockdown of either RNF14 or RNF25 strongly prevented eEF1A degradation, with multiple sgRNAs enriched in the high mCherry-eEF1A population of ternatin-treated cells (**Figure 1.4A**). By contrast, sgRNAs targeting previously characterized ribosome-associated E3 ligases and RQC factors – including ZNF598, LTN1, RNF10, and CNOT4 – had little or no effect on eEF1A degradation (**Figure 1.4B** and **Supplementary Table 1**). To validate RNF14 and

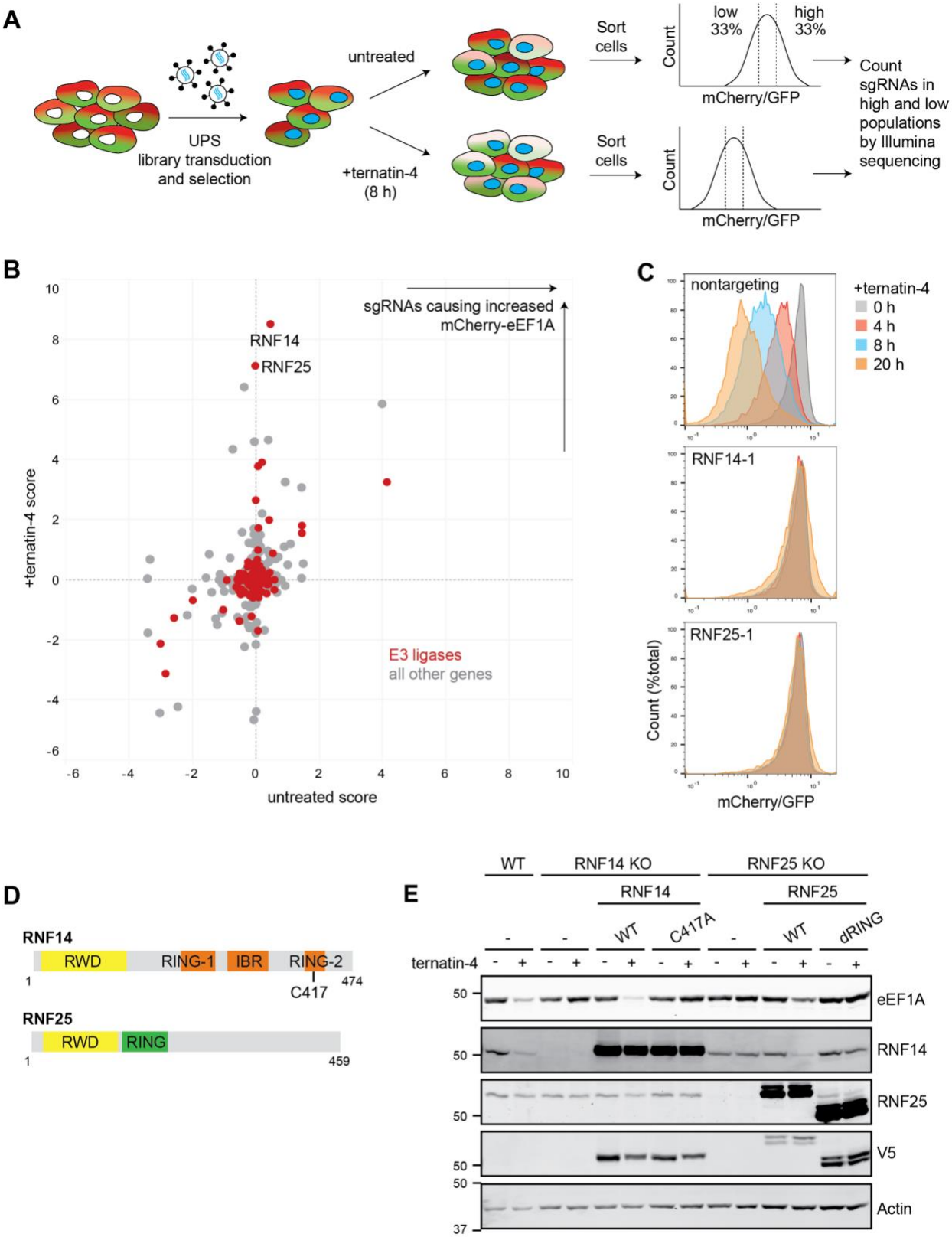
A
UPS
library transduction
and selection
untreated
+ternatin-4
(8 h)
Sort
cells
Count
low
33%
high
33%
mCherry/GFP
Count
sgRNAs in
high and low
populations
by Illumina
sequencing
B
sgRNAs causing increased
mCherry-eEF1A
RNF14
RNF25
E3 ligases
all other genes
+ternatin-4 score
untreated score
C
nontargeting
RNF14-1
RNF25-1
+ternatin-4
0 h
4 h
8 h
20 h
Count (%total)
mCherry/GFP
D
RNF14
RWD
RING-1
IBR
RING-2
C417
RNF25
RWD
RING
E
WT
RNF14 KO
RNF25 KO
RNF14
RNF25
WT
C417A
dRING
ternatin-4
eEF1A
RNF14
RNF25
V5
Actin

Figure 1.3: A CRISPRi screen reveals two E3 ligases required for ternatin-induced eEF1A degradation.
(**A**) Schematic of CRISPRi screen. CRISPRi reporter cells from **Figure 1.1E** were transduced with a library targeting ~1700 genes (5 sgRNAs/gene) related to ubiquitin signaling and proteostasis. Cells selected for sgRNA expression were treated with ternatin-4 for 8 h or left untreated. Cells were sorted into high and low mCherry/GFP populations, and sgRNA counts were determined by deep sequencing. (**B**) CRISPRi scores (based on sgRNA enrichment in high vs. low mCherry/GFP populations) from cells treated with ternatin-4 or left untreated. Knockdown of *RNF14* or *RNF25* stabilizes mCherry-eEF1A1 levels in ternatin-treated but not untreated cells. Scores (plotted for each gene) are the product of the phenotype value (log_2 of the average high/low sgRNA counts for the three most extreme sgRNAs per gene) and the negative log_{10} of the p value. (**C**) CRISPRi screening cells were transduced with the top-scoring *RNF14* and *RNF25* sgRNAs. Transduced cells were treated with ternatin-4 as indicated and analyzed by flow cytometry. (**D**) Domain organization of RNF14 and RNF25. (**E**) RNF14 and RNF25 HeLa KO cells were generated using CRISPR/Cas9. Cells were further transduced with the indicated V5-tagged RNF14 or RNF25 constructs (both with IRES-mCherry) and sorted to produce pure populations. Cells were treated for 20 h with ternatin-4 and analyzed by immunoblotting.

RNF25, we retested individual, top-scoring sgRNAs in our mCherry-eEF1A reporter cells and observed a complete loss of ternatin-induced degradation (**Figure 1.3C**).

RNF14 (also called ARA54) (Kang et al., 1999) belongs to the Ring-Between-Ring (RBR) class of E3 ligases, which transfer ubiquitin from an E2 bound to the RING1 domain to a conserved catalytic cysteine (Cys417 in RNF14) in the RING2 domain (Dove and Klevit, 2017; Walden and Rittinger, 2018). By contrast, RNF25 (also called AO7) (Lorick et al., 1999) is a RING-type E3 ligase. Deletion of RNF25 was recently found to sensitize cells to the alkylating agent methyl methanesulfonate (MMS), but not other DNA damaging agents, indicating a potential role in repairing methylated DNA (Hundley et al., 2021). We note that MMS also methylates RNA and was found to activate the RQC pathway in yeast (Yan and Zaher, 2021), suggesting that MMS hypersensitivity of RNF25 KO cells could also stem from effects related to translation. Both RNF14 and RNF25 contain N-terminal RWD domains (**Figure 1.3D**), protein interaction domains found in ~30 diverse human proteins exemplified by the ribosome-associated stress kinase, GCN2. Overall, the biological functions of RNF14 and RNF25 remain poorly understood.

To further validate RNF14 and RNF25, we generated HeLa knockout cell lines using CRISPR/Cas9. Similar to our CRISPRi knockdown results with mCherry-eEF1A, knockout of either RNF14 or RNF25 abolished ternatin-induced degradation of endogenous eEF1A, while having no effect on eEF1A levels in untreated cells (**Figure 1.3E**). This phenotype was consistently observed across multiple RNF14 and RNF25 KO clones (**Figure 1.4C**). Concomitant with eEF1A degradation, ternatin-4 treatment of wild type HeLa cells caused a

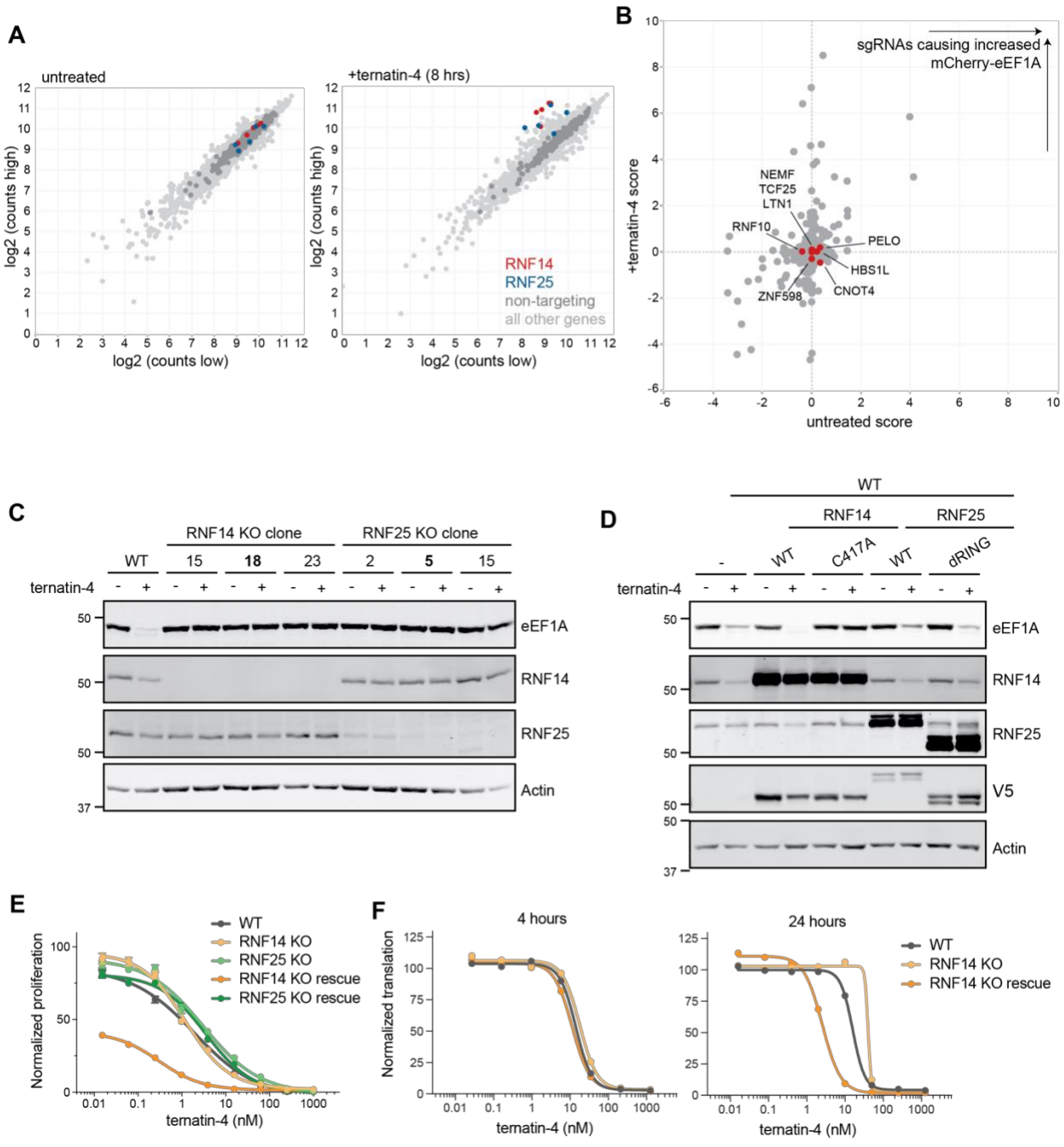

Figure 1.4: RNF14 and RNF25 are both required for eEF1A degradation.
(**A**) sgRNA sequencing counts for high and low fluorescence cell populations (± ternatin-4) from the CRISPRi screen, highlighting RNF14 and RNF25 sgRNAs. (**B**) CRISPRi scores from Figure 1.3B are shown in red for HBS1L, PELO, LTN1, ZNF598, NEMF, RNF10, and CNOT4. (**C**) Knockout of RNF14 or RNF25 prevents ternatin-induced eEF1A degradation across multiple HeLa cell clones. Cells were treated with ternatin-4 for 20 h and analyzed by immunoblotting. Clones 18 (RNF14) and 5 (RNF25) were utilized for further experiments. (**D**) Overexpression of V5-tagged RNF14, but not RNF25, increases eEF1A degradation in wild type HeLa cells. Stable cell lines were generated as in **Figure 1.3E** and treated for 20 h with ternatin-4. (**E**) HeLa WT, KO, and the corresponding rescue cell lines were treated for 72 h, and live cell counts were measured by CellTiter-Glo. Values were normalized to DMSO for each cell line. (**F**) HeLa WT, RNF14 KO, and rescue cells were treated with ternatin-4 for 4 h or 24 h and pulsed 1 h with O-propargyl puromycin. OPP incorporation was measured by FACS and normalized to DMSO.

dramatic reduction in endogenous RNF14 levels. Remarkably, this effect was also abolished in RNF25 KO cells (**Figure 1.3E**). These results suggest: (1) RNF14, while an essential mediator of eEF1A destruction, is also degraded in response to ternatin-4 treatment, and (2) RNF25 plays an essential role in ternatin-induced degradation of both eEF1A and RNF14.

Reintroduction of wild type RNF14 and RNF25 into their respective KO cells restored eEF1A degradation, confirming an essential role for both E3 ligases (**Figure 1.3E**). Overexpression of wild type RNF14 rescued and further enhanced eEF1A degradation in the KO cells, whereas overexpression of the catalytic Cys417 to Ala mutant failed to restore degradation. Importantly, C-terminally tagged RNF14 was inactive in our rescue experiments (data not shown). Likewise, expression of wild type RNF25, but not a RING deletion mutant, restored degradation of both eEF1A and RNF14 in the RNF25 KO cells (**Figure 1.3E**). Overexpression of RNF14, but not RNF25, in wild type cells also led to enhanced eEF1A degradation, whereas a catalytically dead mutant of RNF14 (but not RNF25) acted in a dominant negative manner, completely abrogating eEF1A degradation (**Figure 1.4D**). These results suggest that the ubiquitin ligase activity of RNF14 is rate-limiting for eEF1A degradation and that overexpression of catalytically dead RNF14 can saturate a binding site required to promote eEF1A degradation. While WT and knockout cells were similarly sensitive to ternatin-4, overexpression of RNF14 sensitized cells to ternatin-4 (**Figure 1.4E**). This effect is likely

attributable to greater translation inhibition in RNF14-overexpressing cells (**Figure 1.4F**), which may result from more complete degradation of eEF1A.

RNF14 and RNF25 mediate ubiquitination of eEF1A and ribosomal proteins

Having established the essential roles of RNF14 and RNF25 E3 ligase activity in eEF1A degradation, we sought to determine the global landscape of RNF14/RNF25-dependent ubiquitination sites in an unbiased manner. To do this, we used an established SILAC proteomics workflow in which tryptic peptides containing a ubiquitin-derived diGly remnant (attached to a substrate lysine residue) are immuno-enriched and quantified by mass spectrometry (Kim et al., 2011). We first treated cells stably overexpressing RNF14 with or without ternatin-4 for 4 h in two biological replicates (SILAC light/heavy label swaps; see Methods). Cell lysates from each treatment condition (± ternatin-4) were combined and digested with trypsin, prior to enrichment of diGly peptides (**Figure 1.6A**). Mass spectrometry analysis revealed >800 ubiquitination sites, 7 of which were strongly and reproducibly increased by ternatin-4 (log_2-fold change >2, **Figure 1.5A**). Strikingly, all 7 top-ranked sites were found either in eEF1A (4 sites) or the ribosomal proteins RPLP0, RPS13, and RPS17. Several ubiquitination sites in proteins relevant to translation elongation – including 7 additional eEF1A sites – were induced to a somewhat lower extent (log_2-fold change >1) or were identified in only one biological replicate (**Figure 1.5B** and **Supplementary Table 2**), as is typical in data-dependent acquisition (DDA) mass spectrometry. Of all identified ubiquitination sites, eEF1A K385 was induced most strongly by ternatin, increasing by at least 75-fold (**Figure 1.5B** and **1.6B**). In addition, ternatin-4 treatment led to increased ubiquitination of multiple sites within the C-terminal region of the ribosome collision sensor, GCN1 (**Figure 1.5B** and **1.6B**), as well as ABCF3 (ortholog of yeast Gcn20) and the ribosomal proteins, RPL12 and RPS27A (**Figure 1.5B**). We repeated the diGly SILAC-MS experiment (± ternatin-4) in RNF14-overexpressing

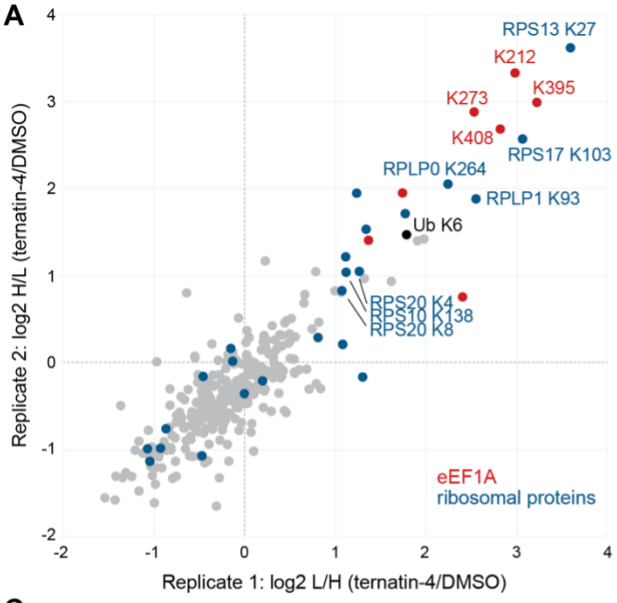

B

Gene	Position	R1 log2 L/H	R2 log H/L
EEF1A1	K385	6.3	
GCN1	K2237	3.7	
RPS13	K27	3.6	3.6
GCN1	K1992	3.3	
GCN1	K2027	3.3	
EEF1A1	K395	3.2	3.0
RPL12	K48	3.2	
RPS17	K103	3.1	2.6
GCN1	K2066		3.0
EEF1A1	K212	3.0	3.3
EEF1A1	K244	2.8	
EEF1A1	K408	2.8	2.7
GCN1	K2072	2.8	
RPLP1	K93	2.5	1.9
EEF1A1	K273	2.5	2.9
EEF1A1	K219	2.4	0.8
RPLP0	K264	2.2	2.1
EEF1A1	K44	2.1	
ABCF3	K294	1.9	1.4
Ubiquitin	K6	1.8	1.5
EEF1A1	K392	1.7	2.0
RPS27A	K113	1.3	-0.2
RPL12	K83	1.2	2.0
RPS27A	K107		1.1

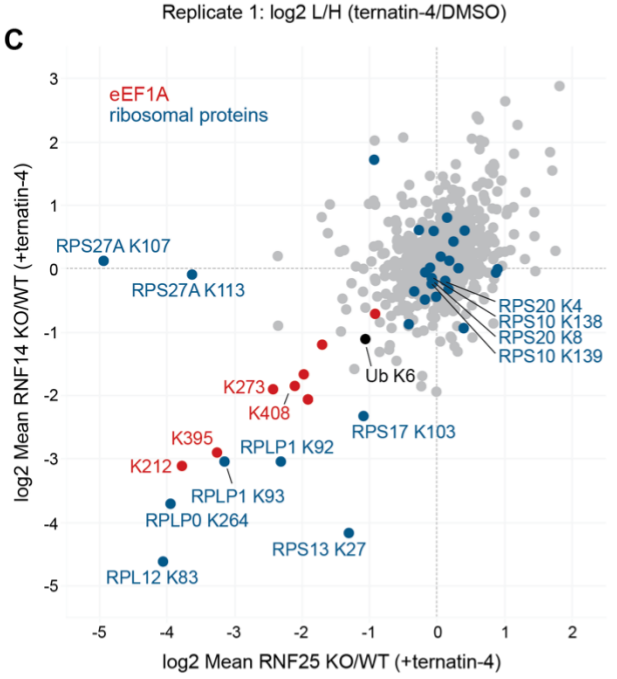

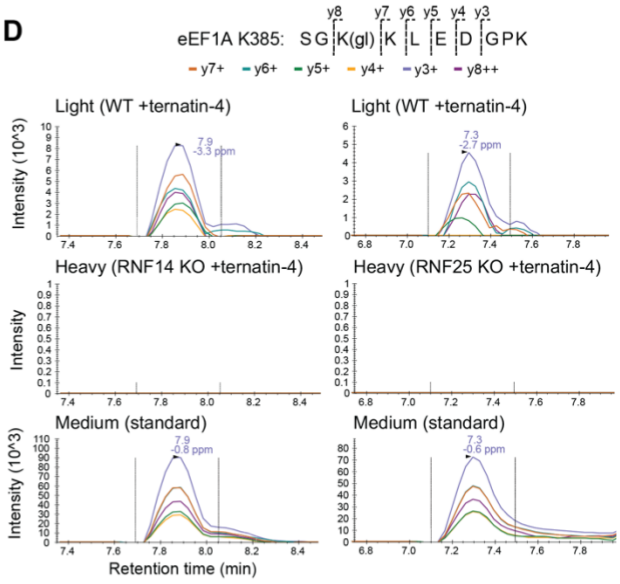

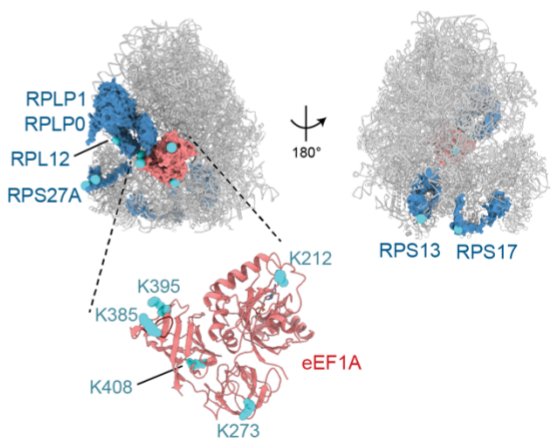

Figure 1.5: Ternatin-4 promotes RNF14 and RNF25-dependent ubiquitination of eEF1A and ribosomal proteins.
(**A**) HeLa cells stably overexpressing RNF14 were labeled in SILAC media and treated for 4 h ± ternatin-4. Lysates from ternatin-4 and DMSO-treated cells were mixed. Tryptic peptides containing diGly ubiquitin remnants were immuno-enriched and analyzed by LC-MS/MS. Shown are SILAC ratios for each diGly site identified in both biological replicates. (**B**) SILAC ratios for top-ranked diGly sites (eEF1A and ribosome-associated proteins) from each of the two biological replicates from part (**A**). (**C**) HeLa WT and RNF14 or RNF25 KO cells were treated for 4 h with ternatin-4. KO and WT SILAC pairs were mixed before processing as in (**A**). Mean KO/WT SILAC ratios were calculated from two biological replicates (H/L label swaps) for both RNF14 KO and RNF25 KO experiments. (**D**) Samples from (**C**) were analyzed by PRM-MS for eEF1A K385 ubiquitination. Chromatograms are shown for one biological replicate each for RNF14 and RNF25 KO samples. MS2 transitions were monitored for light (WT cells), heavy (KO cells), and medium (synthetic peptide standard) variants of SGK[diGly]KLEDGPK, corresponding to eEF1A K385-Ub. (**E**) Cartoon showing location of ternatin-induced and RNF14/25-dependent ubiquitination sites (cyan spheres) on eEF1A and ribosomal proteins based on cryo-EM models (PDB: 5LZS; RPLP0/RPLP1 based on PDB: 4V6X). The loop containing eEF1A K385 (residues 379-386) is colored in dark red in the ribbon model**.**

cells co-treated with a proteasome inhibitor and in wild type cells (without proteasome inhibitor treatment or RNF14 overexpression), and we observed similar levels of ternatin-induced eEF1A and ribosomal protein ubiquitination (**Figures 1.6B** and **1.6C, Supplementary Table 2**).

We next employed SILAC-MS to quantify ternatin-induced ubiquitination sites in RNF14 or RNF25 KO cells, relative to the parental wild type cells. Consistent with their obligate roles in eEF1A degradation, knockout of either RNF14 or RNF25 dramatically reduced eEF1A ubiquitination at multiple sites (**Figure 1.5C** and **Supplementary Table 2**). Ubiquitination of a discrete set of ribosomal protein sites (including RPLP0 K264, RPLP1 K92, RPLP1 K93, and RPL12 K83), were similarly reduced in both knockout cell lines. In striking contrast, ubiquitination of RPS27A at K107 and K113 was reduced in RNF25 KO but not RNF14 KO cells, suggesting that these ubiquitination events are selectively mediated by RNF25 (**Figure 1.5C**). Ubiquitination of ZNF598-dependent sites on RPS10 and RPS20 (Garzia et al., 2017; Juszkiewicz et al., 2018; Sundaramoorthy et al., 2017) was unaffected by either RNF14 or RNF25 knockout (**Figure 1.5C** and **Supplementary Table 2**), despite increasing ~2-fold in response to ternatin-4 treatment (**Figure 1.5B** and **Supplementary Table 2**). These data

suggest that ternatin-induced stalls can activate distinct ribosome-associated ubiquitination events, which are mediated independently by ZNF598 and RNF14/RNF25.

The ubiquitination site most strongly induced by ternatin-4, eEF1A K385, was not identified in every biological replicate; this is likely due to the presence of a missed trypsin cleavage site after K386, as the fully trypsinized tetrapeptide would be too short to identify

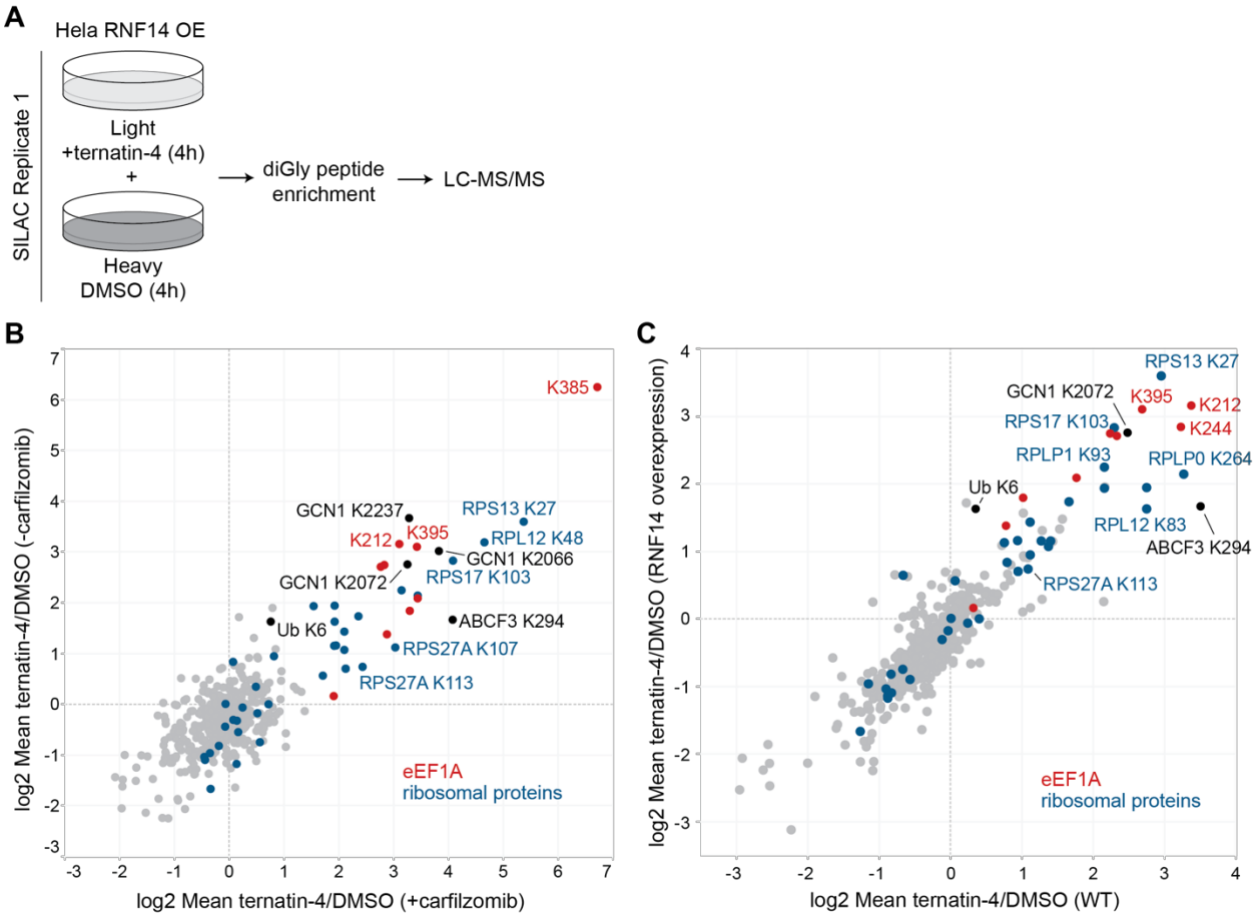

Figure 1.6: Proteomic analysis of ternatin-induced ubiquitination sites.
(**A**) Schematic for the SILAC-based diGly proteomics method to identify ternatin-induced ubiquitination sites. Sample configuration is shown for the experiment in **Figures 1.5A** and **1.5B**. Replicate 2 was performed identically except heavy and light labels (Arg/Lys in growth media) were swapped. (**B**) HeLa cells stably overexpressing RNF14 were labeled in SILAC media as in (**A**) and treated for 4 h with 500 nM carfilzomib ± ternatin-4 (50 nM). Mean SILAC ratios (log_2) for each ubiquitination site (2 replicates, label swaps) were plotted against corresponding log_2 ratios from the experiment shown in **Figure 1.5A** and **1.5B** (without carfilzomib). (**C**) HeLa cells (without RNF14 overexpression) were labeled in SILAC media as in (**A**) and treated for 4 h ± ternatin-4 (50 nM). Mean SILAC ratios (log_2) for each ubiquitination site (2 replicates, label swaps) were plotted against the corresponding log_2 ratios from the experiment shown in **Figure 1.5A** and **1.5B** (HeLa RNF14 OE).

unambiguously. However, across multiple independent SILAC-MS experiments in which it was identified, K385 ubiquitination was consistently and dramatically induced by ternatin treatment, suggesting its likely dependence on RNF14/RNF25. To test this rigorously, we spiked in a synthetic 'medium heavy' peptide standard (SGK[diGly]KLEDGPK, synthesized with heavy Leu), which facilitated identification and quantification of the endogenous SILAC-derived peptides (SGK[diGly]KLEDGPK, containing 3 light or heavy Lys) via parallel reaction monitoring (PRM) mass spectrometry instead of DDA-MS (see Methods for details). These experiments unambiguously revealed diGly-modified eEF1A K385 in ternatin-treated wild type cells, whereas it was undetectable in either RNF14 or RNF25 knockout cells (**Figure 1.5D**).

We conclude that ternatin-induced elongation stalls promote ubiquitination of multiple sites on eEF1A and a discrete set of ribosomal proteins. Most ternatin-induced ubiquitination sites are dependent on both RNF14 and RNF25, whereas RPS27A ubiquitination selectively requires RNF25. Several of the ribosomal ubiquitination sites we identified – including those on RPLP0, RPLP1, RPL12, and RPS27A – are proximal to the GTPase center where eEF1A binds, consistent with the notion that RNF14/RNF25-dependent eEF1A ubiquitination occurs on elongation-stalled ribosomes (**Figure 1.5E**). By contrast, RPS13 and RPS17 sites – which are also ternatin-induced and RNF14/RNF25-dependent – localize to a distinct region of the 40S subunit near the interface of collided di-ribosomes.

K385 is required for efficient eEF1A degradation and is directly ubiquitinated by RNF14

To assess the functional relevance of ternatin-induced, RNF14/RNF25-dependent eEF1A ubiquitination sites identified by mass spectrometry, we introduced lysine to arginine mutations into the mCherry-eEF1A reporter. With the exception of K385, mutation of individual lysines had little or no effect on eEF1A degradation kinetics. By contrast, ternatin-induced degradation of K385R eEF1A was impaired (**Figure 1.7A** and **1.7B**). K385 resides on a flexible loop in the C-terminal beta-barrel domain of eEF1A (**Figure 1.5E**). This loop lies near the

interface between the C-terminal domain and the N-terminal GTPase domain of ribosome-bound eEF1A and directly contacts the ternatin/didemnin binding site (Carelli et al., 2015; Shao et al., 2016). The mutagenesis results suggest that K385 ubiquitination, which is dramatically increased in the context of ternatin-induced stalls, plays a critical role in subsequent events

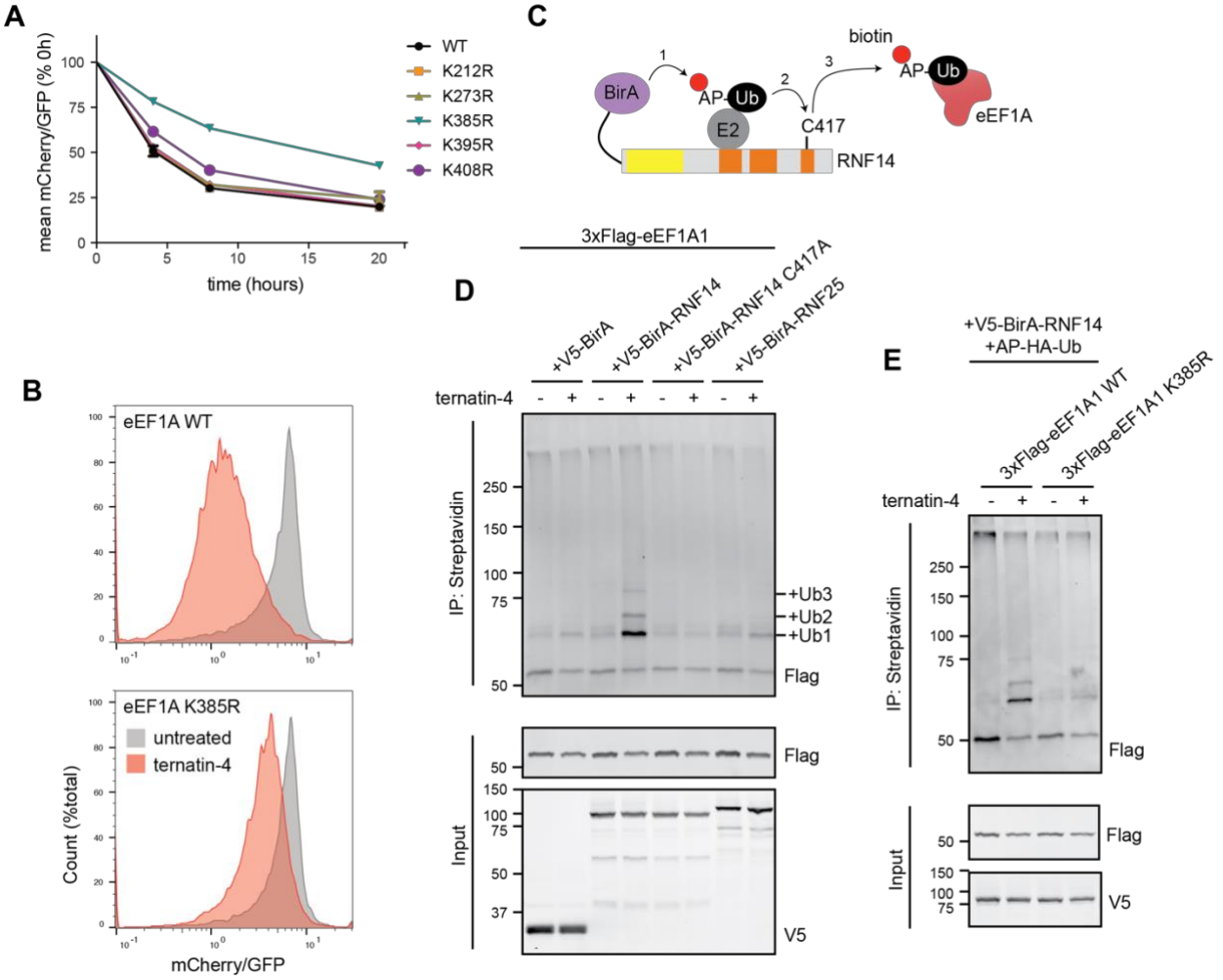

Figure 1.7: eEF1A K385 is required for efficient degradation and is directly ubiquitinated by RNF14.
(**A**) Ternatin-resistant HCT116 cells expressing WT and Lys mutant mCherry-eEF1A reporter constructs were treated with ternatin-4 as indicated and analyzed by flow cytometry. Plotted are the mean mCherry/GFP ratios (n=3, ± SEM) relative to t=0 h for each mutant. (**B**) Histograms for cells from (**A**) expressing WT or K385R eEF1A and treated ± ternatin-4 for 8 h. (**C**) Schematic for proximity-based biotin transfer from E3 (BirA-RNF14) to ubiquitin/E2 to substrates (eEF1A). Acceptor peptide (AP)-ubiquitin is biotinylated when bound to E2 and the biotin ligase BirA-RNF14 fusion. Biotinylated AP-Ub is subsequently transferred to E3 substrates, which are enriched via streptavidin. (**D**) Ternatin-4 induces proximity-mediated eEF1A ubiquitination by RNF14, but not RNF25. Ternatin-resistant HCT116 cells stably expressing 3xFlag-eEF1A1 were co-transfected with AP-HA-Ub and the indicated BirA fusion constructs. Cells were treated with 50 μM biotin ± ternatin-4 for 4 h. (**E**) Cells expressing WT or K385R 3xFlag-eEF1A were transfected with AP-HA-Ub and BirA-RNF14 and treated with biotin ± ternatin-4.

leading to proteasome-dependent eEF1A degradation. Additional ternatin-induced ubiquitination sites, as revealed by our SILAC-MS experiments, may also contribute collectively to promote efficient eEF1A degradation.

Based on the genetic evidence implicating RNF14 and RNF25 in ternatin-induced eEF1A ubiquitination and degradation, we hypothesized that one or both E3 ligases directly ubiquitinate eEF1A K385. To test whether this occurs in cells, we turned to a biotin-transfer assay in which an E3 of interest is fused to the biotin ligase BirA (Deshar et al., 2016, 2019; Yoo et al., 2019). This proximity-based biotinylation assay relies on the specificity of BirA for an acceptor peptide fused to ubiquitin (AP-Ub). Expression of the BirA-E3 fusion protein results in biotinylation of a proximal E2-bound AP-Ub, followed by transfer of biotin-AP-Ub to an adjacent substrate (**Figure 1.7C**). Enrichment of biotinylated proteins with streptavidin-conjugated beads allows detection of ubiquitinated substrates specific to the BirA-E3 ligase of interest.

We established the BirA-E3 proximity biotinylation assay in our ternatin-resistant HCT116 cell line (eEF1A1$^{A399V/A339V}$), modified to stably express Flag-eEF1A. Strikingly, treatment of cells co-expressing BirA-RNF14 and AP-Ub with ternatin-4 for 4 h resulted in the specific enrichment of one major (mono-Ub) and two minor (di- and tri-Ub) higher-molecular weight forms of Flag-eEF1A (**Figure 1.7D** and **1.8A**). Transfer of biotin-AP-Ub to Flag-eEF1A was not observed in cells expressing similar levels of BirA or an active site mutant of BirA-RNF14 (C417A), and it was barely detectable in cells expressing BirA-RNF25 (**Figure 1.7D**). Conversely, BirA-RNF25 (but not BirA-RNF14 or catalytically dead BirA-RNF25-dRING) promoted robust ubiquitination of RPS27A K113 (**Figure 1.8B**), consistent with the SILAC-MS data (**Figure 1.5C**). Finally, we observed a drastic decrease in BirA-RNF14-mediated ubiquitination of K385R Flag-eEF1A (**Figure 1.7E**). These results suggest that RNF14 can directly promote eEF1A K385 ubiquitination in response to ternatin-induced elongation stalls. By contrast, the essential role of RNF25 in the eEF1A degradation pathway likely involves direct ubiquitination of RPS27A K113 (see below).

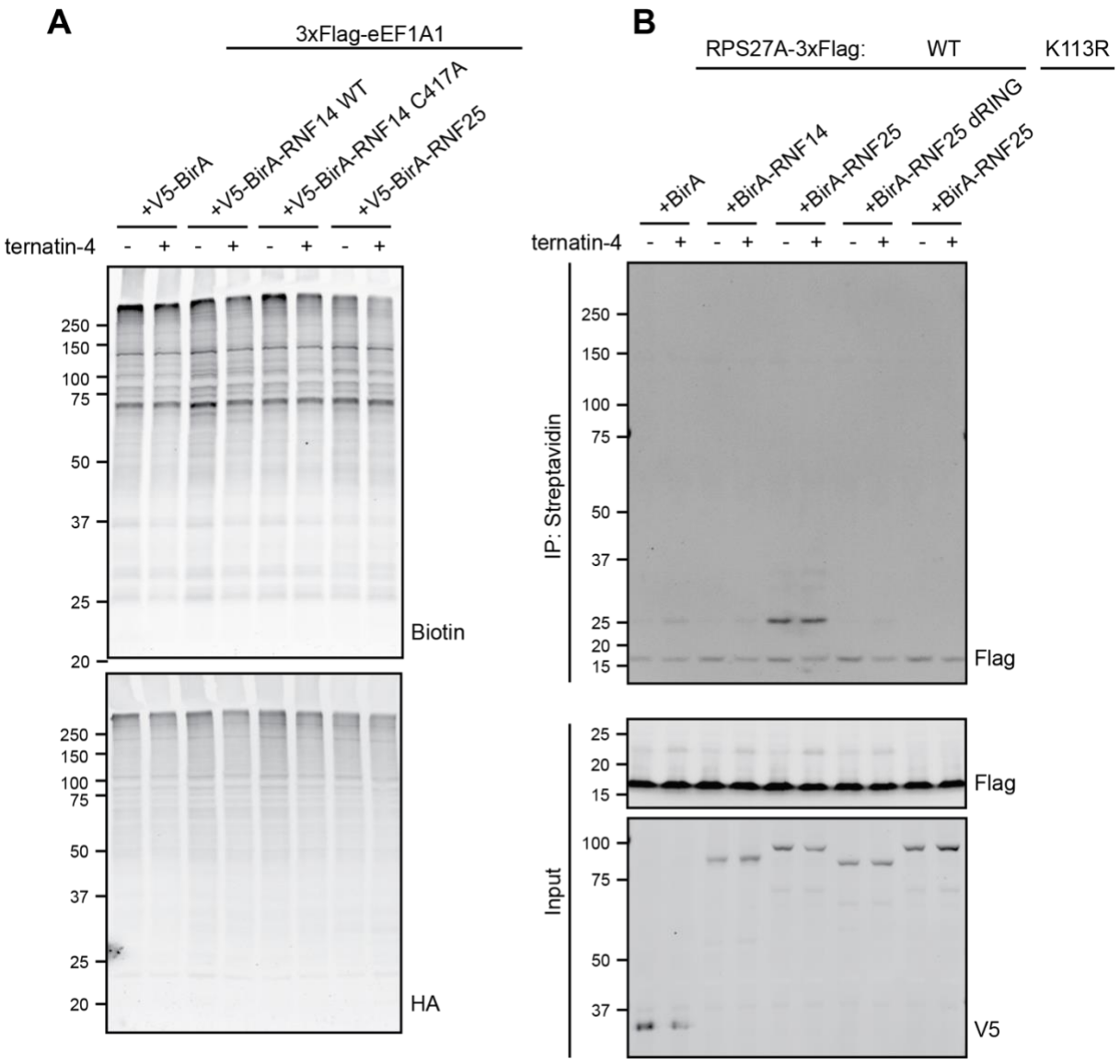

Figure 1.8: Proximity-mediated biotinylation of RNF14/RNF25 substrates.
(**A**) Cell lysates from **Figure 1.7D** were analyzed by immunoblotting for AP-HA-Ub (anti-HA) and biotinylated proteins (streptavidin). (**B**) HeLa cells stably expressing WT or K113R mutant RPS27A-3xFlag were transfected with AP-HA-Ub and the indicated V5-tagged BirA constructs. Cells were treated with 50 μM biotin ± ternatin-4 (50 nM) for 1 h, and biotinylated products were subsequently enriched and analyzed by immunoblotting as in **Figure 1.7**.

GCN1 interacts with RNF14 and is essential for eEF1A degradation

Besides eEF1A and ribosomal proteins, our diGly proteomics experiments revealed multiple ternatin-induced ubiquitination sites on GCN1. GCN1 is a conserved ribosome-associated scaffolding protein that binds the RWD domain of the integrated stress response

kinase, GCN2 (Sattlegger and Hinnebusch, 2000; Kubota et al., 2000). In addition, GCN1 was recently shown to interact with collided, elongation-stalled ribosomes in yeast (Pochopien et al., 2021) and human cells (Wu et al., 2020), although the relative binding affinities of GCN1 for monosomes vs. disomes, trisomes, etc. remain unknown. We postulated that GCN1 (which was not included in the CRISPRi screen) might play a direct role in RNF14/RNF25-mediated eEF1A degradation.

To evaluate potential interactions with GCN1, we immunoprecipitated Flag-tagged RNF14 or RNF25 (stably expressed in HeLa cells). Because previous studies employed chemical crosslinking to stabilize protein interactions with GCN1 (Sattlegger and Hinnebusch, 2005; Wu et al., 2020), we briefly treated cells with 0.1% formaldehyde (22˚C, 10 min) prior to preparing detergent lysates for immunoprecipitation. This experiment revealed a specific interaction between Flag-RNF14 and endogenous GCN1 in cells treated with or without ternatin (**Figure 1.9A**). A higher-molecular weight, likely multi-ubiquitinated form of GCN1 was specifically enriched in Flag-RNF14 immunoprecipitates from ternatin-treated cells, whereas this higher-molecular weight GCN1 species was not detected in immunoprecipitates from untreated cells or from ternatin-treated cells expressing a catalytically dead mutant (C417A) of Flag-RNF14 (**Figure 1.9A** and **1.10A**). Multi-ubiquitinated GCN1 bound to Flag-RNF14 was observed in cells treated for 1 h with intermediate but not high concentrations of ternatin-4 (**Figure 1.10B**), providing additional evidence that RNF14 is activated by ribosome collisions. Relative to Flag-RNF14, Flag-RNF25 enriched GCN1 to a lesser extent, yet robustly immunoprecipitated endogenous 40S and 60S ribosomal proteins, even in the absence of chemical crosslinking (**Figure 1.9A**). These results suggest that RNF14 and RNF25 can form complexes containing GCN1 and ribosomes, consistent with a requirement for both E3 ligases in ternatin-induced ubiquitination of eEF1A and ribosomal proteins (**Figure 1.5**) and the established role of GCN1 as a sensor for elongation-stalled ribosomes (Meydan and Guydosh, 2020; Pochopien et al., 2021; Wu et al., 2020; Yan and Zaher, 2021). The data also suggest that RNF14 may directly

ubiquitinate GCN1 in response to ternatin-induced stalls, although the functional relevance of these marks is unclear.

GCN1-interacting proteins other than GCN2 remain relatively unexplored in higher eukaryotes. By contrast, a conserved C-terminal region of yeast Gcn1, which includes R2259, has been shown to mediate interactions with the RWD domains of yeast Gcn2, Yih1, and Gir2

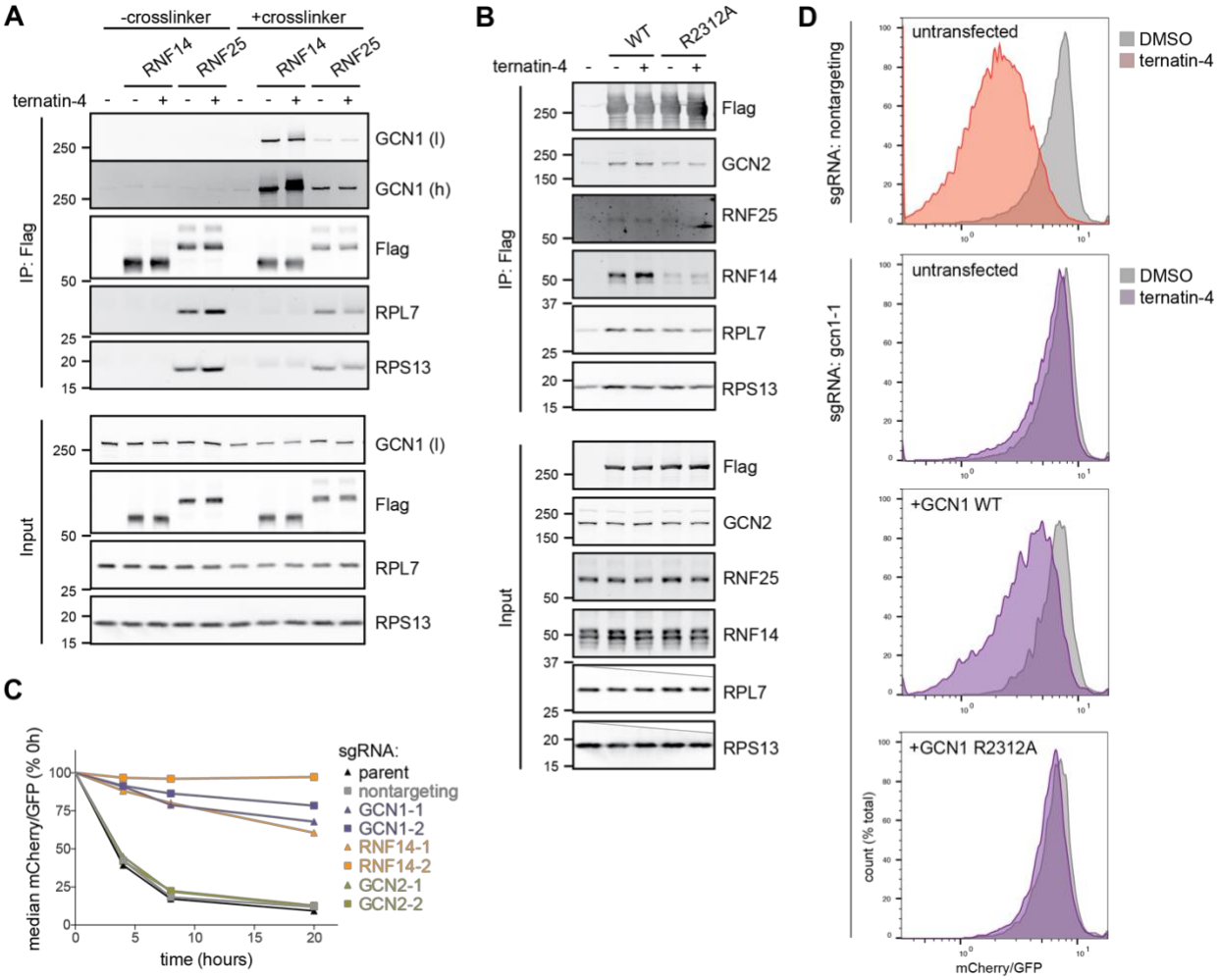

Figure 1.9: GCN1 interacts with RNF14 and is essential for eEF1A degradation.
(**A**) HeLa cells stably expressing 3xFlag-tagged RNF14 or RNF25 were treated for 4 h ± ternatin-4 and then crosslinked with 0.1% PFA (10 min, 22 ˚C) prior to cell lysis, Flag immunoprecipitation, and immunoblotting. (**B**) HEK293T cells transiently transfected with WT or R2312A GCN1-3xFlag were treated and analyzed as in part (**A**). (**C**) mCherry-eEF1A/CRISPRi reporter cells were transduced with sgRNAs targeting the indicated genes as in **Figure 1.3**. Cells were treated with ternatin-4 for the indicated times, and mCherry-eEF1A1 levels were analyzed by flow cytometry. (**D**) mCherry-eEF1A/CRISPRi reporter cells were first transduced with nontargeting or GCN1-targeted sgRNAs as in (**C**). Cells were then transfected with WT or R2312A GCN1-3xFlag (or untransfected), treated for 8 h ± ternatin-4, and analyzed by flow cytometry.

(Castilho et al., 2014; Pochopien et al., 2021). Mutation of Gcn1 R2259 (corresponding to R2312 in human GCN1) had no effect on binding to ribosomes or Gcn20, yet abolished interactions with Gcn2 and prevented Gcn2 activation upon amino acid starvation (Sattlegger and Hinnebusch, 2000). Like GCN2, both RNF14 and RNF25 contain RWD domains, which we hypothesized could mediate interactions with the conserved GCN2-binding region of GCN1. Consistent with the above results using overexpressed RNF14/RNF25 (**Figure 1.9A**), reciprocal immunoprecipitation of overexpressed GCN1-Flag confirmed binding to endogenous RNF14, whereas binding to endogenous RNF25 could not be reliably detected over background (**Figure 1.9B**). Importantly, mutation of R2312 in the conserved RWD binding region of GCN1 dramatically reduced interaction with RNF14, but not ribosomal proteins. GCN2 binding was likewise diminished with GCN1 R2312A, although to a lesser extent than RNF14. Expression of both RNF14 and RNF25 was diminished by deletion of the RWD domain, precluding direct assessment of this domain in facilitating GCN1 binding (data not shown).

To test for a functional role of GCN1 in eEF1A degradation, we used CRISPRi and the mCherry-eEF1A reporter assay. Remarkably, GCN1 knockdown diminished ternatin-induced eEF1A degradation to a similar extent as RNF14 knockdown (**Figures 1.9C** and **1.10C**), whereas knockdown of the canonical GCN1 partner, GCN2, had no effect. Impaired eEF1A degradation was partially rescued in the CRISPRi knockdown cells upon overexpression of wild type GCN1. By contrast, the RNF14 binding-defective GCN1 mutant (R2312A) completely failed to restore eEF1A degradation in cells depleted of endogenous GCN1 (**Figure 1.9D** and **1.10D**). Collectively, the results in **Figure 1.9** demonstrate that GCN1, which has previously been linked to activation of the integrated stress response kinase GCN2, forms a distinct functionally relevant complex with the E3 ligase RNF14.

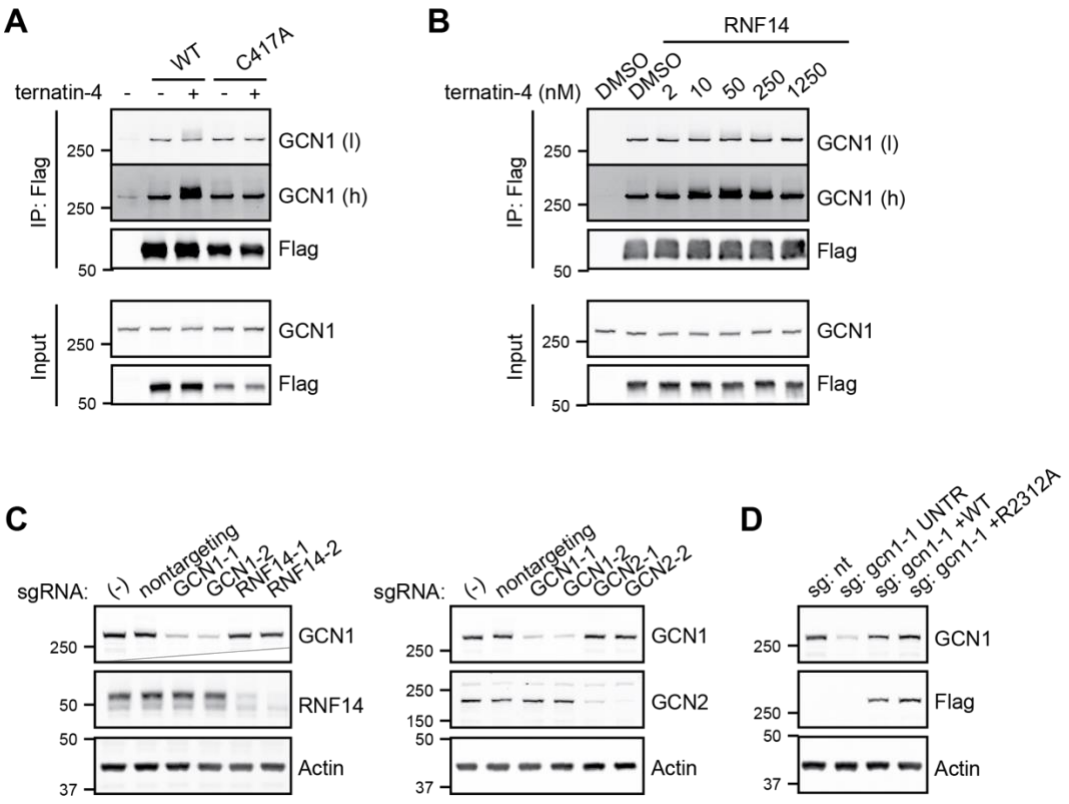

Figure 1.10: RNF14 associates with ubiquitinated GCN1.
(**A**) Ternatin-induced GCN1 modification requires the catalytic cysteine (C417) of RNF14. As in **Figure 1.9A**, HeLa WT cells stably expressing WT or C417A 3xFlag-RNF14 were treated for 4 h with ternatin-4 (50 nM) prior to crosslinking with 0.1% PFA, Flag immunoprecipitation, and immunoblotting. Low and high intensity immunoblot images for GCN1 are shown to indicate higher-MW, presumably multi-ubiquitinated forms of GCN1. (**B**) HeLa WT cells stably expressing 3xFlag-RNF14 were treated with the indicated concentrations of ternatin-4 for 1 h. Samples were crosslinked with 0.1% PFA prior to Flag immunoprecipitation and immunoblotting as in part (**A**). (**C**) Immunoblot analysis of lysates from sgRNA-expressing cells used in **Figure 1.9C**. Cells were puromycin selected and collected 8 days after sgRNA transduction. All samples were prepared from the same experiment but are depicted on different blots. (**D**) WT and R2312A GCN1 rescue constructs are expressed at similar levels. Cells puromycin-selected for sgRNA expression were transfected with the indicated GCN1-3xFlag_IRES-iRFP constructs to give ~20% iRFP+ cells. Lysates from the untreated cells used in **Figure 1.9D** were analyzed by immunoblotting to show knockdown of endogenous GCN1 and overexpression of exogenous WT and R2312A GCN1-3xFlag.

RNF25-dependent ubiquitination of RPS27A K113 is essential for eEF1A degradation

The mechanistic experiments presented above support a specific role for RNF14, which forms a complex with GCN1 and directly ubiquitinates eEF1A, but they do not account for the essential role of RNF25 in the pathway. Our diGly proteomics data provided a potential clue to

this puzzle, which was further corroborated by the BirA-RNF25 assay (**Figure 1.8B**). Ubiquitination of RPS27A (aka eS31) at K107 and K113 was found to be uniquely dependent on RNF25, and not RNF14, whereas ubiquitination of eEF1A and other ribosomal proteins required both RNF25 and RNF14 (**Figure 1.5C**). These data are consistent with an E3 signaling cascade: RNF25 directly promotes RPS27A ubiquitination, which is essential for subsequent RNF14-mediated ubiquitination events on stalled ribosomes. To test whether RPS27A

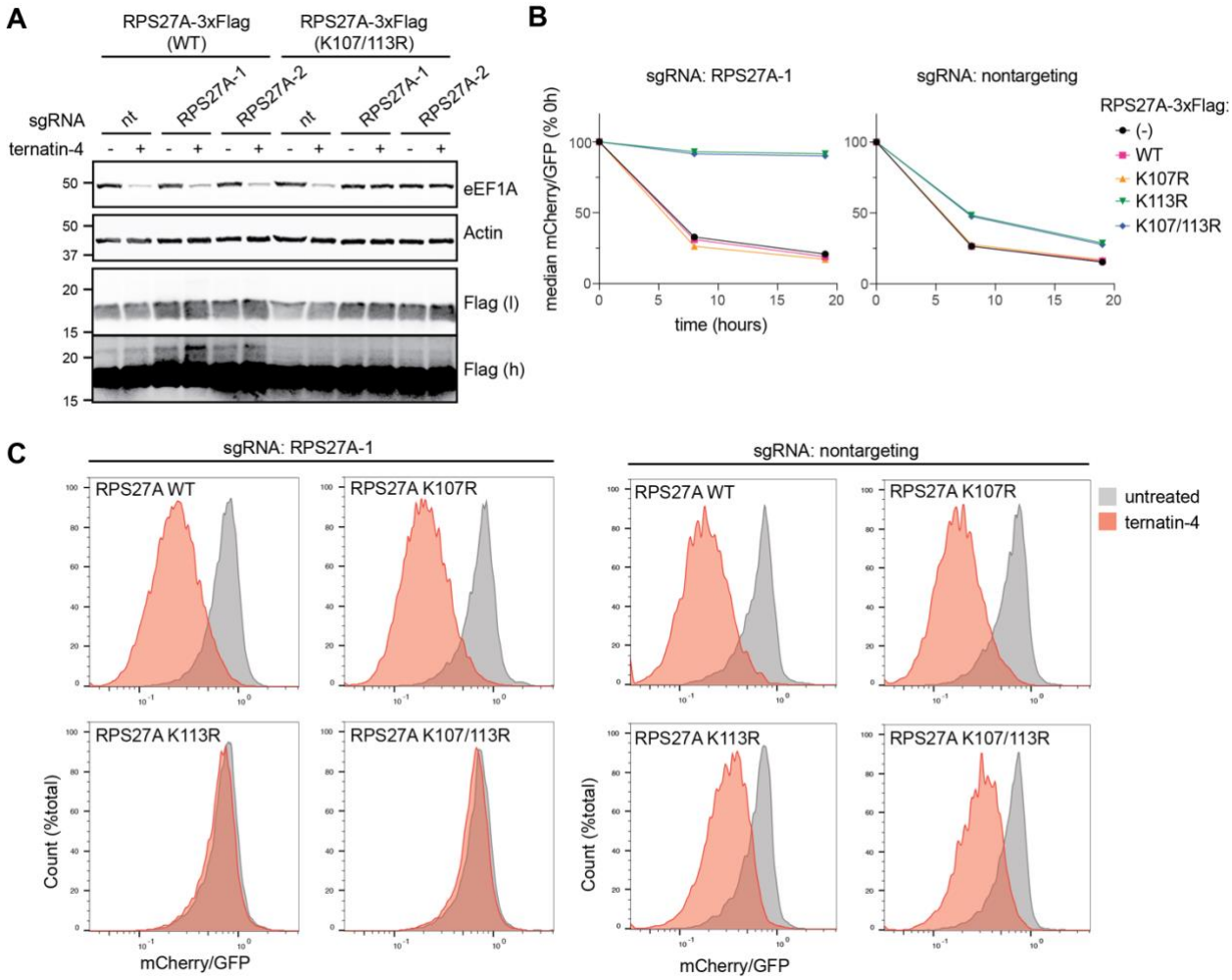

Figure 1.11: Ubiquitination of RPS27A/eS31 K113 is essential for eEF1A degradation. (**A**) HeLa CRISPRi cells stably expressing WT or K107/113R RPS27A-3xFlag were transduced with sgRNAs targeting endogenous RPS27A or a nontargeting sgRNA (nt). Cells selected for sgRNA expression were treated for 20 h ± ternatin-4 and analyzed by immunoblotting. (**B**) mCherry-eEF1A/CRISPRi reporter cells (**Figure 1.1E**) were transduced with RPS27A-3xFlag (WT, K107R, K113R, or K107/113R). Cells were then transduced with sgRNAs as in (**A**), treated with ternatin-4, and analyzed by flow cytometry. (**C**) Flow cytometry histograms are shown for the cells in (**B**) treated for 8 h ± ternatin-4.

ubiquitination is required for eEF1A degradation, we employed a CRISPRi-mediated knockdown and rescue strategy. HeLa CRISPRi cells (stably expressing dCas9-BFP-KRAB) were first transduced with lentiviral constructs encoding either WT or K107/113R mutant RPS27A-Flag. The resulting cell lines, which stably express exogenous RPS27A, were next transduced with sgRNAs to selectively knock down endogenous RPS27A (**Figure 1.12A**). Upon treatment with ternatin-4, we observed robust eEF1A degradation in cells expressing WT RPS27A-Flag (**Figure 1.11A**). By contrast, eEF1A degradation was abolished in RPS27A knockdown cells expressing the K107/113R mutant, strongly supporting a role for RNF25-dependent ubiquitination of K107 and/or K113. Immunoblot analysis of the cells expressing WT RPS27A-Flag, but not the K107/113R mutant, revealed low levels of a higher molecular weight band consistent with mono-ubiquitination of K107 and/or K113.

We confirmed and extended these results by monitoring mCherry-eEF1A degradation in the HCT116 CRISPRi cells, which were engineered to stably express the following RPS27A-Flag constructs: WT, K107R, K113R, or K107/113R. Strikingly, mCherry-eEF1A degradation was completely prevented in ternatin-treated cells expressing K113R RPS27A-Flag (or the K107/113R double mutant) and transduced with an sgRNA targeting endogenous RPS27A (**Figure 1.11B** and **1.11C**). By contrast, the K107R single mutant was indistinguishable from WT RPS27A-Flag and supported robust degradation of mCherry-eEF1A. Even without sgRNA-mediated knockdown of endogenous RPS27A, expression of exogenous K113R or K107/113R RPS27A-Flag partially reduced mCherry-eEF1A degradation (**Figure 1.11B** and **1.11C**).

Stable overexpression of RNF25 (but not RNF14) in HeLa cells resulted in increased levels of mono-ubiquitinated WT (but not K113R) RPS27A-Flag (**Figure 1.12B**), facilitating its analysis by sucrose density gradient centrifugation. Using these cells, we confirmed that ubiquitinated and unmodified RPS27A-Flag cofractionate with 80S monosomes and polysomes, indicating that both forms of RPS27A-Flag are constituents of actively translating ribosomes (**Figure 1.12C**). Upon treatment of cell lysates with micrococcal nuclease, RPS27A-Flag

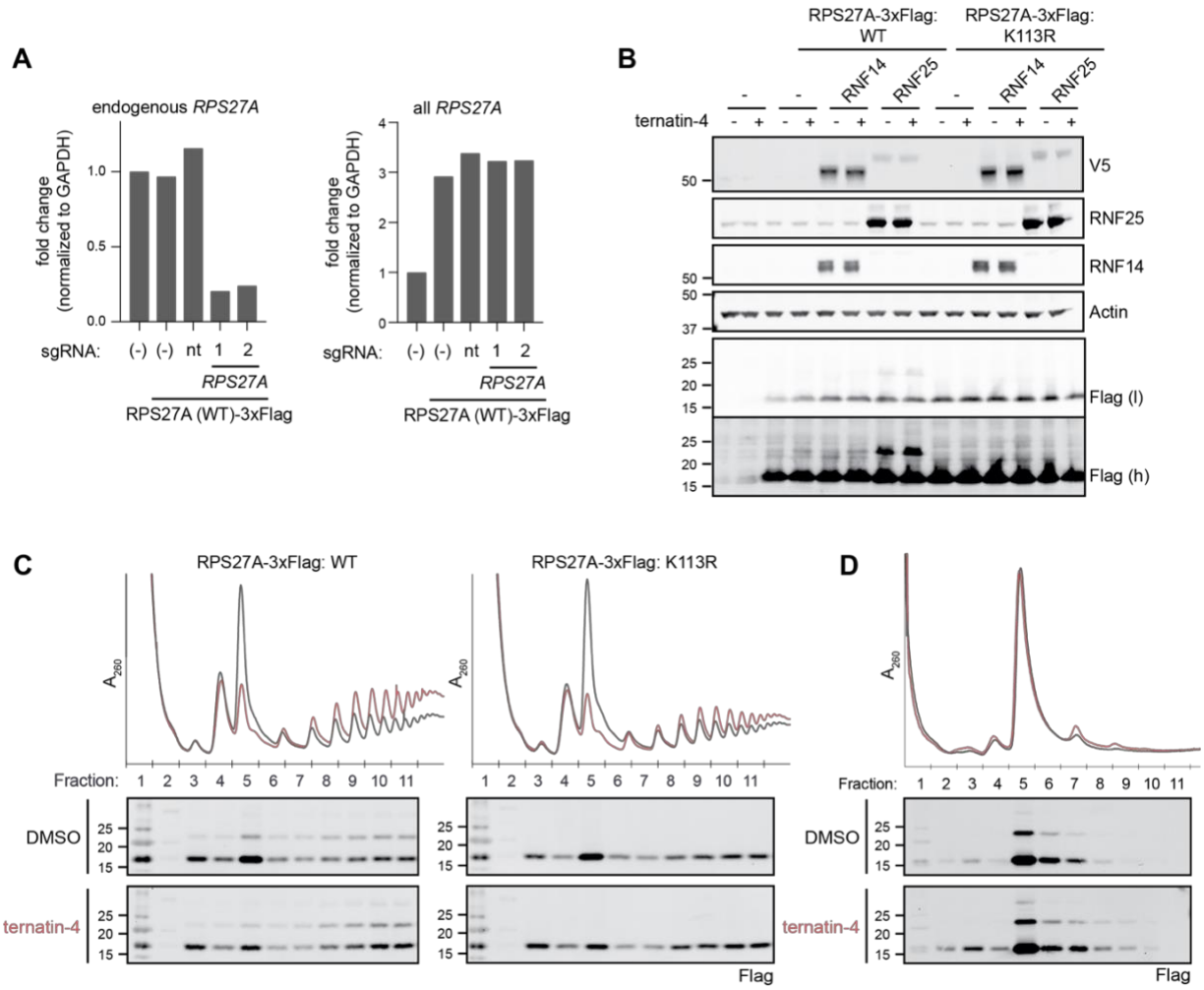

Figure 1.12: Ubiquitinated RPS27A cofractionates with actively translating ribosomes. (**A**) Cells from **Figure 1.11A** (pure populations of HeLa CRISPRi cells expressing RPS27A-3xFlag and the indicated sgRNAs) were subjected to qPCR analysis for both endogenous and exogenous *RPS27A*, or *GAPDH*. *RPS27A* mRNA levels were normalized to *GADPH* expression and are plotted relative to parental HeLa CRISPRi cells. Note that the CRISPRi system targets the endogenous *RPS27A* transcriptional start site (not the *RPS27A* coding sequence), thus allowing for continued expression of exogenous RPS27A. (**B**) HeLa CRISPRi cells stably expressing WT or K113R mutant RPS27A-3xFlag and V5-RNF14 or RNF25 were treated 1 h with ternatin-4 and analyzed by immunoblotting. (**C**) HeLa cells stably expressing V5-RNF25 and WT or K113R mutant RPS27A-3xFlag were treated for 1 h with ternatin-4. Lysates were resolved by ultracentrifugation through 10-50% sucrose gradients, analyzed by A_{260}, and fractionated. Equal amounts of each fraction were analyzed by immunoblotting. (**D**) HeLa cells stably expressing V5-RNF25 and WT RPS27A-3xFlag were treated 1 h with ternatin-4. Lysates were digested with micrococcal nuclease prior to fractionation through 10-40% sucrose gradients and analysis as in (**C**).

predominantly cofractionated with 80S monosomes; however, both ubiquitinated and unmodified forms were also detected in fractions containing nuclease-resistant disomes, and in ternatin-treated cells, trisomes (**Figure 1.12D**).

Ubiquitin-mediated activation of the related RBR E3 ligases Parkin, HOIP, and RNF216 has previously been reported (Cotton et al., 2022; Lechtenberg et al., 2016; Wauer et al., 2015). Parkin is allosterically activated by phospho-Ser65 Ub, and in turn ubiquitinates proteins at the mitochondrial outer membrane, promoting a feed-forward loop (Gundogdu et al., 2021). Key binding interactions between Parkin and allosteric Ub (alloUb) exist at phospho-Ser65, the Ub Ile44 hydrophobic patch, and the ubiquitin C-terminus. Mutation of *hs*Parkin Ala320 (which engages the alloUb Ile44 hydrophobic patch) to arginine was found to reduce alloUb binding and ubiquitination activity (Wauer et al., 2015). Likewise, HOIP binds and is activated by ubiquitin in part through Ile807 and Glu809, which interact with the ubiquitin C-terminus, and Arg770, which interacts with Ub Lys63 and Glu64 (Lechtenberg et al., 2016). These key interaction motifs on Parkin and HOIP reside in an alpha helix at the end of the RING1 domain and in a beta strand at the beginning of the RBR domain (**Figure 1.13A-B**). Ubiquitin binding

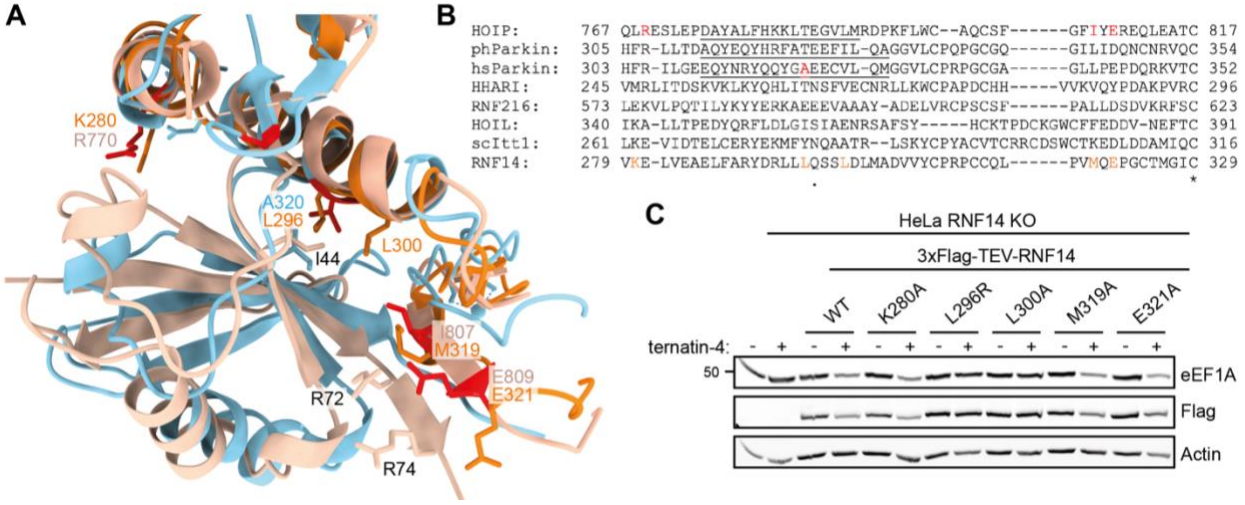

Figure 1.13: Activation of RBR E3 ligases is mediated by allosteric binding to ubiquitin. (**A**) Overlay of the crystal structures of *Pediculus humanus* Parkin/alloUb (blue; PDB: 5CAW), HOIP/alloUb (tan; PDB: 5EDV), and the RNF14 AlphaFold model (orange). Note that structural studies in Wauer et al. employed *Pediculus humanus* Parkin, while functional studies employed *Homo sapiens* Parkin; labeling denotes *hs*Parkin. Residues that were experimentally shown to modulate the ubiquitin binding and ligase activity of Parkin or HOIP are shown in red sticks. Residues tested for their requirement in RNF14-mediated eEF1A degradation are shown in orange sticks. (**B**) Alignment of the ubiquitin binding regions of Parkin and HOIP, with alpha helices underlined and residues from (**A**) mediating ubiquitin interactions in red. Aligned regions from HHARI, RNF216, HOIL, *saccharomyces cerevisiae* Itt1, and RNF14 are shown, with mutated RNF14 residues in orange. (**C**) The indicated RNF14 constructs were introduced into RNF14 KO cells. Transduced cells were sorted on the basis of mCherry positivity, treated with ternatin-4 for 20 h, and eEF1A levels were analyzed by immunoblotting.

promotes straightening of this helix and destabilization of autoinhibitory RBR interactions, allowing subsequent E2 binding and thus providing a rationale for activation.

An overlay of the AlphaFold model for RNF14 with functionally validated residues in the Parkin and HOIP structures revealed several candidate residues, Lys280, Leu296, Met319, and Glu321, which may likewise facilitate RNF14/ubiquitin binding. An additional residue, Leu300, resides adjacent to Leu296 in the alpha helix and may also contact the Ile44 hydrophobic patch. We tested the ability of RNF14 mutations at these sites to restore ternatin-induced eEF1A degradation in RNF14 KO cells. Strikingly, although they were expressed equivalently to WT Flag-RNF14, mutation of either Leu296 to Arg, or Leu300 to Ala, was unable to rescue eEF1A degradation (**Figure 1.13C**). While the ability of L296R and L300A RNF14 mutants to bind GCN1 and ribosomes remains to be assessed, our results suggest that interactions between RNF14 and the Ub Ile44 hydrophobic patch may be required for RNF14 activation.

Collectively, our RPS27A knockdown/rescue experiments strongly suggest that direct RNF25-dependent ubiquitination of RPS27A on K113 plays an essential upstream role in the E3 signaling cascade, ultimately promoting RNF14-dependent eEF1A ubiquitination and degradation on stalled ribosomes (**Figure 1.14A**). A recent cryo-EM structure of yeast Gcn1 bound to a stalled ribosome reveals that RPS27A K113 lies in close proximity to the RWD-binding domain of Gcn1, as well as the ribosomal A site (**Figure 1.14B**), suggesting that K113-Ub could potentially activate GCN1-bound RNF14 (see Discussion).

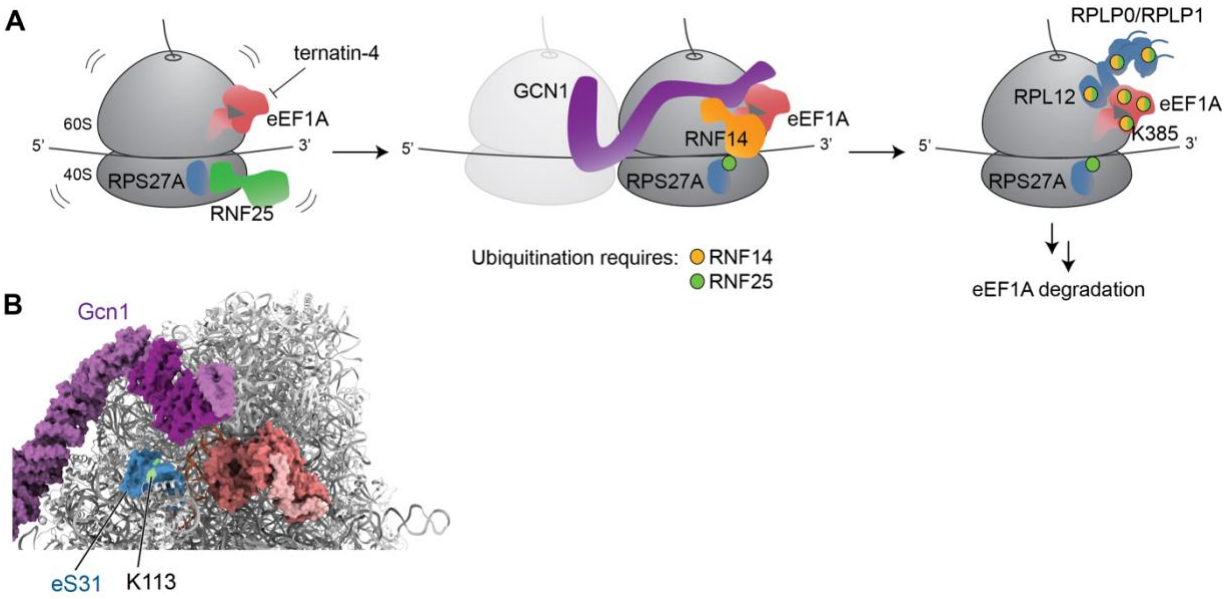

Figure 1.14: Model for ternatin-induced eEF1A degradation.
(**A**) Model for GCN1/RNF14/RNF25 surveillance pathway. RNF25 binds translating ribosomes in unstressed cells and ubiquitinates RPS27A K113 in response to transient stalling events. Upon ternatin-induced stalling, GCN1-bound RNF14 is recruited to ribosome collisions, leading to ubiquitination of trapped eEF1A and the adjacent ribosomal proteins RPL12, RPLP0, and RPLP1. Ubiquitination of eEF1A at K385 and other sites leads to proteasome-dependent eEF1A degradation. (**B**) CryoEM-derived model of yeast Gcn1/di-ribosome complex (PDB: 7NRC) showing Gcn1 (purple) bound to the leading (stalled) ribosome. The C-terminal RWD-binding region of Gcn1 (bright purple) is proximal to K113 (green) of eS31 (blue; yeast ortholog of human RPS27A/eS31) and the GTPase center, which in this structure contains the yeast Gir2/Rbg2 complex (pink/red) bound to peptidyl-tRNA in the A site. Maximal RNF14 E3 ligase activity may require interactions with GCN1 and the RNF25-dependent ubiquitin mark linked to RPS27A/eS31 K113.

Discussion

In this study, we investigated the cellular response to elongation stalls induced by ternatin-4, which traps eEF1A on the ribosome and prevents aa-tRNA accommodation (Wang et al., 2022). We discovered that ternatin-4 robustly induces eEF1A degradation, and we used this phenotype as a foothold to elucidate a novel signaling pathway requiring two poorly characterized E3 ligases, RNF14 and RNF25. RNF14 and RNF25 act in concert with the ribosome collision sensor GCN1 – best known as an upstream activator of the integrated stress response kinase GCN2 – to promote ubiquitination and proteasome-dependent degradation of eEF1A.

Integrating our data with recently published work, we propose a detailed model for eEF1A ubiquitination on stalled ribosomes (**Figure 1.14A**). Because a fraction of RNF25 interacts with ribosomes even in unstressed cells, we propose that it plays an essential upstream surveillance role by promoting RPS27A K113 ubiquitination in response to pausing or stalling events. Consistent with this idea, we detected RPS27A K113 ubiquitination in untreated cells, which subsequently increased ~2-fold after treatment with ternatin-4 (**Figure 1.5B**, **1.5C**, and **Supplementary Table 2**). Of note, ubiquitination of RPS27A K113 was uniquely and solely dependent on RNF25 (and not RNF14), and expression of K113R RPS27A in cells depleted of endogenous RPS27A abolished ternatin-induced eEF1A degradation. This represents one of only a few reported examples of functionally characterized ribosome ubiquitination sites in human cells (Garshott et al., 2021; Garzia et al., 2021; Juszkiewicz and Hegde, 2017; Sundaramoorthy et al., 2017). Elevated RPS27A K113 ubiquitination requiring active translation has previously been observed in cells lacking the deubiquitinase USP16 (Montellese et al., 2020) or treated with low-dose emetine (Sinha et al., 2020). Although the relevant E3 ligase was not identified in either study, our results reveal RNF25 as a strong candidate. We propose that RNF25, likely via direct ubiquitination of RPS27A K113 (**Figure 1.8B**), provides one of two signaling inputs required to activate the RBR-type E3 ligase, RNF14; a potential mechanism for this requirement is described below.

GCN1 provides a second essential signaling input, most likely by recruiting and activating RNF14 near the A site of elongation-stalled ribosomes. The cryo-EM structure of yeast Gcn1 bound to collided di-ribosomes suggests a potential mechanism (Pochopien et al., 2021), as the RWD binding domain of Gcn1 is positioned adjacent to the A site of the leading (stalled) ribosome (**Figure 1.14B**). Hence, binding of this highly conserved region to the N-terminal RWD domain of RNF14 could facilitate proximity-based ubiquitination of eEF1A trapped on the ribosome, as well as GCN1 itself (all identified GCN1 Ub sites map to the C-terminal region) and the ribosomal proteins RPL12, RPLP0, and RPLP1. Although further

studies are required to define the functions of these additional ubiquitin marks, we provide evidence here for direct RNF14-mediated ubiquitination of eEF1A K385, which is essential for maximal eEF1A degradation.

The yeast Gcn1/di-ribosome cryo-EM structure also provides clues to a potential role for RNF25-dependent ubiquitination of RPS27A/eS31 K113. This ubiquitination site resides at the tip of the small ribosomal subunit 'beak' and is immediately adjacent to the RWD binding domain of Gcn1 (**Figure 1.14B**). This arrangement suggests a mechanism whereby RNF14 could receive two proximal signaling inputs: one provided by GCN1 binding to the RNF14 RWD domain, and a second provided by mono-ubiquitinated K113 on RPS27A. K113-Ub could potentially engage a conserved allosteric ubiquitin binding site in the RBR domain of RNF14. Although speculative, this model is consistent with structural and biochemical studies of other RBR-type E3 ligases (e.g., parkin and HOIP), which are autoinhibited and require allosteric activation – including by ubiquitin itself – to unveil the E2 binding and catalytic sites (Cotton and Lechtenberg, 2020).

Historically, natural products with distinct proteotoxic mechanisms have been used to elucidate cellular stress response pathways, including the UPR (tunicamycin), mitochondrial UPR (antimycin), and ribotoxic stress response (anisomycin). A strength of our study is the use of ternatin-4 to acutely induce ribosome stalls with trapped eEF1A, providing a robust elongation stress signal that culminates in ubiquitin-dependent eEF1A degradation. A key question for the future concerns the physiological and environmental stressors that activate the GCN1/RNF14/RNF25 pathway in cells and organisms. One potential environmental stressor is RNA- damaging UV light, which was recently shown to induce ribosome collisions (Wu et al., 2020). Interestingly, a previously published diGly proteomics dataset identified UV-induced ubiquitination sites on eEF1A, ribosomal proteins, and GCN1 (Elia et al., 2015).

In addition to RNA damage, altered post-transcriptional RNA modifications – in particular, decreased methoxycarbonylmethylation or thiolation of the anticodon wobble uridine

(U_{34}) in certain tRNAs – could result in codon-specific stalls that locally activate GCN1/RNF14/RNF25. Preliminary support for this idea is provided by a recent study that correlated genome-wide CRISPR knockout effects (https://depmap.org) across 485 cancer cell lines (Wainberg et al., 2021). Based on statistical analysis of gene-gene correlations ('co-essentiality'), RNF25 was placed in the same biological pathway as ELP3 and CTU2. The latter enzymes promote tRNA U_{34} methoxycarbonylmethylation and thiolation, respectively, and control translation elongation in developmental, homeostatic, and disease contexts (Hawer et al., 2019; Hermand, 2020). Finally, ribosome stalling at termination codons could also activate the GCN1/RNF14/RNF25 pathway, leading to ubiquitination of eEF1A (bound to near-cognate aa-tRNA) or release factors (eRF1/eRF3) trapped in the GTPase center. Consistent with this scenario, overexpression of the RNF14 ortholog Itt1 was found to promote stop codon readthrough in yeast (Urakov et al., 2001), although the mechanism underlying this phenotype remains unclear.

Deletion of GCN1, or even the C-terminal RWD binding region of GCN1, is lethal in mice (Yamazaki et al., 2020), whereas deletion of GCN2 causes only mild phenotypes (Zhang et al., 2002). Hence, GCN1 must have GCN2-independent functions, which have remained enigmatic despite the identification of other RWD domain-containing Gcn1 interactors, including yeast Gir2 and Yih1 (Pochopien et al., 2021; Sattlegger et al., 2004; Wout et al., 2009). Integrating results from our study with previous work, we propose that GCN1 lies at the nexus of multiple translation stress and surveillance pathways requiring RWD domain effectors – including RNF14 and RNF25 – in which pathway selection is determined locally by the status and occupancy of the GTPase center of the stalled ribosome.

Acknowledgments

Funding for this study was provided by the UCSF Invent Fund (J.T.), the National Institutes of Health (DP2 GM119139 to M.K. and P30CA082103 to the UCSF HDFCCC Laboratory for Cell

Analysis Shared Resource Facility), a UCSF Genentech Fellowship (K.O.), a Department of Defense NDSEG fellowship (S.K.S.), and the Tobacco-Related Disease Research Program Postdoctoral Fellowship Awards (28FT-0014 to H.Y.W.). We thank Jong-Bok Yoon for the BirA/AP-Ub plasmids and Scott Blanchard and Davide Ruggero for comments on the manuscript.

Author Contributions

K.O. designed and performed experiments, and analyzed and interpreted data. J.D.C. designed experiments and developed the fluorescent reporter assay. S.K.S. assisted with planning and performing the CRISRPi screen and analyzed screen data. T.Y. collected mass spectrometry data and assisted with mass spectrometry data analysis. H.Y.W. synthesized key reagents. M.K. assisted with planning the CRISPRi screen and interpreted data. J.T. supervised the study. J.D.C., K.O., and J.T. conceived the study. J.T. and K.O. wrote the manuscript with input from all authors.

Table 1.1: Key Resources

Reagent or Resource	Source	Identifiers
Antibodies		
Mouse monoclonal anti-eEF1A, clone CBP-KK1	EMD Millipore	Cat# 05-235; RRID: AB_309663
Rabbit monoclonal anti-beta Actin (13E5)	Cell Signaling Technology	Cat# 4970S; RRID: AB_2223172
Mouse monoclonal anti-RNF14 (B-10)	Santa Cruz Biotechnology	Cat# sc-376701; RRID: AB_11150281
Rabbit polyclonal anti-RNF25	Abcam	Cat# ab140514
Rabbit monoclonal anti-V5 (D3H8Q)	Cell Signaling Technologies	Cat# 13202S; RRID: AB_2687461
Mouse monoclonal anti-Flag	Sigma-Aldrich	Cat# F3165; RRID: AB_259529
Mouse monoclonal anti-HA (6E2)	Cell Signaling Technologies	Cat# 2367S; RRID: AB_10691311
Rabbit polyclonal anti-GCN1L1	Novus Biologicals	Cat# NBP1-83383; RRID: AB_11022056
Rabbit polyclonal anti-GCN2	Cell Signaling Technologies	Cat# 3302S; RRID: AB_2277617
Rabbit polyclonal anti-RPL7	Bethyl Laboratories	Cat# A300-741A; RRID: AB_2301241
Rabbit polyclonal anti-RPS13	Proteintech	Cat# 16680-1-AP; RRID: AB_2182500
Goat polyclonal anti-mouse IgG IRDye 680RD	LI-COR	Cat# 926-68070; RRID: AB_10956588
Goat polyclonal anti-mouse IgG IRDye 800CW	LI-COR	Cat# 926-32210; RRID: AB_621842
Goat polyclonal anti-rabbit IgG IRDye 680RD	LI-COR	Cat# 926-68071; RRID: AB_10956166
Goat polyclonal anti-rabbit IgG IRDye 800CW	LI-COR	Cat# 926-32211; RRID: AB_621843
Chemicals, Peptides, and Recombinant Proteins		
Ternatin-4	Wang et al., 2022	n/a
Cycloheximide	Sigma-Aldrich	Cat# C7698
Homoharringtonine	MedChemExpress	Cat# HY-14944
Carfilzomib	Abcam	Cat# ab216469
CB-5083	ApexBio	Cat# B6032
O-propargyl puromycin (OPP)	Liu et al., 2012	n/a
Puromycin	InvivoGen	Cat# ant-pr-1
Biotin	Sigma-Aldrich	Cat# B4501
Chloroacetamide	Sigma-Alrich	Cat# 22790
$^{13}C_6$ $^{15}N_4$ L-arginine hydrochloride	Cambridge Isotope Laboratories	Cat# CNLM-539-H-0.1
$^{13}C_6$ $^{15}N_2$ L-lysine hydrochloride	Cambridge Isotope Laboratories	Cat# CNLM-291-H-0.1
Zombie Aqua Fixable Viability Kit	BioLegend	Cat# 423101

Reagent or Resource	Source	Identifiers
CF647 azide	Biotium	Cat# 92084
eEF1A K385 standard peptide SGK[diGly]KLEDGPK, with 13C6,15N-Leu	Peptide Specialty Laboratories	n/a
3xFlag Peptide	Sigma-Aldrich	Cat# M4799
EDTA-free Protease Inhibitor Cocktail	Roche	Cat# 11873580001
Q5 Hot Start PCR Master Mix	New England Biolabs	Cat# M094
RNase Inhibitor, Human Placenta	New England Biolabs	Cat# M0307
SUPERaseIn RNase Inhibitor	Invitrogen	Cat# AM2694
Micrococcal nuclease	Roche	Cat# 10107921001
TURBO DNase	Invitrogen	Cat# AM2238
Trypsin	Promega	Cat# V5113
IRDye 800CW Streptavidin	LI-COR	Cat# 926-32230
Pierce Streptavidin Magnetic Beads	Thermo Fisher Scientific	Cat# 88817
Anti-Flag M2 Magnetic Beads	Sigma-Aldrich	Cat# M8823
Mirus TransIT-LT1 Transfection Reagent	Mirus Bio	Cat# MIR2300
Lipofectamine 2000	Invitrogen	Cat# 11668-019
Lipofectamine LTX	Invitrogen	Cat# 15338030
ViralBoost Reagent	Alstem Cell Advancements	Cat# VB100
Hexadimethrine bromide (polybrene)	Sigma-Aldrich	Cat# TR-1003-G
16% Paraformaldehyde Solution	Electron Microscopy Sciences	Cat# 15710
Critical Commercial Assays		
NucleoSpin Blood L Kit	Macherey-Nagel	Cat# 740954.20
PTMScan® Ubiquitin Remnant Motif (K-ε-GG) Kit	Cell Signaling Technology	Cat# 5562
RNeasy Mini Kit	Qiagen	Cat# 74104
High-Capacity cDNA Reverse Transcription Kit	Applied Biosystems	Cat# 4368813
Luna Universal qPCR Master Mix	New England Biolabs	Cat# M3003
CellTiter-Glo Luminescent Cell Viability Assay	Promega	Cat# G7572
Experimental Models: Cell Lines		
HeLa	ATCC	CCL-2
HEK293T	ATCC	CRL-3216
HCT116 eEF1A1 A399V/A399V	Krastel et al., 2015	n/a
HCT116 eEF1A1 A399V/A399V Flag-mCherry-eEF1A1_IRES-GFP dCas9-HA-NLS-BFP-KRAB	This paper	n/a
HCT116 eEF1A1 A399V/A399V Flag-mCherry-eEF1A1_IRES-GFP	This paper	n/a
HCT116 eEF1A1 A399V/A399V Flag-mCherry-eEF1A1 A399V_IRES-GFP	This paper	n/a

Reagent or Resource	Source	Identifiers
HCT116 eEF1A1 A399V/A399V Flag-mCherry-eEF1A1 K212R_IRES-GFP	This paper	n/a
HCT116 eEF1A1 A399V/A399V Flag-mCherry-eEF1A1 K273R_IRES-GFP	This paper	n/a
HCT116 eEF1A1 A399V/A399V Flag-mCherry-eEF1A1 K385R_IRES-GFP	This paper	n/a
HCT116 eEF1A1 A399V/A399V Flag-mCherry-eEF1A1 K395R_IRES-GFP	This paper	n/a
HCT116 eEF1A1 A399V/A399V Flag-mCherry-eEF1A1 K408R_IRES-GFP	This paper	n/a
HCT116 eEF1A1 A399V/A399V 3xFlag-eEF1A1	This paper	n/a
HCT116 eEF1A1 A399V/A399V 3xFlag-eEF1A1 K385R	This paper	n/a
HeLa RNF14 KO	This paper	n/a
HeLa RNF25 KO	This paper	n/a
HeLa RNF14 KO V5-RNF14	This paper	n/a
HeLa RNF14 KO V5-RNF14 C417A	This paper	n/a
HeLa RNF14 KO 3xFlag-TEV-RNF14	This paper	n/a
HeLa RNF14 KO 3xFlag-TEV-RNF14 K280A	This paper	n/a
HeLa RNF14 KO 3xFlag-TEV-RNF14 L296R	This paper	n/a
HeLa RNF14 KO 3xFlag-TEV-RNF14 L300A	This paper	n/a
HeLa RNF14 KO 3xFlag-TEV-RNF14 M321A	This paper	n/a
HeLa RNF14 KO 3xFlag-TEV-RNF14 E321A	This paper	n/a
HeLa RNF25 KO V5-RNF25	This paper	n/a
HeLa RNF25 KO V5-RNF25 dRING (aa 135-201)	This paper	n/a
HeLa V5-RNF14	This paper	n/a
HeLa V5-RNF14 C417A	This paper	n/a
HeLa V5-RNF25	This paper	n/a
HeLa V5-RNF25 dRING (aa 135-201)	This paper	n/a
HeLa 3xFlag-TEV-RNF14	This paper	n/a
HeLa 3xFlag-TEV-RNF14 C417A	This paper	n/a
HeLa 3xFlag-TEV-RNF25	This paper	n/a
HeLa dCas9-HA-NLS-BFP-KRAB	This paper	n/a
HeLa RPS27A-3xFlag dCas9-HA-NLS-BFP-KRAB	This paper	n/a
HeLa RPS27A K113R-3xFlag dCas9-HA-NLS-BFP-KRAB	This paper	n/a
HeLa RPS27A K107/113R-3xFlag dCas9-HA-NLS-BFP-KRAB	This paper	n/a
HeLa V5-RNF14 RPS27A-3xFlag dCas9-HA-NLS-BFP-KRAB	This paper	n/a
HeLa V5-RNF14 RPS27A K113R-3xFlag dCas9-HA-NLS-BFP-KRAB	This paper	n/a
HeLa V5-RNF25 RPS27A-3xFlag dCas9-HA-NLS-BFP-KRAB	This paper	n/a

Reagent or Resource	Source	Identifiers
HeLa V5-RNF25 RPS27A K113R-3xFlag dCas9-HA-NLS-BFP-KRAB	This paper	n/a
Recombinant DNA		
pLX304 Flag-mCherry-eEF1A1_IRES-GFP	This paper	n/a
pLX302 Flag-mCherry-eEF1A1_IRES-GFP	This paper	n/a
pLX302 Flag-mCherry-eEF1A1 A399V_IRES-GFP	This paper	n/a
pLX302 Flag-mCherry-eEF1A1 K212R_IRES-GFP	This paper	n/a
pLX302 Flag-mCherry-eEF1A1 K273R_IRES-GFP	This paper	n/a
pLX302 Flag-mCherry-eEF1A1 K385R_IRES-GFP	This paper	n/a
pLX302 Flag-mCherry-eEF1A1 K395R_IRES-GFP	This paper	n/a
pLX302 Flag-mCherry-eEF1A1 K408R_IRES-GFP	This paper	n/a
pLX302 3xFlag-eEF1A1_IRES-GFP	This paper	n/a
pLX302 3xFlag-eEF1A1 K385R_IRES-GFP	This paper	n/a
pHR V5-RNF14_IRES-mCherry	This paper; RNF14 sequence from DNASU Clone # HsCD00436670	n/a
pHR V5-RNF14 C417A_IRES-mCherry	This paper	n/a
pHR V5-RNF25_IRES-mCherry	This paper; RNF25 sequence from DNASU Clone # HsCD00438677	n/a
pHR V5-RNF25 dRING (aa 135-201)_IRES-mCherry	This paper	n/a
pHR V5-BirA_IRES-mCherry	This paper; BirA sequence from Deshar et al., 2016	n/a
pHR V5-BirA-RNF14_IRES-mCherry	This paper	n/a
pHR V5-BirA-RNF14 C417A_IRES-mCherry	This paper	n/a
pHR V5-BirA-RNF25_IRES-mCherry	This paper	n/a
pHR V5-BirA-RNF25 dRING (aa 135-201)_IRES-mCherry	This paper	n/a
pHR 3xFlag-TEV-RNF14_IRES-mCherry	This paper	n/a
pHR 3xFlag-TEV-RNF14 C417A_IRES-mCherry	This paper	n/a
pHR 3xFlag-TEV-RNF14 K280A_IRES-mCherry	This paper	n/a
pHR 3xFlag-TEV-RNF14 L296R_IRES-mCherry	This paper	n/a
pHR 3xFlag-TEV-RNF14 L300A_IRES-mCherry	This paper	n/a
pHR 3xFlag-TEV-RNF14 M319A_IRES-	This paper	n/a

Reagent or Resource	Source	Identifiers
mCherry		
pHR 3xFlag-TEV-RNF14 E321A_IRES-mCherry	This paper	n/a
pHR 3xFlag-TEV-RNF25_IRES-mCherry	This paper	n/a
pLenti6.3 GCN1-3xFlag_IRES-iRFP	This paper; GCN1 sequence from DNASU Clone # HsCD00946315	n/a
pLenti6.3 GCN1 R2312A-3xFlag_IRES-iRFP	This paper	n/a
pHR RPS27A-3xFlag_IRES-AcGFP	This paper; RPS27A sequence from Addgene Plasmid #69561	n/a
pHR RPS27A K113R-3xFlag_IRES-AcGFP	This paper	n/a
pHR RPS27A K107/113R-3xFlag_IRES-AcGFP	This paper	n/a
pHR RPS27A-3xFlag_IRES-iRFP	This paper	n/a
pHR RPS27A K107R-3xFlag_IRES-iRFP	This paper	n/a
pHR RPS27A K113R-3xFlag_IRES-iRFP	This paper	n/a
pHR RPS27A K107/113R-3xFlag_IRES-iRFP	This paper	n/a
pcDNA3.1 AP-HA-Ub	Deshar et al., 2016	n/a
pHR dCas9-HA-NLS-BFP-KRAB	Innovative Genomics Institute	Plasmid #IGI_P0152
pLG15	Horlbeck et al., 2016	n/a
CRISPRi UPS pooled library	Chen et al., 2019	n/a
pCMV-dR8.91	Gift from Didier Trono	Addgene Ref #2221
pMD2.G	Gift from Didier Trono	Addgene Plasmid #12259
PX458 pSpCas9(BB)-2A-GFP	Ran et al., 2013	Addgene Plasmid #48138
Sequence-Based Reagents		
Nontargeting CRISPRi sgRNA: 5'-GGACTAAGCGCAAGCACCTA-3'	Tian et al., 2019	n/a
RNF14-1 CRISPRi sgRNA: 5'-GGGCGAGCTGAACCCAGACT-3'	This paper	n/a
RNF14-2 CRISPRi sgRNA: 5'-GGGCGGCCGGAAGGTACGGT-3'	This paper	n/a
RNF25-1 CRISPRi sgRNA: 5'-GCGGGCCGGTGAAGATATGG-3'	This paper	n/a
GCN1-1 CRISPRi sgRNA: 5'-GGGCGGCGCAGGCAGACCGC-3'	This paper	n/a
GCN1-2 CRISPRi sgRNA: 5'-GGGCGGACACGCAGGTGAGG-3'	This paper	n/a
GCN2-1 CRISPRi sgRNA: 5'-GCTCCAGGGCCTGTAGCTCG-3'	This paper	n/a
GCN2-2 CRISPRi sgRNA: 5'-GCAGCGCTGCGCCCAAGGCA-3'	This paper	n/a

Reagent or Resource	Source	Identifiers
RPS27A-1 CRISPRi sgRNA: 5'-GAGACACCCACCGCAGATGG-3'	This paper	n/a
RPS27A-2 CRISPRi sgRNA: 5'-GGCGGTGGGTGTCTGCACTT-3'	This paper	n/a
sgRNA targeting exon 5 of *RNF14*: 5'-GACAATATTCAAGTATGCTA-3'	This paper	n/a
sgRNA targeting exon 3 of *RNF25*: 5'-AAAGTGATGTAGATCTCCCA-3'	This paper	n/a
Software and Algorithms		
GraphPad Prism	GraphPad Prism software	n/a
Image Studio Lite	LI-COR	n/a
FlowJo	BD Biosciences	n/a
Tableau	Tableau software	n/a
MaxQuant	Cox and Mann, 2008	n/a
Skyline	Maclean et al., 2010	n/a
Adobe Illustrator	Adobe	n/a
Adobe Photoshop	Adobe	n/a

Experimental Methods

Cell lines and culture conditions

HEK293T and HeLa cells were maintained in Dulbecco's Modified Eagle's Medium (DMEM) supplemented with 10% fetal bovine serum (FBS), 100 U/mL penicillin, and 100 µg/mL streptomycin. HCT116 eEF1A1 A399V/A399V cells were originally described in Krastel et al., (2015), and were maintained in McCoy's media supplemented with 10% FBS, 100 U/mL penicillin, and 100 µg/mL streptomycin. Antibiotics were omitted for all transfection-based experiments. Cells were grown in a humidified incubator at 37 °C with a 5% CO_2 atmosphere. Unless indicated otherwise, all treatment conditions utilized a vehicle control, 50 nM ternatin-4, 50 µg/mL cycloheximide, 2 µg/mL homoharringtonine, 500 nM carfilzomib or 2.5 µM CB-5083 as described in figure legends.

Plasmid Generation

Plasmids encoding the indicated genes, epitope tags, and IRES sequences were constructed by Gibson cloning. Point mutations and the RNF25 RING deletion (residues 135-201) were created by site-directed mutagenesis. All eEF1A1-encoding constructs were expressed from a pLX302 vector containing IRES-AcGFP, except the mCherry-eEF1A1 reporter used for the CRISPRi screen, which was expressed from a pLX304 vector. RNF14, RNF25, and RPS27A-encoding constructs were expressed from a pHR vector containing IRES-mCherry (RNF14 and RNF25) or IRES-AcGFP or iRFP (RPS27A). GCN1 was expressed in a modified pLenti6.3 vector with the SV40 promoter and blasticidin resistance marker removed, and IRES-iRFP added. Plasmids encoding individual sgRNAs were constructed by ligating complementary oligonucleotides (sequences indicated above in **Sequence-Based Reagents**) into the BlpI and BstXI restriction enzyme sites of pLG15 (CRISPRi) or the BbsI restriction enzyme sites of PX458 (CRISPR KO). All plasmids were verified by Sanger sequencing.

Lentivirus and stable cell line generation

Lentivirus was generated by transfecting HEK293T cells growing at approximately 60% confluency in 6-well dishes with lipid complexes containing 1.5 µg of a construct of interest, 1.35 µg pCMV-dR8.91, 165 ng pMD2-G, and 7.5 µL Mirus TransIT-LT1 diluted in OPTI-Mem. Alstem ViralBoost was added to cells after addition of the transfection mix. Two days post-transfection, an additional 1.5 mL complete DMEM was added to cells. The viral supernatant was collected on the third day and filtered through 0.45 µm sterile SFCA syringe filters (Thermo Scientific). Supernatant was used immediately or stored at -20 °C.

For stable cell line generation, media containing 8 µg/mL polybrene was added to cells, lentivirus was added, and cells were incubated overnight. Lentivirus was removed from cells, and cells were expanded until cell sorting using a BD FACS Aria II. Transduced cells were typically sorted to at least 95% purity.

CRISPR knockout cell lines

CRISPR knockout cells were generated as previously described (Ran et al., 2013). sgRNA sequences targeting exon 5 of RNF14 and exon 3 of RNF25 were identified using the Broad CRISPR design tool (crispr.mit.edu/v1) and ligated into the PX458 (pSpCas9(BB)-2A-GFP) plasmid. HeLa cells were transfected using Lipofectamine 2000 and sorted for GFP positivity after 3 days. Eight days post-transfection, cells were plated into a 96-well plate at 0.5 cells per well. After appearance of visible colonies (approximately 2 weeks), wells containing individual colonies were collected by trypsinization and expanded to 6-well dishes. Clones were screened for RNF14/RNF25 expression by Western blotting and Sanger sequencing prior to selection for experiments.

Immunoblot analysis

Cells were washed once with ice-cold PBS and stored at -80 °C or immediately lysed using lysis buffer (50 mM HEPES pH 7.4, 150 mM NaCl, 1% NP-40, 2x Roche EDTA-free protease inhibitors). Lysates were collected by scraping and were cleared by centrifugation at 16,100 *g* for 10 minutes at 4 °C. Total protein was quantified using the Bradford method and normalized prior to electrophoresis using hand-cast 7.5% polyacrylamide gels. Proteins were transferred to 0.45 µm nitrocellulose membranes (Bio-Rad) using a Bio-Rad Criterion transfer system. Membranes were blocked for 1 hour at room temperature using blocking buffer (5% BSA, 0.1% sodium azide in TBS-T). Membranes were incubated with primary antibodies diluted in blocking buffer for 1 hour at room temperature or overnight at 4 °C. Membranes were rinsed with TBS-T (3 x 5 minutes at room temperature) and incubated with secondary antibodies diluted in blocking buffer for 1 hour at room temperature. Membranes were rinsed with TBS-T (3 x 5 minutes at room temperature) and were imaged using a Li-Cor Odyssey system. The resulting images were quantified using Image Studio Lite (Li-Cor). Where indicated, intensities were normalized to vehicle controls.

Protein synthesis measurements

Cells were grown to 70% confluency in 12-well plates and treated as indicated (ternatin-4 or vehicle; 20 h). Following treatment, O-propargyl puromycin (OPP) was added to all wells at a final concentration of 30 µM, and cells were incubated for an additional hour. Cells were collected by trypsinization and transferred to a 96-well V-bottom plate for the remainder of the experiment. All centrifugation steps were performed at 2,100 *g* for 3 minutes at 4°C, and all washes and incubations were done with 200 µL buffer unless indicated otherwise. Cells were washed once with cold PBS and then stained with 100 µL Zombie Aqua (BioLegend; 1:1000 in PBS) for 30 min at RT. Incubations from this step onwards were performed in the dark. Cells were washed once (2% FBS in PBS) and fixed with 4% paraformaldehyde (PFA) in PBS for 15

min at 4 °C. Cells were washed once (2% FBS in PBS) and incubated in permeabilization buffer (3% FBS, 0.1% saponin in PBS) for 5 min at RT. Click chemistry mix was prepared by adding the following components to final concentrations in the order listed: 50 mM HEPES pH 7.5, 150 mM NaCl, 400 µM TCEP, 250 µM TBTA, 5 µM CF647 azide (Biotium), 200 µM $CuSO_4$. Cells were resuspended in 25 µL permeabilization buffer, 100 µL click chemistry mix was added, and cells were incubated overnight at RT. Cells were washed twice with permeabilization buffer and twice with FACS buffer (2% FBS, 100 U/mL penicillin, 100 µg/mL streptomycin, and 2 mM EDTA in PBS lacking Ca^{+2}/Mg^{+2}). Samples were analyzed on a Thermo Attune NxT (see below). Data was processed in FlowJo (BD) with a gating hierarchy as follows: debris were excluded (FSC-H vs. SSC-A), doublets were excluded (FSC-H vs. FSC-W), and dead cells were excluded on the basis of Zombie Aqua positivity. Mean fluorescent intensity (MFI) was calculated for each sample and normalized to vehicle control samples.

Cell proliferation assays

HeLa cells were plated (1000 cells/well, 90 µL media) into white 96-well plates, excluding the outer edges. Three rows were plated for each treatment condition. The following day, 10X drug stocks were prepared (0.1% DMSO final per well) and added to cells. Cells were incubated for 72 h (37 °C; 5% CO_2 atmosphere). CellTiter-Glo reagent (Promega) was prepared by adding 1 part reagent to 4 parts PBS. The dilution was added directly to cells (100 µL/well) and luminescence was immediately measured using a Molecular Devices Spectra Max M5 plate reader. Measurements from biological replicate wells for each condition were averaged, normalized to DMSO wells, and nonlinear regression curves were plotted in GraphPad Prism.

Flow cytometry

Cells were harvested by trypsinization, transferred to 96-well V-bottom plates, centrifuged at 2,100 *g* for 3 minutes at 4 °C, and resuspended in FACS buffer (2% FBS, 100 U/mL penicillin,

100 µg/mL streptomycin, and 2 mM EDTA in PBS lacking Ca^{+2}/Mg^{+2}). Samples were analyzed using a Thermo Attune NxT equipped with 405 nm, 488 nm, 561 nm, and 637 nm lasers. Single cells were analyzed using FlowJo (BD) software. For all samples, debris (FSC-H vs. SSC-A), and doublets (FSC-H vs. FSC-W) were excluded. Flow cytometry data was quantified using the mean fluorescent intensity (MFI; protein synthesis measurements), or median mCherry/GFP ratio (eEF1A degradation reporter), across a single cell population. MFI values were normalized to the vehicle control for an indicated cell line.

CRISPRi screen

CRISPRi screening cells were generated by transducing ternatin-resistant HCT116 eEF1A1 A399V/A399V cells with lentivirus encoding dCas9-HA-NLS-BFP-KRAB. Cells were sorted twice for BFP positivity. The resulting dCas9-containing cells were transduced with the eEF1A FACS reporter (pLX304 Flag-mCherry-eEF1A1_IRES-AcGFP) and were sorted twice for GFP positivity.

Throughout the screen, a minimum of 1000x representation was maintained for sgRNA elements. A sgRNA library targeting elements of the ubiquitin proteasome system (Chen et al, 2019; 9,564 sgRNAs total) was utilized. Several sgRNAs targeting additional eEF1A or RQC-related genes (*EF1A1*, *EF1A2*, *HBS1L*, *PELO*, *NEMF*, *TCF25*, *PUM2*, *PCBP1*) were individually cloned (5 sgRNAs/gene) and added to the library. Lentivirus was generated by transfecting two 15 cm dishes of HEK293T cells each with 9 µg of library, 8 µg of pCMV-dR8.91, and 1 µg of pMD2-G per dish using Mirus Trans-IT LT1 and Alstem ViralBoost. Viral supernatant was collected after two days and filtered. Six 15 cm dishes of CRISPRi screening cells were transduced with all freshly harvested virus, yielding a transduction efficiency of approximately 55% (measured by FACS two days post-transduction). Puromycin selection for sgRNA-containing cells began three days post-transduction and was conducted for 48 hours, with daily

replenishment of media containing 2 µg/mL puromycin. Six days post-transduction, cells were plated into two sets of 8 15 cm dishes (96 million cells per set) for treatment and cell sorting the following day.

Cells at approximately 70% confluency were left untreated or treated for 8 hours with 50 nM ternatin-4. Cells were harvested by trypsinization, resuspended in FACS buffer (2% FBS, 100 U/mL penicillin, 100 µg/mL streptomycin, and 2 mM EDTA in PBS lacking Ca^{+2}/Mg^{+2}), and sorted on a BD FACS Aria II equipped with BD FACSDiva software. Single, BFP positive cells were separated into high, middle, and low thirds based on the calculated ratio of mCherry to GFP for each cell, with approximately 9 million cells collected for each population. Sorted cell populations were washed once with PBS and stored at -80°C until genomic DNA extraction.

Sorted samples were prepared for next-generation sequencing as previously described (Tian et al., 2019). Briefly, genomic DNA was isolated from samples using the Machery-Nagel Blood Midi kit (catalog number 740954.20) according to the manufacturer's instructions. TSS (transcription start site)-specific sgRNA sequences were PCR amplified using all genomic DNA, indexed PCR primers, and 2x Q5 Hot Start PCR Master Mix (NEB M094). In total, approximately 40-55 60 µL PCR reactions were prepared for each sample. PCR products were size-selected using SPRI-select beads to remove PCR primers and genomic DNA, and samples were sequenced using an Illumina HiSeq 4000.

CRISPRi screen analysis

Sequencing data was analyzed as previously described (Kampmann et al., 2013; Tian et al., 2019). Briefly, raw sequencing data was aligned to the reference library sequences using Bowtie, and the number of reads for each sgRNA were counted. Sequencing counts were normalized to the total number of counts within each sequenced sample. Phenotype scores for

each sgRNA were calculated as the $\log_2$ ratio of high mCherry/GFP sequencing counts divided by low mCherry/GFP counts. An epsilon value was calculated by averaging the three most extreme phenotype scores for each transcription start site (TSS). A p value for each TSS was calculated using the Mann-Whitney U test against nontargeting controls. A gene score was calculated for each TSS as the product of the epsilon score and the $-\log_{10}$(p value). Epsilon values, p values, and products for all genes targeted in the library are included in **Supplementary Table 1**.

Individual sgRNA knockdown and rescue

Lentivirus was generated for plasmids encoding individual sgRNAs. CRISPRi reporter cells (ternatin-resistant HCT116 eEF1A1 A399V/A399V expressing Flag-mCherry-eEF1A1_IRES-AcGFP and dCas9-BFP-KRAB) were transduced, and sgRNA-expressing cells were selected three days post-transduction with 2 μg/mL puromycin for 48 hours. For RPS27A knockdown experiments, HeLa CRISPRi cells expressing RPS27A-3xFlag (sorted on the basis of GFP positivity after transduction with RPS27A-3xFlag_IRES-AcGFP), or CRISPRi mCherry-eEF1A reporter cells expressing RPS27A-3xFlag (~50% of cells as judged by iRFP positivity after transduction with RPS27A-3xFlag_IRES-iRFP), were transduced with sgRNA-encoding lentivirus and subjected to puromycin selection as above. For GCN1 rescue experiments, puromycin-selected, sgRNA-containing cells were transfected in 6-well dishes with 1 μg of the indicated GCN1 constructs (1 well/construct) using the manufacturer's protocol for Lipofectamine 2000 (Thermo Fisher).

The resulting cells were plated for experiments (typically 6 days post-transduction) in media lacking puromycin; the next day, cells were treated and analyzed as indicated in figure legends. For FACS-based analyses, cells were plated in 12-well dishes, and for immunoblotting experiments, cells were plated in 6-well dishes. For GCN1 rescue experiments, cells were

plated approximately 24 hours post-transfection. For FACS-based experiments, following gating of debris and doublets, cells were gated on expression of sgRNAs (BFP positivity) and RPS27A or GCN1 (iRFP positivity), as applicable.

RT-qPCR

Cells were collected from 6-well dishes, washed once with cold PBS, and RNA was extracted using the RNeasy Mini Kit (Qiagen). cDNA was synthesized from 1 µg RNA per sample using the High-Capacity cDNA Reverse Transcription Kit (Applied Biosystems). $1/10^{th}$ of each RT reaction was analyzed using Luna Universal qPCR Master Mix (NEB) according to the manufacturer's instructions and a BioRad CFX Touch Real-Time PCR instrument. mRNA abundance was quantified by the $\Delta\Delta C_q$ method, with GAPDH as the reference gene. Primer pairs for endogenous RPS27A or common to endogenous and transgenic RPS27A were designed using Primer Blast (NIH). The GAPDH primer pair was from the Harvard Medical School PrimerBank (PrimerBank ID 378404907c2; Spandidos et al., 2010). Primer sequences were as follows.

RPS27A-endo_fwd: 5'-GGAGCCGCCACCAAAAT-3',
RPS27A-endo_rev: 5'-GCTTGCCAGCAAAGATCAGTC -3',
RPS27A-common_fwd: 5'-AGGCCAAGATCCAGGATAAGG-3',
RPS27A-common_rev: 5'-CACCACCACGAAGTCTCAACA-3',
GAPDH_fwd: 5'-ACAACTTTGGTATCGTGGAAGG-3',
GAPDH_rev: 5'-GCCATCACGCCACAGTTTC-3'

DiGly peptide enrichment

Cells were grown in light (Arg0/Lys0) or heavy (Arg10/Lys8) SILAC DMEM (Thermo Scientific) supplemented with 10% dialyzed FBS, 100 U/mL penicillin,100 µg/mL streptomycin, 80 µM

lysine0 or lysine8, and 40 µM arginine0 or arginine10 for 12 days prior to indicated treatments. Typically, 5-6 15 cm dishes were used per label and treatment condition, yielding approximately 10-15 mg total protein. A label swap was performed as a biological replicate for all experimental conditions. Cells were harvested at room temperature by quickly aspirating media from dishes, rinsing once with ice-cold PBS, and scraping cells into cell lysis buffer (20 mM HEPES pH 8.0, 9 M urea, 1 mM sodium orthovanadate, 2.5 mM sodium pyrophosphate, 1 mM beta-glycerophosphate). Lysates were sonicated using three 15-second bursts from a microtip sonicator, and lysates were clarified by centrifugation at 19,000 *g* for 15 minutes at RT. Cleared lysates were quantified using the BCA method, and equal amounts of heavy and light samples were pooled (20-30 mg total). Samples were reduced with 4.5 mM DTT for 30 minutes at 55 °C. Samples were allowed to cool to room temperature and alkylated with 10.2 mM chloroacetamide for 30 minutes at RT. Lysates were diluted 4-fold with 20 mM HEPES pH 8.0 to a final concentration of approximately 2 M urea, sequencing-grade trypsin (Promega V5113) was added at a 1:300 w/w ratio, and samples were digested by rotating overnight at RT. The next day (approximately 18 hours later), trypsin digestion was stopped by addition of TFA to 1% final concentration. Samples were incubated on ice for 15 minutes and centrifuged at 1,780 *g* for 15 minutes at RT. Peptides were desalted using Waters 500 mg C18 SepPaks (WAT036945). SepPak cartridges were conditioned with 7 mL acetonitrile and equilibrated with 3 sequential washes of 1.4 mL, 4.2 mL, and 8.4 mL Solvent A (0.1% TFA in water) prior to loading of the clarified peptide solution. Peptides were loaded onto columns by gravity flow, and columns were washed 3 times using 1.4 mL, 7 mL, and 8.4 mL Solvent A. Peptides were eluted by 3 sequential additions of 2.8 mL solvent B (0.1% TFA, 40% acetonitrile in water). Samples were frozen and lyophilized for a minimum of 48 hours prior to immunoprecipitation of diGlycine-containing peptides.

Ubiquitin remnant-containing peptides were isolated using the Cell Signaling Technologies PTMScan Ubiquitin Remnant Motif Kit (CST #5562). Lyophilized peptides were collected by centrifugation at 2,000 *g* for 5 minutes at RT and dissolved in 1.4 mL ice-cold Immunoaffinity Purification (IAP) buffer (50 mM MOPS pH 7.2, 10 mM disodium phosphate, 50 mM NaCl). The peptide solution was cleared by centrifugation at 10,000 *g* for 5 minutes at 4 °C. The peptide supernatant was added to a tube containing immunoaffinity beads pre-washed 4x with 1 mL of cold PBS. All centrifugation steps with antibody beads were done at 2,000 *g* for 30 seconds at 4 °C. Immunoprecipitations were performed using a predetermined ratio of 10 mg input protein per 10 µL of antibody bead slurry (Udeshi et al., 2013). Samples were rotated for 2 hours at 4 °C, and subsequently, peptide supernatant was removed from beads. Beads were washed twice with 1 mL ice-cold IAP buffer and 3 times with 1 mL ice-cold HPLC water. Peptides were eluted from beads with two consecutive incubations of 55 µL and 50 µL 0.15% TFA for 10 minutes at RT with gentle agitation every 2-3 minutes. Eluants were desalted using Agilent OMIX C18 tips (A57003100), dried by vacuum concentration, and stored at -80 °C until analysis.

LC-MS/MS data acquisition (DDA)

One half of each sample was resuspended in 10 µL 0.1% FA or 10 µL 0.1% FA containing 2.5 nM eEF1A K385 standard peptide (SGK[diGly]KLEDGPK, with $^{13}C_6$,^{15}N-Leu). One quarter of each reconstituted sample (2.5 µL; 12.5% of total sample) was analyzed on an Orbitrap Fusion Lumos (Thermo Scientific) equipped with an ACQUITY M-Class UPLC (Waters) and an EASY-Spray C18 column (Thermo Scientific #ES800; 75 µm x 15 cm, 3 µm particle size, 100 Å pore size). Solvent A was 0.1% FA in water, and Solvent B was 0.1% FA in acetonitrile. Peptides were loaded onto the warmed column (45 ˚C), and equilibrated with 0% B for 13 min using a flow rate of 600 nL/min, followed by 0-30% B over 120 min at 300 nL/min, 30-80% B over 20 min, 80% B for 5 min, 80%-0% B over 2 min, and 0% B for 10 min with the flow rate changed

back to 600 nL/min. The entire method ran for a total of 170 min. Mass spectra were acquired in data dependent mode. MS1 scans were collected in the orbitrap at a resolution of 120,000, a scan range of 375-1500 m/z, an automatic gain control (AGC) target of 4E5, and a maximum injection time of 50 ms. Ions with a peptide-like isotopic distribution (MIPS set to “peptide”) that exceeded an intensity threshold of 2E4 and contained a charge between 2 and 7 were selected for HCD fragmentation. MS2 spectra of HCD-fragmented peptides were collected using a 1.6 m/z isolation window and an HCD collision energy of 30%. Fragment ions were measured in the orbitrap at a resolution of 30,000 and were collected with an AGC target of 5E4 and a maximum injection time of 100 ms. Peptides selected for fragmentation were dynamically excluded for the following 30 seconds using a 10-ppm window. The maximum duty cycle was set to 3 s.

Mass spectrometric site identification and quantification

The raw data were searched against the human Uniprot database (73,651 entries) using MaxQuant (version 1.6.7.0) with a list of common laboratory contaminants added. ‘Arg10’ and ‘Lys8’ were selected as heavy labels. The digestion enzyme was set to trypsin, a maximum of three missed cleavages were allowed, and the minimum peptide length was set to 7. Cysteine carbamidomethylation was specified as a fixed modification, and N-terminal protein acetylation and methionine oxidation were set as variable modifications. Internal lysine diGlycine modifications, and lysine diGlycine modifications at the protein C-terminus were additionally set as variable modifications. The remainder of the search parameters were left at default settings. Peptide requantification was enabled for calculation of H/L SILAC ratios. DiGly site identifications and normalized SILAC ratios were obtained from the MaxQuant sites file. SILAC ratios were inverted for label swap experiments. Site values were averaged between biological replicates, $\log_2$-transformed, and reported in **Supplementary Table 2**.

PRM analysis of eEF1A K385 ubiquitination

Sample reconstitution and liquid chromatography proceeded identically to DDA preparations (see above). For each cycle of the PRM method, an MS1 scan was first collected with a scan range of 360-1300 m/z, a resolution of 60,000, an automatic gain control (AGC) target of 4E5, and a maximum injection time of 50 ms. Subsequently, targeted MS2 scans were collected for heavy, light, and standard (medium) eEF1A K385 peptides (z = 3; m/z = 399.5614, 391.5472, and 393.8862, respectively). MS2 precursors were fragmented by HCD using a collision energy of 30%. MS2 scans utilized an isolation window of 0.7 m/z, a resolution of 15,000, an AGC target of 1E5, and a maximum injection time of 150 ms. The entire scan cycle was repeated over the entire gradient. Data was analyzed with Skyline using a reference library constructed from previous DDA runs with the same samples. The six most highly ranked (most intense) b or y ions were chosen for generation of extracted ion chromatograms.

Proximity-based ubiquitination assay

Ternatin-resistant HCT116 cells (eEF1A1 A399V/A399V) stably expressing 3xFlag-eEF1A were cultured in DMEM, which does not contain biotin, supplemented with 10% fetal bovine serum. The assay was based on Deshar et al., (2016), with some modifications. Cells were grown to 70% confluency in 10 cm dishes and were co-transfected with 1.8 µg AP-HA-Ub (pcDNA3.1) and 8.8 µg V5-BirA or V5-BirA-RNF (pHR) constructs using the manufacturer's protocol for Lipofectamine 2000. The next day, cells were treated with 50 µM biotin and with DMSO or 50 nM ternatin-4 for 4 h. For analysis of RPS27A ubiquitination, Hela cells stably expressing RPS27A-3xFlag were grown to 70% confluency in 15 cm dishes, co-transfected with 2 ug AP-HA-Ub and 8 ug V5-BirA constructs using the manufacturer's protocol for Lipofectamine LTX, and treated the next day with 50 µM biotin and DMSO or 50 nM ternatin-4 for 1 h.

Following treatment, cells were washed once with ice-cold PBS and collected by scraping into PBS. Cells were centrifuged at 1000 *g* for 3 minutes at 4 °C, and cell pellets were frozen in liquid nitrogen and stored at -80 °C or immediately lysed. Cells were lysed in lysis buffer (50 mM HEPES pH 7.4, 150 mM NaCl, 1% NP-40, 2x Roche EDTA-free protease inhibitors, and 50 mM chloroacetamide) and lysate was cleared by centrifugation at 16,100 *g* for 10 minutes at 4 °C. SDS was added to supernatants to 1% final concentration, and samples were boiled for 10 minutes. Denatured lysates were quantified by the Bradford method, normalized, and diluted 10-fold in lysis buffer. Diluted lysates were filtered through 0.45 µm SFCA syringe filters (Thermo Scientific) and were added to tubes containing streptavidin magnetic beads (Pierce; 40 µL beads per 1 mg protein). Samples were rotated for 2 hours at 4 °C. Supernatants were removed from beads, and beads were washed twice with wash buffer 1 (50 mM HEPES pH 7.4, 150 mM NaCl, 1% NP-40, 0.1% SDS), and twice with wash buffer 2 (50 mM HEPES pH 7.4, 500 mM NaCl, 1% NP-40). Bound proteins were eluted by boiling beads for 10 minutes in elution buffer (50 mM HEPES pH 7.4, 150 mM NaCl, 1% NP-40, 5 mM biotin, and 1x SDS loading buffer). 10 µg of input protein (typically < 3% total input protein) and 40% of eluants were loaded on 7.5% gels and analyzed by immunoblotting.

Co-immunoprecipitations

For GCN1-3xFlag immunoprecipitations, HEK293T cells growing in a 15 cm dish at approximately 70% confluency were transfected with 8 µg plasmid (pLenti6.3) using Lipofectamine 2000. The next day, cells were split between two 15 cm dishes. Cells were treated approximately 48 hours post-transfection. For 3xFlag-RNF14 or RNF25 immunoprecipitations, HeLa cells stably expressing the indicated construct were were grown to approximately 70% confluency and treated in 10 cm dishes.

Cells were harvested by scraping into ice-cold PBS and centrifuged at 1000 *g* for 3 minutes at 4 °C. Unless otherwise indicated, cells were crosslinked as described by Shi et al., (2017), as follows: cells were resuspended in 1 mL PBS containing 0.1% PFA (Electron Microscopy Sciences) and were rotated for 10 minutes at room temperature; crosslinking was stopped by addition of 100 µL quench solution (2.5 M glycine, 25 mM Tris pH 7.4), and cells were centrifuged at 1000 *g* for 3 minutes at 4 °C. Cells were lysed in lysis buffer (50 mM HEPES pH 7.4, 100 mM KOAc, 5 mM $Mg(OAc)_2$, 0.1% NP-40, 40 U/mL RNAse inhibitor (NEB), 2x Roche EDTA-free protease inhibitors, and 50 mM chloroacetamide) for 5 minutes on ice, and lysates were cleared by centrifugation at 15,000 *g* for 10 minutes at 4 °C. Lysates were quantified by the Bradford method and normalized. Samples were added to tubes containing Flag M2 magnetic beads (Sigma) and rotated for 1 hour at 4 °C. For GCN1-3xFlag IPs, 40 µL bead slurry was used per 1 mg protein, and for 3xFlag-RNF14 and RNF25 IPs, 20 µL bead slurry was used per 1 mg protein. After binding, supernatants were removed and beads were washed 3 times using wash buffer (50 mM HEPES pH 7.4, 100 mM KOAc, 5 mM $Mg(OAc)_2$, 0.1% NP-40). Two sequential elutions were performed by incubating 200 µg/mL 3xFlag peptide in wash buffer with rotation for 30 minutes at 4°C. 10 µg input protein (typically < 2% total input protein) and 40% of IP eluates were loaded onto 4-12% Bis-Tris gradient gels (Invitrogen) and analyzed by immunoblotting.

Sucrose density gradient ultracentrifugation

HeLa cells were grown to approximately 80% confluency in 15 cm dishes prior to treatment. Cells were harvested by scraping into ice-cold PBS and were centrifuged at 1000 *g* for 3 minutes at 4 °C. Cells were lysed (50 mM HEPES pH 7.4, 100 mM KOAc, 15 mM $Mg(OAc)_2$, 0.1% NP-40, 5 U/mL Turbo DNAse (Invitrogen), 20 U/mL SUPERaseIn (Invitrogen), 2x Roche EDTA-free protease inhibitors, and 50 mM chloroacetamide) for 5 minutes on ice. For samples intended for nuclease digestion, SUPERaseIn was omitted from the lysis buffer. Lysates were

cleared by centrifugation at 15,000 *g* for 10 minutes at 4 °C, and supernatants were normalized based on NanoDrop (Thermo Scientific) readings at 260 nm (typically 60 – 120 µg RNA). Where indicated, RNA was digested as follows: $CaCl_2$ was added to a final concentration of 1 mM, 20 U micrococcal nuclease (Roche) was added per 40 µg RNA, and samples were shaken (500 rpm) on a Thermomixer for 45 minutes at RT. Digestion was quenched by adding EGTA to a final concentration of 2 mM, and 12 U SUPERaseIn was added per 40 µg RNA.

Prepared samples were layered onto 10-50% sucrose gradients for polysome analysis, and 10-40% or 10-50% gradients for analysis of nuclease-digested samples, as indicated. All gradients were composed of 50 mM HEPES pH 7.4, 100 mM KOAc, and 15 mM $Mg(OAc)_2$, and were formed using a Biocomp Gradient Station. Samples were resolved by ultracentrifugation through gradients using an SW-41 rotor (Beckman Coulter) spun at 4 °C for 3 hours at 35,000 rpm. Samples were fractionated (typically 930 µL per fraction) and absorbance at 260 nm was monitored using a Biocomp fractionator and a Triax flow cell. Equal amounts of each fraction (typically 10 µL) were loaded onto 4-12% Bis-Tris gradient gels (Invitrogen) and analyzed by immunoblotting.

Chapter 2: Identification of additional RNF14/RNF25 activators and substrates

Abstract

Ribosomes may pause or stall due to a growing list of innate and environmental stressors. We recently reported that ternatin-4, which traps eEF1A/aa-tRNA at the ribosome A site, promotes eEF1A degradation through the E3 ligases RNF14 and RNF25 and the collision sensor GCN1. It is unclear if this pathway is activated by additional stimuli, or if it recognizes additional A site factors. Here we investigate the susceptibility of the eEF1A isoforms, eEF1A1 and eEF1A2, to ternatin-induced degradation, and find that eEF1A2 is degraded with enhanced kinetics. Leveraging quantitative proteomics datasets, we find that the translational GTPase DRG1 is also a substrate for RNF14/RNF25, and that the RNF14/RNF25 pathway is additionally activated by ultraviolet light. In the presence of the small-molecule SRI-41315 or when inhibited by a hydrolysis-deficient AAQ mutation, the translation termination factor eRF1 is likewise degraded by RNF14/RNF25. SRI-41315 and ternatin-4 each elicit K6-linked ubiquitination of GCN1 and the corresponding translation factor, suggesting common features of pathway activation. Deeper investigation of the mechanisms of pathway activation for each stress/substrate pair is an exciting question for future work.

Introduction

During protein synthesis, multiple factors access the ribosome A site. In the final step of initiation, the GTPase eIF5B binds the 40S A site, promoting subunit joining with the 60S. In yeast, GTP hydrolysis by eIF5B was proposed to gate the transition from initiation to elongation (Jackson et al., 2010; Wang et al., 2019). During translation elongation, the eEF1A/GTP/aa-tRNA ternary complex binds the A site, delivering the amino acids necessary for the growing nascent chain. After peptide bond formation, the GTPase eEF2 binds to the A site, promoting translocation of the peptidyl-tRNA to the P site and resetting the ribosome for another cycle of aa-tRNA selection (Dever et al., 2018). When a stop codon is reached, translation termination begins with the recruitment of the eRF3 GTPase, in complex with eRF1. eRF1 facilitates stop

codon recognition, promoting GTP hydrolysis and dissociation of eRF3 from the ribosome. The ATPase ABCE1 subsequently binds eRF1, promoting ribosome splitting (Hellen, 2018).

In addition to these “canonical” A site binding factors, a number of additional proteins access the ribosome A site. eEF1A possesses two isoforms, eEF1A1, which is nearly ubiquitously expressed in human tissues, and eEF1A2, which, following a transition from eEF1A1 expression during development, is expressed in the heart, brain, and skeletal muscle (Khalyfa et al., 2001). A number of additional translational GTPases exist (Leipe et al., 2002), several with documented ability to bind the ribosome A site. A related GTPase, eEFSec, is uniquely responsible for delivery of selenocysteine-tRNA to UGA stop codons upstream of a mRNA selenocysteine insertion sequence (Gonzalez-Flores et al., 2012; Simonović and Puppala, 2018). The GTPase HBS1L, in complex with Pelota, binds in the empty ribosome A site of a stalled ribosome, leading to the recruitment of ABCE1 to promote ribosome splitting. Similar to HBS1L, the proteins GTPBP1 and GTPBP2 are expressed in many eukaryotes and are thought to also participate in ribosome surveillance (Ishimura et al., 2014; Zinoviev et al., 2018). Recently, the yeast translational GTPase Rbg2 (DRG2 in humans), was identified at the GTPase-associated center (GAC) of the leading ribosome in a Gcn1-bound disome unit (Pochopien et al., 2021). The related yeast GTPase Rbg1 (DRG1 in humans) was similarly found to bind the GAC of 80S ribosomes (Zeng et al., 2021), although the precise roles of these factors during translation is unclear.

We recently described the mechanism for degradation of the translation elongation factor eEF1A, when trapped in a pre-accommodated state at the ribosome by ternatin-4. Two E3 ligases, RNF14 and RNF25, as well as the ribosome collision sensor GCN1, are required for eEF1A degradation. Given the complexity of this degradation mechanism, it is likely this pathway evolved to sense additional translation pausing or stalling events at the ribosome A site. Identification of additional cues for eEF1A degradation, or additional substrates of RNF14/RNF25, may provide further insight into the physiological basis for this pathway.

Apart from eEF1A inhibitors and the mechanistically related bacterial inhibitor kirromycin, there are relatively few known inhibitors that directly target A site translation factors, either at the ribosome or freely in solution. In bacteria, EF-Tu is also targeted by pulvomycin and GE2270A, which prevent aa-tRNA binding and thus inhibit translation (Parmeggiani et al., 2006). The natural product sordarin inhibits fungal, but not mammalian, eEF2 by trapping eEF2 in a post-translocation state at the ribosome (Dmitriev et al., 2020; Shao et al., 2022; Spahn et al., 2004). An unrelated molecule, bouvardin, is thought to similarly trap eEF2 at the ribosome and is active in human cells (Stickel et al., 2015). Small molecule-induced degradation of the termination factor eRF3 has been reported via the cereblon ligands CC-885 and CC-90009, which have been evaluated for their therapeutic potential against acute myeloid leukemia (Matyskiela et al., 2016; Surka et al., 2021) and other cancers. More recently, a small molecule, SRI-41315, was reported to cause degradation of the eRF3 binding partner, eRF1 (Sharma et al., 2021), but not eRF3. eRF1 degradation was shown to be proteasome-dependent, although a mechanism for how this compound promotes degradation was not proposed. SRI-41315-induced eRF1 degradation holds therapeutic potential by promoting readthrough of disease-causing premature stop codons, with a proof of concept demonstrated in the *CFTR* gene.

In addition compounds that interact with the A-site translation machinery, translation stressors may provide hints to activators of RNF14/RNF25. Loss of RNF25 was shown to sensitize cells to the alkylating agent methyl methansulfonate (MMS), and not other DNA damaging agents (Hundley et al., 2021). In addition to DNA damage, MMS also damages RNA, eliciting translation stress and activating the integrated stress response and Hel2-driven ribosome quality control in yeast (Yan and Zaher, 2021; Yan et al., 2019). In yeast, oxidative stress causes ribosome stalling in a pre-translocation state in part through K63-linked ubiquitination of the ribosome P stalk, which prevents eEF2 binding (Zhou et al., 2020). Stalled ribosomes result from multiple additional stresses, including heat shock, nascent chain misfolding agents, ultraviolet (UV) irradiation, nutrient deprivation, and arsenite (Bartok et al.,

2020; Darnell et al., 2018; Knutsen et al., 2015; Liu et al., 2013; Moon et al., 2020; Shalgi et al., 2013; Shenton et al., 2006; Wu et al., 2019). Collectively, drawing from this list of translation factors, inhibitors, and stresses, we set out to identify additional instances of RNF14/RNF25 activity.

Results

eEF1A isoform 2 displays faster degradation kinetics relative to isoform 1

In eukaryotes, eEF1A is encoded by two separate genes, termed isoform 1 and isoform 2. eEF1A1 and eEF1A2 share over 90% protein similarity. Expression of eEF1A2 is restricted to the heart, skeletal muscle, and brain, which largely consist of non-proliferating cells and switch from eEF1A1 expression earlier in development. By contrast, eEF1A1 is otherwise ubiquitously expressed (Khalyfa et al., 2001). Perturbations to eEF1A2 have been linked to cancer and neurodevelopmental disorders. Overexpression of eEF1A2, but not eEF1A1, has been noted in some ovarian cancers, and introduction of an eEF1A2 transgene into NIH3T3 cells accelerated cell proliferation and colony formation (Anand et al., 2002). Hyper-methylation of eEF1A Lys55 by METTL13 has been linked to cancer cell proliferation through an increase in GTPase activity and global translation, although an isoform-specific contribution was not assessed (Liu et al., 2019). Heterozygous mutations to eEF1A2 (G70S, E122K, and R266W, among others) have been identified in patients displaying epilepsy and intellectual disability, although whether this is a result of loss of function or toxic gain of function is unclear (Carvill et al., 2020; Lam et al., 2016). Purified eEF1A1 has been shown to have a slightly higher affinity for GTP vs. GDP (0.82), whereas eEF1A2 has a higher affinity for GDP vs. GTP (1.50). However, both isoforms had equivalent GTP hydrolysis rates and promoted equivalent levels of protein synthesis (Kahns et al., 1998).

We assessed ternatin-induced degradation of eEF1A1 and eEF1A2 across four different cell lines (**Figure 2.1A**), of which MCF7 and HCT116 cells expressed higher levels of eEF1A2

relative to HEK293T and HeLa cells. Following 20 h treatment with ternatin-4, eEF1A2 was dramatically decreased relative to eEF1A1, suggesting unequal rates of ternatin-induced degradation between the two isoforms. To confirm that this result does not reflect a trivial difference in eEF1A1 and eEF1A2 half-lives, we leveraged our mCherry-linked FACS reporter assay in ternatin-resistant HCT116 cells, in which global translation should be unaffected by

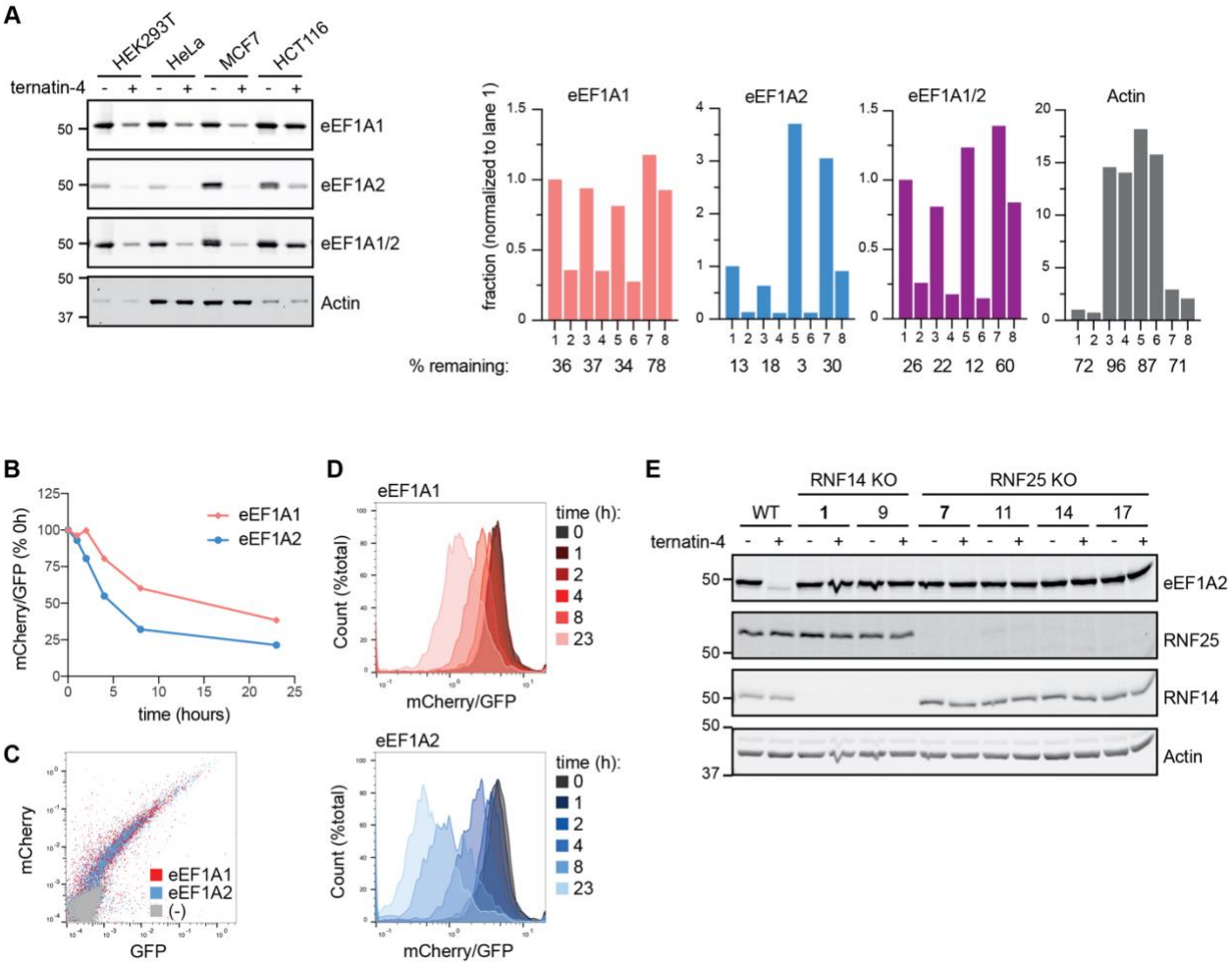

Figure 2.1: Ternatin-4 promotes more rapid degradation of eEF1A isoform 2.
(**A**) HEK293T, HeLa, MCF7, and HCT116 cells were treated for 20 h with ternatin-4. Separate membranes were probed for eEF1A1 and eEF1A2. (**B**) mCherry-eEF1A2 is degraded more rapidly than mCherry-eEF1A1. Ternatin-resistant HCT116 cells were transduced with either construct and treated with ternatin-4 for the indicated times. Median mCherry/GFP levels were normalized to 0 hours for the given construct. (**C**) Scatter plot depicting mCherry-eEF1A and GFP. eEF1A1 and eEF1A2 are expressed at identical steady-state levels. (**D**) mCherry/GFP histograms for transduced (GFP+) cells. (**E**) RNF14 and RNF25 KO cells were generated from ternatin-resistant HCT116 cells. Individual KO clones were treated with ternatin-4 for 8 h.

ternatin-4 treatment. Although both proteins were similarly expressed under steady-state levels, eEF1A2 levels diminished more rapidly following ternatin-4 treatment, with approximately 30% eEF1A2 remaining after 8 hours, compared to 60% eEF1A1 remaining (**Figure 2.1B-D**). Interestingly, a lag was observed in mCherry-eEF1A1 degradation between 0 and 2 hours of ternatin-4 treatment (**Figure 2.1B**). This may be caused by competition between endogenous wild type eEF1A2 and mCherry-eEF1A1, either for ribosome binding or limiting RNF14. Utilizing our ternatin-resistant HCT116 cells (eEF1A1 A399V), we generated CRISPR KO cells lacking RNF14 and RNF25, confirming that eEF1A2 is a bona fide substrate of this pathway (**Figure 2.1E**).

The GTPase DRG1 is directly ubiquitinated by RNF14

The developmentally regulated GTPase family is conserved in eukaryotes and archaea and has two eukaryotic paralogs, DRG1 and DRG2 (Rbg1 and Rbg2 in yeast), with relatively unknown functions (Westrip et al., 2021). These proteins were initially discovered in a search for genes that were expressed during development of the mouse central nervous system but downregulated in adults (Kumar et al., 1992). Both DRG1 and DRG2 are expressed across most tissues (Sazuka et al., 1992; Westrip et al., 2021). A recent study identified DRG1 mutations in patients from three families who exhibited neurodevelopmental disorders, likely due to reduced DRG1 protein levels (Westrip et al., 2022).

DRG1 and DRG2 are highly similar (57% in humans); however, they exhibit distinct properties in cells. Each protein possesses a GTPase domain, a helix-turn-helix (HTH) domain, a ribosomal protein S5 like domain (S5D2L), and a TGS domain (Westrip et al., 2021). Rbg1 and Rbg2 both interact with the ribosome A site via the S5D2L domain (Pochopien et al., 2021; Zeng et al., 2021). Each GTPase has a dedicated binding partner, DFRP1 (DRG family regulatory protein 1, also known as ZC3H15) for DRG1, and DFRP2 for DRG2. In the absence of their regulatory subunit, DRG1 and DRG2 are unstable and are degraded (Ishikawa et al.,

2005). Both DFRPs interact similarly with the corresponding DRG through interactions with the GTPase and TGS domains (Francis et al., 2012; Pochopien et al., 2021; Zeng et al., 2021). Apart from the DFRP domain, DFRP1 and DFRP2 differ substantially and direct distinct cellular roles for DRG1 and DRG2. Of note, DFRP2, also known as RWDD1 (Gir2 in yeast), possesses an RWD domain. Under overexpression conditions, the Gir2 RWD domain competes with Gcn2 for Gcn1 binding and dampens the Gcn2 axis of the integrated stress response (Castilho et al., 2014). In yeast and human cells, DRG1 constitutively associates with polysomes, while DRG2 does not (Westrip et al., 2021).

Recent work has begun to elaborate on the functions of these factors. While single or double knockout of Rbg1 and Rbg2 had no effect on growth in yeast, triple knockout of Rbg1, Rbg2, and the RQT complex member Slh1 (ASCC3 in humans) impaired cell growth and caused ribosomes to shift from polysome to 80S monosome fractions (Daugeron et al., 2011). Consistent with a role in translation, both DRG1 and DRG2 were recently shown to co-immunoprecipitate with the ribosome-associated chaperone HSPA14 and DNAJC2 (Piette et al., 2021).

Further insight into these proteins has been gained at a molecular level. A cryoEM structure of a Gcn1-bound disome unit revealed density for Rbg2 at the GTPase-associated center of the leading ribosome (Pochopien et al., 2021). Rbg2 connected to Gcn1 through its regulatory protein Gir2, which bound Gcn1 through its RWD domain. The leading ribosome was found in an unrotated, pre-translocation conformation, with eIF5A in the ribosome E site and peptidyl-tRNA in the ribosome A site. The authors speculated that slowed translation, perhaps due to difficulty in peptide bond formation, may recruit the Gcn1/Gir2/Rbg2 complex, allowing Rbg2 to promote peptide bond formation and thus continued translation, in lieu of more drastic action by the integrated stress response kinase Gcn2. An additional study found that Rbg1 also

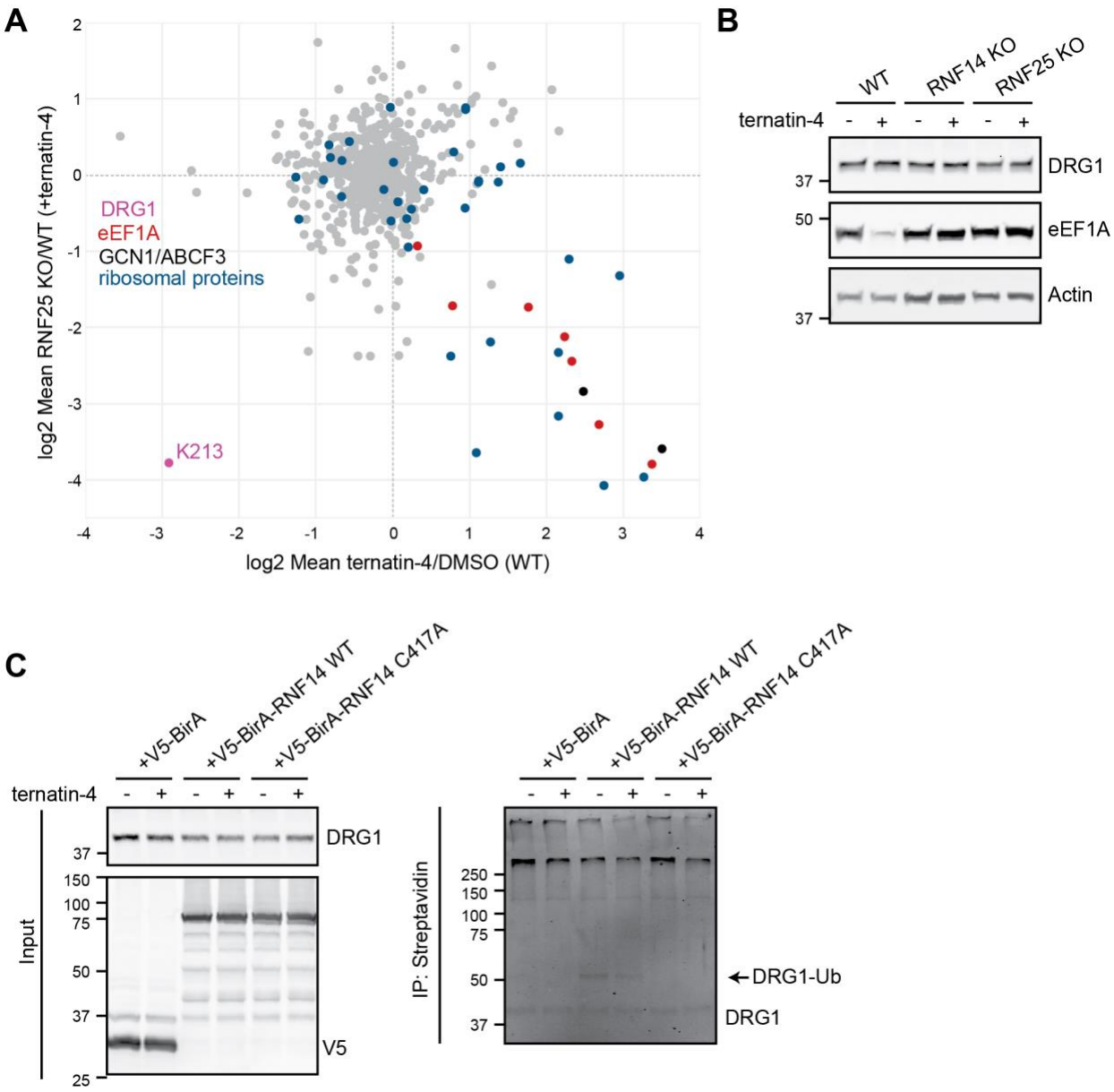

Figure 2.2: The GTPase DRG1 is directly ubiquitinated by RNF14.
(**A**) DRG1 ubiquitination at K213 is reduced by ternatin-4 treatment and is RNF25 dependent. Ternatin-induced ubiquitination sites (x-axis) and RNF25-dependent ubiquitination sites (y-axis) identified by SILAC proteomics in **Figure 1.5** are depicted. HeLa WT cells were treated with ternatin-4 or DMSO for 4 h to measure the extent of ubiquitination site induction, and HeLa WT and RNF25 KO cells were both treated with ternatin-4 to measure RNF25 dependence. (**B**) Steady-state DRG1 levels are not modulated by RNF14 or RNF25. HeLa WT, RNF14 KO, or RNF25 KO cells were treated with ternatin-4 for 20 h, and DRG1 levels were analyzed by immunoblotting. (**C**) Endogenous DRG1 is directly ubiquitinated by RNF14. HEK293T cells were co-transfected with the indicated BirA constructs and AP-HA-Ub. Cells were treated 2 h with ternatin-4 and biotin, lysed, and biotinylated products were enriched.

binds at the GTPase-associated center, and that knockout of Rbg1 leads to an increase of ribosome stalls at lysine- and arginine-rich coding sequences. Interestingly, the ribosome was also found in the pre-translocation state, with peptidyl-tRNA in the A site and eIF5A in the ribosome E site (Zeng et al., 2021).

During our study of ternatin-induced and RNF14/RNF25-dependent ubiquitination sites, we consistently identified a peptide corresponding to DRG1 ubiquitinated at Lys213, which resides in the S5D2L domain (**Supplementary Table 2**). Ubiquitination at this site decreased 4-8 fold after ternatin-4 treatment, and we observed a further >8-fold decrease in ternatin-treated RNF25 KO cells, relative to ternatin-treated WT HeLa cells (**Figure 2.2A**). These results suggest that under steady state conditions, DRG1 is constitutively ubiquitinated. Although DRG1 ubiquitination decreases under conditions where the RNF14/RNF25 pathway is activated, paradoxically, ubiquitination also requires this pathway. One likely explanation for these results is that DRG1 may compete with eEF1A for ribosome binding and ubiquitination, with the latter dominating in the presence of ternatin-4. We investigated the effect of RNF14 or RNF25 on steady state DRG1 levels and observed no change in untreated or ternatin-treated cells (**Figure 2.2B**). Thus, DRG1 ubiquitination may occur with low stoichiometry, or function as a regulatory mark rather than a signal for degradation.

While we were not able to detect the K213 ubiquitination site in our proteomics experiments with RNF14 KO cells, we hypothesized that by analogy to eEF1A ubiquitination, RNF14, rather than RNF25, would likely mediate DRG1 ubiquitination. To determine if DRG1 ubiquitination is a direct consequence of RNF14 activity, we turned to our BirA assay. Enrichment of biotinylated proteins from cells cotransfected with AP-HA-Ub and BirA-RNF14 revealed a single faint band corresponding to mono-ubiquitinated endogenous DRG1 (**Figure 2.2C**). This band was reduced in the presence of ternatin-4 and was absent in cells expressing C417A BirA-RNF14 or isolated BirA. Thus, DRG1 may represent the first constitutive substrate

identified for RNF14. Under ternatin-4 treatment conditions, the ribosome A site is likely saturated with eEF1A/aa-tRNA, preventing DRG1 ubiquitination.

RNF14 and RNF25 promote degradation of the termination factor eRF1

In addition to ternatin-mediated eEF1A stalls, the RNF14/RNF25 pathway may monitor other translation factors at the A site, including DRG1. Interestingly, a synthetic small molecule, SRI-41315, was recently shown to induce degradation of the termination factor eRF1, while eRF3 was unaffected. While a mechanism for degradation was not proposed, eRF1 depletion resulted in enhanced stop codon readthrough, suggesting a potential therapeutic use for SRI-41315 (Sharma et al., 2021). We hypothesized that SRI-41315 might impair eRF1 functions during translation termination and thus activate the RNF14/RNF25 pathway. Consistent with the previous report (Sharma et al., 2021), treatment of HeLa cells with SRI-41315 for 20 h resulted in a dramatic loss of eRF1. Strikingly, eRF1 degradation was completely prevented in RNF14 KO or RNF25 KO cells and rescued by reintroduction of the corresponding E3 ligase (**Figure 2.3A**). SRI-41315 was previously reported to have no effect on eRF3 levels, although ABCE1 levels were not examined (Sharma et al., 2021). In our experiments, we noted no significant reduction to ABCE1 following 20 h treatment. Examination of eRF1 levels at early time points in WT cells revealed an increase in a faint, higher molecular weight band suggestive of ubiquitinated eRF1 (**Figure 2.3B**). Simultaneous treatment with SRI-41315 and either cycloheximide or homoharringtonine prevented eRF1 degradation (**Figure 2.3C**), demonstrating a requirement for active translation.

To test directly whether impaired eRF1 activity is sufficient to promote RNF14-dependent degradation, we took advantage of a catalytically inactive eRF1 variant in which the conserved GGQ motif is mutated to AAQ. Such eRF1 mutants can recognize stop codons in the A site (Brown et al., 2015; Shao et al., 2016), but they fail to catalyze peptidyl-tRNA hydrolysis, thus promoting ribosome collisions (Juszkiewicz et al., 2018; Yan and Zaher, 2021). RNF14 KO

or rescue cells were stably transduced with Flag-tagged WT or mutant eRF1 linked to an IRES-GFP and analyzed by flow cytometry. In RNF14 rescue cells, steady-state levels of Flag-eRF1-AAQ were drastically reduced compared to WT Flag-eRF1 (**Figure 2.3D**). By contrast, there was no apparent difference between WT and mutant eRF1 levels in RNF14 KO cells. Similar results were obtained by immunoblotting for WT and mutant Flag-eRF1 (**Figure 2.3E**).

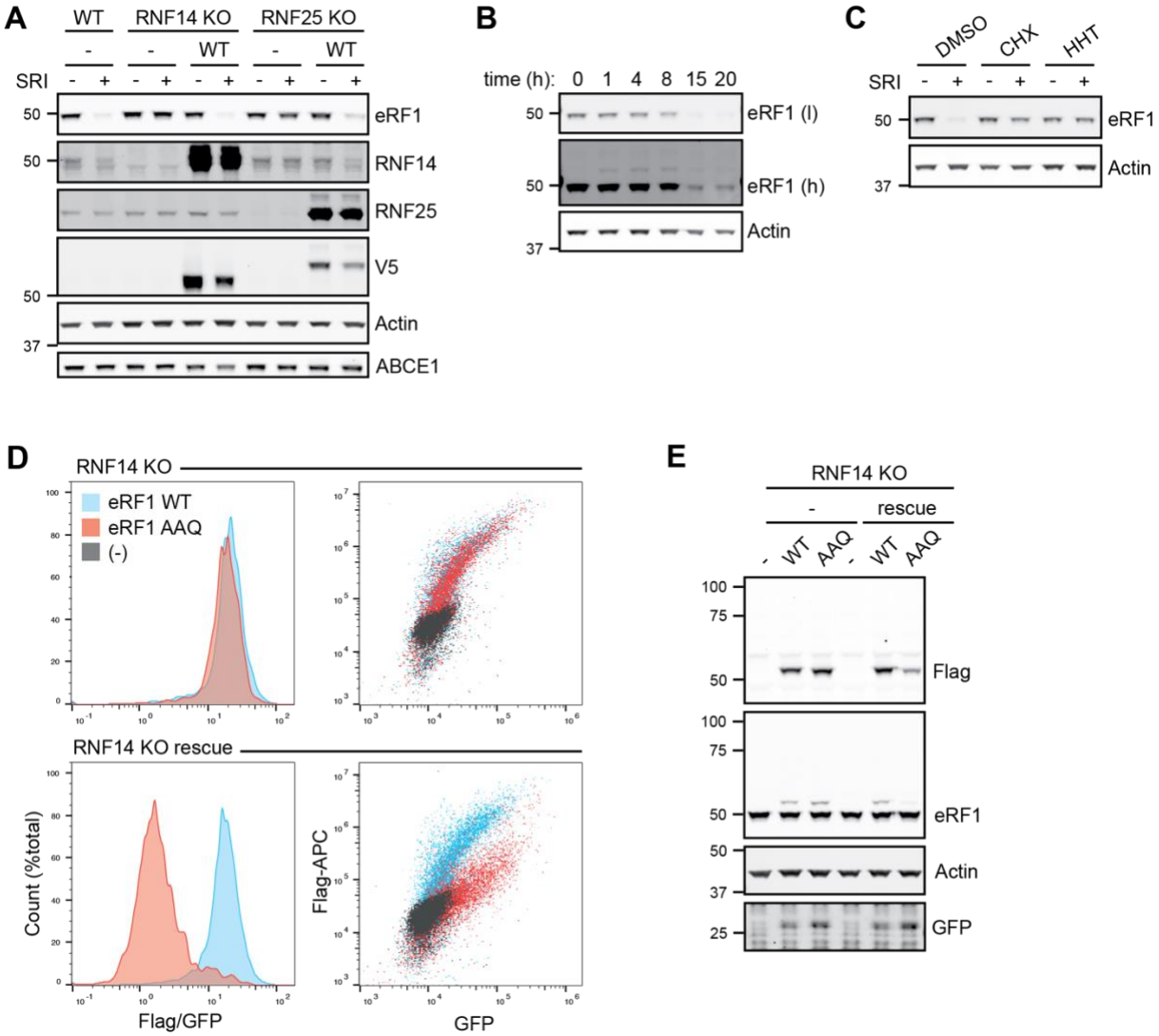

Figure 2.3: RNF14 and RNF25 promote degradation of the termination factor eRF1. (**A**) HeLa WT, KO, or rescue cells (**Figure 1.3E**) were treated ± 10 μM SRI-41315 for 20 h. (**B**) HeLa WT cells were treated with SRI-41315 for the indicated times. (**C**) HeLa WT cells were treated with SRI-41315 in the presence or absence of CHX or HHT for 20 h. (**D**) HeLa RNF14 KO or rescue cells were transduced with constructs containing WT or AAQ 3xFlag-eRF1 and IRES-GFP. Cells were fixed, permeabilized, stained with anti-Flag-APC, and analyzed by flow cytometry. GFP-positive cells are displayed in mCherry/GFP histograms. (**E**) Cells as in part (**D**) were analyzed by immunoblotting.

Collectively, our data suggest that the RNF14/RNF25 pathway can monitor the ribosomal A site during translation termination, promoting degradation of stalled eRF1.

Ultraviolet irradiation triggers RNF14-dependent ubiquitination of eEF1A and the ribosome

While inhibitor-mediated stalls provide a valuable tool to study the RNF14/RNF25 pathway, its physiological role, and the innate or environmental stalls it may sense, remains a major outstanding question. During our study of ternatin-induced, RNF14/RNF25-dependent ubiquitination sites (**Figure 1.5**), we noted that many of the same sites are also induced by UV irradiation, as revealed by a previously published dataset (**Figure 2.4A**) (Elia et al., 2015).

We performed a diGly SILAC-MS experiment comparing UV-irradiated RNF14 KO vs. rescue cells. UV-induced ubiquitination of eEF1A K392 and ribosomal protein sites (e.g., RPLP1 K92/K93, RPLP0 K264, and RPL12 K48) was diminished in the absence of RNF14 (**Figure 2.4B**), whereas ubiquitination of DNA damage response proteins (e.g., FANCI K523, XPC K174, and PCNA K164) was unaffected (**Supplementary Table 2**). Interestingly, similar to our observations with ternatin-4 treatment, DRG1 ubiquitination at K213 was also reduced by UV irradiation. This dataset revealed additional ubiquitination sites at DRG1 K126 and K159, which reside in the GTPase domain. Combined with our experiments with ternatin, which identified K213 as an RNF25-dependent ubiquitination site, this result strongly suggests that DRG1 ubiquitination is dependent on both RNF14 and RNF25 activity. We additionally noted an approximately 3-fold increase in ubiquitination at K397 of the ribosome splitting factor ABCE1, which was likewise diminished by RNF14 KO. These data indicate that UV irradiation, an environmental stressor that induces ribosome collisions via photo-damaged mRNA (Wu et al., 2020), can also activate the RNF14/RNF25 pathway. Recovery of cells after UV irradiation revealed no change in eEF1A levels (**Figure 2.4C**), suggesting UV-mediated stalls likely occur with much lower frequency compared to ternatin-induced stalls.

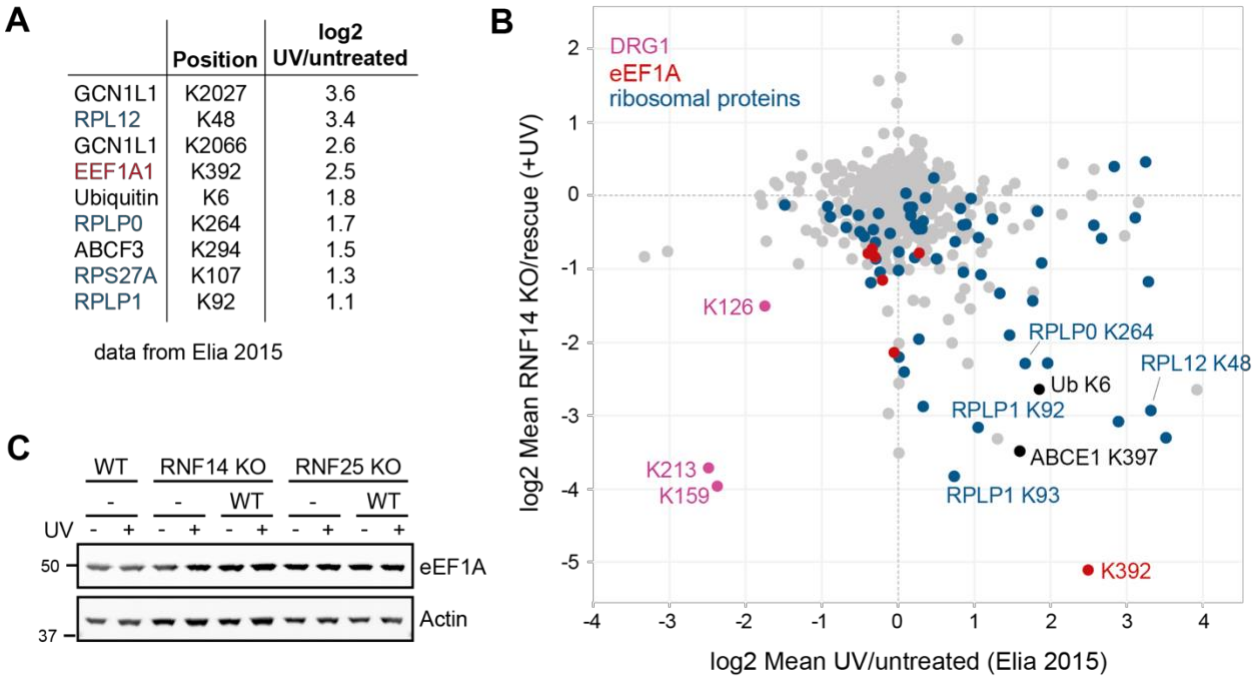

Figure 2.4: Ultraviolet irradiation triggers RNF14-dependent ubiquitination of eEF1A and the ribosome.
(**A**) Published SILAC diGly proteomics data (Elia et al., 2015) derived from HeLa cells irradiated with UV light (40 J/m^2) and then allowed to recover for 1 h. UV-induced diGly sites (log_2 SILAC ratio >1) also induced by ternatin-4 are tabulated (UV/untreated, mean of 3 replicates). (**B**) Comparison of UV-induced ubiquitination sites (Elia et al., 2015) and ubiquitination sites from HeLa RNF14 KO and rescue cells both irradiated with UV light (40 J/m^2) and allowed to recover for 1 h. Data from Elia et al. are shown as the log_2 UV/untreated ratio from the mean of three biological replicates. RNF14 KO vs. rescue data are shown as the log_2 (KO/rescue) ratio from the mean of three technical replicates. (**C**) eEF1A levels are unaffected following overnight recovery from UV irradiation. HeLa WT, KO, and rescue cells from **Figure 1.3** were irradiated with UV light (40 J/m^2) and allowed to recover for 20 h.

RNF14 and RNF25 promote K6-linked ubiquitination of multiple factors in response to cellular stress

Across our diGly proteomics experiments employing both ternatin-4 and ultraviolet irradiation, we noted a striking increase in K6-linked ubiquitin, but not other ubiquitin linkage types (**Figure 2.5A** and **Supplementary Table 2**). RNF14 overexpression stimulated K6-linked ubiquitination to a greater extent than in WT cells, while comparison of KO and WT cells revealed a similar dependence of K6-linked ubiquitination on both RNF14 and RNF25. Although increased K6-linked polyubiquitination was previously observed in response to UV irradiation or

p97/VCP inhibitors (Elia et al., 2015; Heidelberger et al., 2018), the specific functions of this linkage type remain poorly understood.

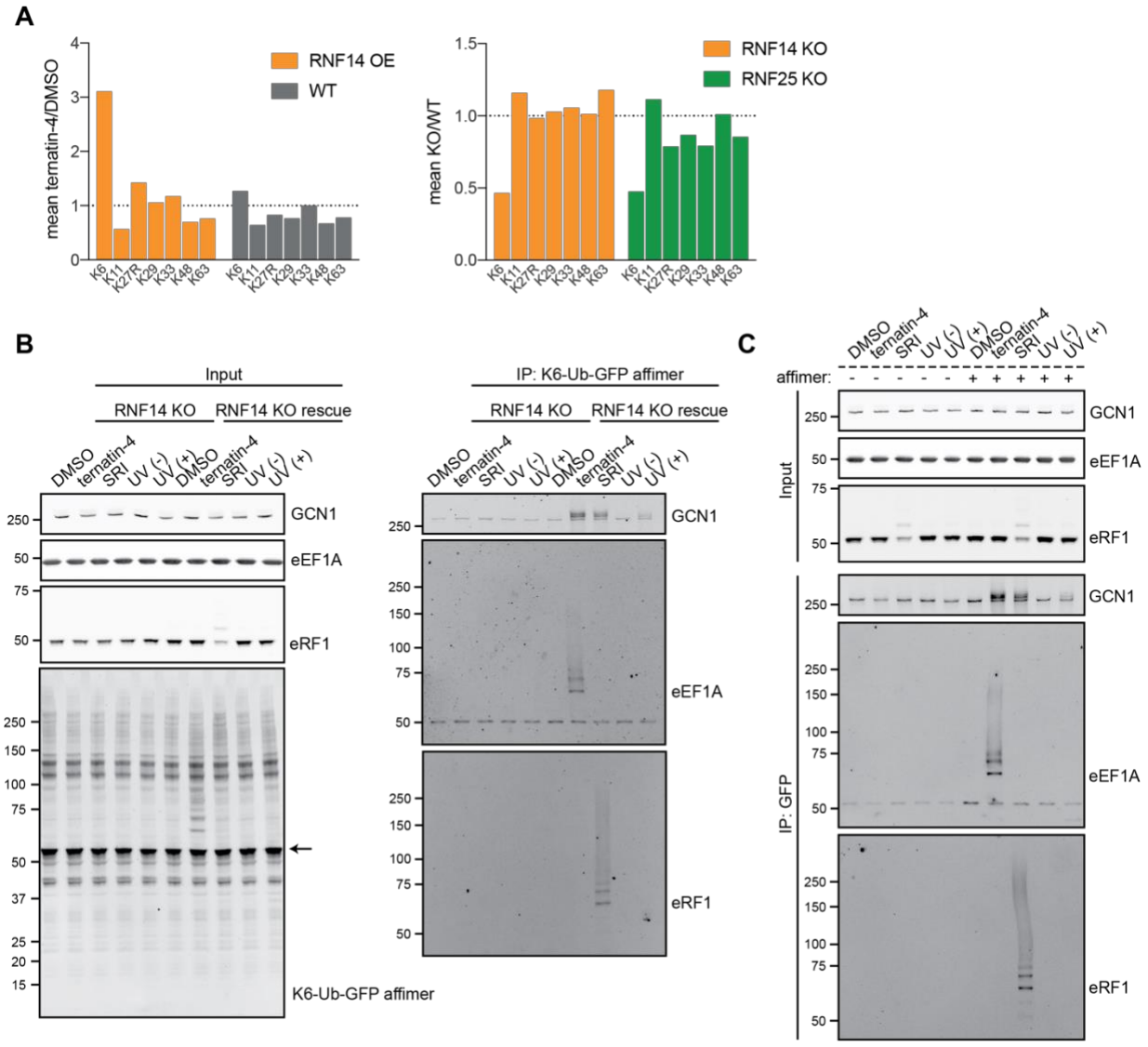

Figure 2.5: RNF14 and RNF25 promote K6-linked ubiquitination of multiple factors in response to cellular stress.
(**A**) SILAC ratios for ubiquitin linkages from the experiments in **Figure 1.3**. Ubiquitination site induction was measured following treatment with ternatin-4 or DMSO for 4 h. RNF dependence was measured in HeLa WT and RNF14 KO or RNF25 KO cells both treated with ternatin-4. (**B**) HeLa RNF14 KO or rescue cells were treated with DMSO, ternatin-4, or SRI-41315 for 1 h, or were irradiated ± 40 J/m^2 UV and allowed to recover for 1 h. Cell lysates were incubated with a GFP-conjugated affimer for K6-linked ubiquitin, and bound species were enriched using a GFP nanobody. (**C**) HeLa RNF14 KO rescue cells were treated as in (**B**). Cell lysates were incubated with or without a GFP-conjugated affimer for K6-linked ubiquitin, and bound species were enriched using a GFP nanobody.

We leveraged a recently described affimer specific to K6-ubiquitin (Michel et al., 2017) to measure this linkage in RNF14 KO and rescue cells treated with ternatin-4, SRI-41315, or UV for 1 h (**Figure 2.5B**). Interestingly, ternatin-4 treatment caused the appearance of multiple discrete bands in whole cell lysates, in a manner reminiscent of the banding pattern observed for Flag-eEF1A in our BirA assay (**Figure 1.7**). Treatment of cells with SRI-41315 or UV did not lead to a similar increase in total K6-linked ubiquitin chains. However, in RNF14 rescue cells treated with SRI-41315, total eRF1 levels decreased by >50% and resulted in the formation of higher molecular weight, presumably ubiquitinated eRF1 species. Consistent with eEF1A and eRF1 ubiquitination, affinity enrichment with the K6-specific affimer revealed a dramatic increase in K6-ubiquitinated eRF1 (but not eEF1A) in cells treated with SRI-41315, and in K6-ubiquitinated eEF1A (but not eRF1) in cells treated with ternatin-4. This effect was RNF14-dependent (**Figure 2.5B**) and specific to samples with affimer added prior to enrichment via GFP nanobody resin (**Figure 2.5C**). Likewise, ternatin-4, SRI-41315, and UV-treated treatment stimulated RNF14-dependent, K6-linked GCN1 ubiquitination, albeit to a lesser extent with UV.

While we were not able to detect eEF1A-Ub by immunoblotting against whole cell lysates with our anti-eEF1A antibody, the robust signal afforded by the K6-linked affimer suggests the high abundance of ternatin-induced eEF1A-Ub, relative to SRI-41315 induced eRF1-Ub (**Figure 2.5B-C**). Likewise, ternatin-4 stimulated GCN1 ubiquitination to a greater degree than SRI-41315. Affimer enrichment after UV irradiation revealed a more modest increase in K6-ubiquitinated GCN1, but not eRF1 or eEF1A, presumably reflecting weaker activation of the RNF14/RNF25 pathway by UV-damaged RNA.

Discussion

A number of exciting questions remain for future work. In particular, the physiological basis of the RNF14/RNF25/GCN1 pathway remains to be determined. Potential roles may lie in responses to environmental stresses, and/or surveillance of rare, innate defects during

translation elongation. A role for constitutive translation surveillance is suggested by the discovery that the GTPase DRG1 appears to be a substrate for RNF14. Rbg1 was proposed to facilitate peptide bond formation, perhaps in concert with eIF5A (Zeng et al., 2021). At cellular concentrations of approximately 500 nM, DRG1/DFRP1 are vastly exceeded by 35 μM eEF1A, underscoring a more specialized role for this GTPase (Itzhak et al., 2016). K213 resides in the DRG1 S5D2L domain, which contacts the A-site tRNA and may thus provide conformational cues to RNF14. The ubiquitinated lysines we identified in DRG1 are not conserved in yeast Rbg1, and their functional relevance remains to be determined. While we only detected ubiquitination sites in DRG1, we cannot rule out the possibility that ubiquitination also occurs at DRG2, the less abundant of the two GTPases (286 nM) (Itzhak et al., 2016).

Following ternatin-4 treatment, eEF1A2 is degraded more rapidly than eEF1A1. eEF1A1 and eEF1A2 are highly similar and both possess a lysine residue at position 385, which we previously showed was critical for eEF1A1 degradation. This residue is likely also critical for eEF1A2 degradation, and subtle differences near its constituent loop (eEF1A1 G390 and F393 vs. eEF1A2 N390 and S393) may impact its dynamics or conformation. Insights may also be provided by careful examination of eEF1A/ribosome binding affinities and rates, including in the presence of ternatin-4. Identification of additional stresses giving rise to eEF1A degradation may reveal if enhanced eEF1A2 degradation is unique to ternatin-4 or a universal feature. Given the specialized tissue distribution of eEF1A2, an attractive hypothesis is that these nondividing cell types are more reliant on A-site quality control.

Future work will examine how SRI-41315 targets eRF1 and promotes RNF14/RNF25-mediated degradation. RNF14 also promotes degradation of a catalytically dead eRF1 mutant that stalls termination while trapped in the A site (Brown et al., 2015; Shao et al., 2016; Yan and Zaher, 2021), suggesting that SRI-41315 may trap eRF1 in a similar conformation at the ribosome A site. Correspondingly, SRI-41315 was previously shown to have no effect on levels of eRF1's binding partner, the GTPase eRF3, suggesting that SRI-41315 likely acts after eRF3

dissociation and rearrangement of eRF1 in the ribosome A site (Sharma et al., 2021). Likewise, SRI-41315 did not significantly impact ABCE1 levels (**Figure 2.3A**), raising the question of whether ABCE1 binding to eRF1 occurs in the presence of SRI-41315. ABCE1 binds ribosomes stalled with eRF1 AAQ, but whether ABCE1 is also targeted for degradation by this stall is unknown. The requirement for GCN1 and RPS27A ubiquitination in mediating eRF1 degradation, while probable, remains to be determined.

Apart from ternatin-4 and SRI-41315 mediated stalls, we lack a fully defined profile of RNF14/RNF25 activators. Assessment of other commonly utilized translation inhibitors, including anisomycin, emetine, didemnin B, and G418, may prove fruitful. Likewise, many environmental stressors have been utilized to generate ribosome stalls, including UV, oxidative stress, amino acid starvation, heat stress, alkylating agents, misfolding agents, and stalling sequences. We show here that ultraviolet irradiation activates the RNF14/RNF25 pathway, albeit to a lesser degree than ternatin-4 and SRI-41315, and stimulates K6-linked ubiquitination of GCN1. UV was shown to stimulate ubiquitination of both eEF1A and ABCE1, suggesting multiple stages of translation may be altered. Ubiquitination of either factor is likely substoichiometric, and the extent to which degradation may occur is unclear. Further context for the RNF14/RNF25 pathway may also arise from identification of phenotype-causing mutations in development and disease.

Many additional questions remain for future work. Examination of structure activity relationships of both ternatin-4 and SRI-41315 in eliciting degradation, and the associated kinetic parameters and conformational dynamics of eEF1A and eRF1, may add to our understanding of substrate recognition at the ribosome by RNF14. Multiple natural products target eEF1A, including didemnin B, nannocystin, and ansatrienin B, and the effects of these compounds and related analogs on eEF1A levels may provide additional insights into the requirements for eEF1A degradation. At the cellular level, the consequence of RNF14/RNF25-mediated ubiquitination of GCN1 and ribosomes, in addition to eEF1A, is unknown. Whether

these ubiquitination sites are required in this pathway, and if this leads to degradation or de-ubiquitination by an unidentified factor, remains to be determined. Moreover, it is unclear if this pathway functions to allow translation to resume, or to promote ribosome splitting and nascent chain degradation as observed in other pathways. In future studies, it will be interesting to examine crosstalk between additional quality control pathways in the cell (integrated stress response, ribotoxic stress response, RQC), and to identify the preferred pathway for a given stress. Finally, *in vitro* reconstitution of RNF14/RNF25/GCN1-mediated ubiquitination, and eventual structural studies, will provide rich mechanistic insights into this pathway.

Table 2.1: Key Resources

Reagent or Resource	Source	Identifiers
Antibodies		
Mouse monoclonal anti-eEF1A, clone CBP-KK1	EMD Millipore	Cat# 05-235; RRID: AB_309663
Rabbit monoclonal anti-eEF1A1	Abcam	Cat# ab157455
Mouse polyclonal anti-eEF1A2	Abcam	Cat# ab194441
Rabbit monoclonal anti-beta Actin (13E5)	Cell Signaling Technology	Cat# 4970S; RRID: AB_2223172
Mouse monoclonal anti-RNF14 (B-10)	Santa Cruz Biotechnology	Cat# sc-376701; RRID: AB_11150281
Rabbit polyclonal anti-RNF25	Abcam	Cat# ab140514
Rabbit polyclonal anti-DRG1	Proteintech	Cat# 13190-1-AP; RRID: AB_2095275
Rabbit monoclonal anti-V5 (D3H8Q)	Cell Signaling Technologies	Cat# 13202S; RRID: AB_2687461
Rabbit monoclonal anti-ABCE1	Abcam	Cat# ab185548; RRID: AB_2858278
Mouse monoclonal anti-eRF1 (B-11)	Santa Cruz Biotechnology	Cat# sc-365686; RRID: AB_10843214
Mouse monoclonal anti-Flag	Sigma-Aldrich	Cat# F3165; RRID: AB_259529
Chicken polyclonal anti-GFP	Abcam	Cat# ab13970; RRID: AB_300798
Rat monoclonal APC anti-Flag	BioLegend	Cat# 637307; RRID: AB_2561496
Rabbit polyclonal anti-GCN1L1	Novus Biologicals	Cat# NBP1-83383; RRID: AB_11022056
Goat polyclonal anti-mouse IgG IRDye 680RD	LI-COR	Cat# 926-68070; RRID: AB_10956588
Goat polyclonal anti-mouse IgG IRDye 800CW	LI-COR	Cat# 926-32210; RRID: AB_621842
Goat polyclonal anti-rabbit IgG IRDye 680RD	LI-COR	Cat# 926-68071; RRID: AB_10956166
Goat polyclonal anti-rabbit IgG IRDye 800CW	LI-COR	Cat# 926-32211; RRID: AB_621843
Donkey polyclonal anti-chicken IgG IRDye 800CW	LI-COR	Cat# 925-32218; RRID: AB_2814922
Chemicals, Peptides, and Recombinant Proteins		
Ternatin-4	Wang et al., 2022	n/a
SRI-41315	ProbeChem	n/a
Cycloheximide	Sigma-Aldrich	Cat# C7698
Homoharringtonine	MedChemExpress	Cat# HY-14944
Biotin	Sigma-Aldrich	Cat# B4501
Chloroacetamide	Sigma-Alrich	Cat# 22790
$^{13}C_6$ $^{15}N_4$ L-arginine hydrochloride	Cambridge Isotope Laboratories	Cat# CNLM-539-H-0.1

Reagent or Resource	Source	Identifiers
$^{13}C_6$ $^{15}N_2$ L-lysine hydrochloride	Cambridge Isotope Laboratories	Cat# CNLM-291-H-0.1
EDTA-free Protease Inhibitor Cocktail	Roche	Cat# 11873580001
Trypsin	Promega	Cat# V5113
Pierce Streptavidin Magnetic Beads	Thermo Fisher Scientific	Cat# 88817
Anti-Ubiquitin Lys6 specific GFP/His-tag Affimer	EMD Millipore	Cat# MABS1918
GFP-Trap Magnetic Agarose	ChromoTek	Cat# gtma
Mirus TransIT-LT1 Transfection Reagent	Mirus Bio	Cat# MIR2300
ViralBoost Reagent	Alstem Cell Advancements	Cat# VB100
Hexadimethrine bromide (polybrene)	Sigma-Aldrich	Cat# TR-1003-G
16% Paraformaldehyde Solution	Electron Microscopy Sciences	Cat# 15710
Critical Commercial Assays		
PTMScan® Ubiquitin Remnant Motif (K-ε-GG) Kit	Cell Signaling Technology	Cat# 5562
Experimental Models: Cell Lines		
HeLa	ATCC	CCL-2
HEK293T	ATCC	CRL-3216
MCF7	ATCC	HTB-22
HCT116	ATCC	CCL-247
HCT116 eEF1A1 A399V/A399V	Krastel et al., 2015	n/a
HCT116 eEF1A1 A399V/A399V RNF14 KO	This paper	n/a
HCT116 eEF1A1 A399V/A399V RNF25 KO	This paper	n/a
HeLa RNF14 KO	This paper	n/a
HeLa RNF25 KO	This paper	n/a
HeLa RNF14 KO V5-RNF14	This paper	n/a
HeLa RNF25 KO V5-RNF25	This paper	n/a
Recombinant DNA		
pLX302 Flag-mCherry-eEF1A1_IRES-GFP	This paper	n/a
pLX302 Flag-mCherry-eEF1A2_IRES-GFP	This paper; *eEF1A2* sequence from DNASU Clone# HsCD00438271	
pHR V5-RNF14_IRES-mCherry	This paper; *RNF14* sequence from DNASU Clone # HsCD00436670	n/a
pHR V5-RNF25_IRES-mCherry	This paper; *RNF25* sequence from DNASU Clone #	n/a

Reagent or Resource	Source	Identifiers
	HsCD00438677	
pHR V5-BirA_IRES-mCherry	This paper; *BirA* sequence from Deshar et al., 2016	n/a
pHR V5-BirA-RNF14_IRES-mCherry	This paper	n/a
pHR V5-BirA-RNF14 C417A_IRES-mCherry	This paper	n/a
pLX304 3xFlag-eRF1_IRES-AcGFP	This paper	n/a
pLX304 3xFlag-eRF1 G183/184A_IRES-AcGFP	This paper	n/a
pcDNA3.1 AP-HA-Ub	Deshar et al., 2016	n/a
pCMV-dR8.91	Gift from Didier Trono	Addgene Ref #2221
pMD2.G	Gift from Didier Trono	Addgene Plasmid #12259
PX458 pSpCas9(BB)-2A-GFP	Ran et al., 2013	Addgene Plasmid #48138
Sequence-Based Reagents		
sgRNA targeting exon 5 of *RNF14*: 5'-GACAATATTCAAGTATGCTA-3'	This paper	n/a
sgRNA targeting exon 3 of *RNF25*: 5'-AAAGTGATGTAGATCTCCCA-3'	This paper	n/a
Software and Algorithms		
GraphPad Prism	GraphPad Prism software	n/a
Image Studio Lite	LI-COR	n/a
FlowJo	BD Biosciences	n/a
Tableau	Tableau software	n/a
MaxQuant	Cox and Mann, 2008	n/a
Adobe Illustrator	Adobe	n/a
Adobe Photoshop	Adobe	n/a

Experimental Methods

Cell lines and culture conditions

HEK293T, HeLa, and MCF7 cells were maintained in Dulbecco's Modified Eagle's Medium (DMEM) supplemented with 10% fetal bovine serum (FBS), 100 U/mL penicillin, and 100 µg/mL streptomycin. HCT116 eEF1A1 A399V/A399V cells were originally described in Krastel et al., (2015). HCT116 and HCT116 eEF1A1 A399V/A399V cells were maintained in McCoy's media supplemented with 10% FBS, 100 U/mL penicillin, and 100 µg/mL streptomycin. Antibiotics were omitted for all transfection-based experiments. Cells were grown in a humidified incubator at 37 °C with a 5% CO_2 atmosphere. Unless indicated otherwise, all treatment conditions utilized a vehicle control, 50 nM ternatin-4, 10 µM SRI-41315, 50 µg/mL cycloheximide, or 2 µg/mL homoharringtonine as described in figure legends. Ultraviolet irradiation was conducted using a Stratagene UV Stratalinker 2400: cells were washed once with DPBS (containing Ca^{+2}/Mg^{+2}), dry plates were irradiated with 40 J/m^2 UV-C, fresh media was added to plates, and cells were returned to the incubator for the indicated recovery period. Treatment proceeded identically for control samples, except dishes were covered with cardboard during irradiation.

Plasmid Generation

Plasmids encoding the indicated genes, epitope tags, and IRES sequences were constructed by Gibson cloning. eEF1A1 and eEF1A2-encoding constructs were expressed from a pLX302 vector containing IRES-AcGFP. RNF14 and RNF25-encoding constructs were expressed from a pHR vector containing IRES-mCherry. eRF1 was expressed from a pLX304 vector containing IRES-AcGFP. Plasmids encoding individual sgRNAs were constructed by ligating complementary oligonucleotides (sequences indicated above in **Sequence-Based Reagents**) into the BbsI restriction enzyme sites of PX458. All plasmids were verified by Sanger sequencing.

Lentivirus and stable cell line generation

Lentivirus was generated by transfecting HEK293T cells growing at approximately 60% confluency in 6-well dishes with lipid complexes containing 1.5 µg of a construct of interest, 1.35 µg pCMV-dR8.91, 165 ng pMD2-G, and 7.5 µL Mirus TransIT-LT1 diluted in OPTI-Mem. Alstem ViralBoost was added to cells after addition of the transfection mix. Two days post-transfection, an additional 1.5 mL complete DMEM was added to cells. The viral supernatant was collected on the third day and filtered through 0.45 µm sterile SFCA syringe filters (Thermo Scientific). Supernatant was used immediately or stored at -20 °C.

For stable cell line generation, media containing 8 µg/mL polybrene was added to cells, lentivirus was added, and cells were incubated overnight. Lentivirus was removed from cells, and cells were expanded until use in experiments (minimum of two days post-transduction).

CRISPR knockout cell lines

CRISPR knockout cells were generated as previously described (Ran et al., 2013). sgRNA sequences targeting exon 5 of RNF14 and exon 3 of RNF25 were identified using the Broad CRISPR design tool (crispr.mit.edu/v1) and ligated into the PX458 (pSpCas9(BB)-2A-GFP) plasmid. HCT116 eEF1A1 A399V/A399V cells were transfected using Lipofectamine 2000 and sorted for GFP positivity after 2 days. Seven days post-transfection, cells were plated into a 96-well plate at 0.5 cells per well. After appearance of visible colonies (approximately 2 weeks), wells containing individual colonies were collected by trypsinization and expanded to 6-well dishes. Clones were screened for RNF14/RNF25 expression by Western blotting and Sanger sequencing prior to selection for experiments.

Immunoblot analysis

Cells were washed once with ice-cold PBS and stored at -80 °C or immediately lysed using lysis buffer (50 mM HEPES pH 7.4, 150 mM NaCl, 1% NP-40, 2x Roche EDTA-free protease inhibitors). Lysis buffer for eRF1 immunoblotting experiments additionally contained 50 mM chloroacetamide and 5 mM EDTA. Lysates were collected by scraping and were cleared by centrifugation at 16,100 *g* for 10 minutes at 4 °C. Total protein was quantified using the Bradford method and normalized prior to electrophoresis using hand-cast 7.5% polyacrylamide gels or 4-12% Bis-Tris gradient gels (Invitrogen). Proteins were transferred to 0.45 µm nitrocellulose membranes (Bio-Rad) using a Bio-Rad Criterion transfer system. Membranes were blocked for 1 hour at room temperature using blocking buffer (5% BSA, 0.1% sodium azide in TBS-T). Membranes were incubated with primary antibodies diluted in blocking buffer for 1 hour at room temperature or overnight at 4 °C. Membranes were rinsed with TBS-T (3 x 5 minutes at room temperature) and incubated with secondary antibodies diluted in blocking buffer for 1 hour at room temperature. Membranes were rinsed with TBS-T (3 x 5 minutes at room temperature) and were imaged using a Li-Cor Odyssey system.

eEF1A FACS reporter measurements (Figure 2.1B-D)

Cells growing in 12-well dishes were harvested by trypsinization, transferred to 96-well V-bottom plates, centrifuged at 2,100 *g* for 3 minutes at 4 °C, and resuspended in FACS buffer (2% FBS, 100 U/mL penicillin, 100 µg/mL streptomycin, and 2 mM EDTA in PBS lacking Ca^{+2}/Mg^{+2}). Samples were analyzed using a MACSQuant VYB equipped with 405 nm, 488 nm, 561 nm, and 637 nm lasers. Single cells were analyzed using FlowJo (BD) software. For all samples, debris (FSC-H vs. SSC-A), and doublets (FSC-H vs. FSC-W) were excluded. Mean fluorescent intensity (MFI) was calculated for each sample (gated on GFP positivity) and normalized to vehicle control samples within a given cell line.

Flag-APC cell staining (Figure 2.3D)

Cells growing in 6-well dishes were scraped into PBS. All centrifugation steps were performed at 2,100 *g* for 3 minutes at 4°C, and all washes and incubations were done with 200 µL buffer unless indicated otherwise. Cells were washed once (2% FBS in PBS) and fixed with 4% paraformaldehyde (PFA) in PBS for 15 min at RT. Cells were washed once (2% FBS in PBS) and incubated in permeabilization buffer (3% FBS, 0.1% saponin in PBS) for 5 min at RT. Cells were resuspended in 100 µL permeabilization buffer containing 0.1 µg APC-conjugated Flag antibody (BioLegend) and incubated in the dark for 30 min at RT. Cells were washed twice with permeabilization buffer and resuspended in FACS buffer (2% FBS, 100 U/mL penicillin, 100 µg/mL streptomycin, and 2 mM EDTA in PBS lacking Ca^{+2}/Mg^{+2}). Samples were analyzed using a BD CytoFlex S equipped with 405 nm, 488 nm, 561 nm, and 638 nm lasers. For all samples, debris (FSC-H vs. SSC-A), and doublets (FSC-H vs. FSC-W) were excluded.

DiGly peptide enrichment

Cells were grown in light (Arg0/Lys0) or heavy (Arg10/Lys8) SILAC DMEM (Thermo Scientific) supplemented with 10% dialyzed FBS, 100 U/mL penicillin,100 µg/mL streptomycin, 80 µM lysine0 or lysine8, and 40 µM arginine0 or arginine10 for 12 days prior to indicated treatments. Typically, 5-6 15 cm dishes were used per label and treatment condition, yielding approximately 10-15 mg total protein. A label swap was performed as a biological replicate for all experimental conditions, except UV irradiation. Cells were harvested at room temperature by quickly aspirating media from dishes, rinsing once with ice-cold PBS, and scraping cells into cell lysis buffer (20 mM HEPES pH 8.0, 9 M urea, 1 mM sodium orthovanadate, 2.5 mM sodium pyrophosphate, 1 mM beta-glycerophosphate). Lysates were sonicated using three 15-second bursts from a microtip sonicator, and lysates were clarified by centrifugation at 19,000 *g* for 15 minutes at RT. Cleared lysates were quantified using the BCA method, and equal amounts of heavy and light samples were pooled (20-30 mg total). Samples were reduced with 4.5 mM DTT

for 30 minutes at 55 °C. Samples were allowed to cool to room temperature and alkylated with 10.2 mM chloroacetamide for 30 minutes at RT. Lysates were diluted 4-fold with 20 mM HEPES pH 8.0 to a final concentration of approximately 2 M urea, sequencing-grade trypsin (Promega V5113) was added at a 1:300 w/w ratio, and samples were digested by rotating overnight at RT. The next day (approximately 18 hours later), trypsin digestion was stopped by addition of TFA to 1% final concentration. Samples were incubated on ice for 15 minutes and centrifuged at 1,780 *g* for 15 minutes at RT. Peptides were desalted using Waters 500 mg C18 SepPaks (WAT036945). SepPak cartridges were conditioned with 7 mL acetonitrile and equilibrated with 3 sequential washes of 1.4 mL, 4.2 mL, and 8.4 mL Solvent A (0.1% TFA in water) prior to loading of the clarified peptide solution. Peptides were loaded onto columns by gravity flow, and columns were washed 3 times using 1.4 mL, 7 mL, and 8.4 mL Solvent A. Peptides were eluted by 3 sequential additions of 2.8 mL solvent B (0.1% TFA, 40% acetonitrile in water). Samples were frozen and lyophilized for a minimum of 48 hours prior to immunoprecipitation of diGlycine-containing peptides.

Ubiquitin remnant-containing peptides were isolated using the Cell Signaling Technologies PTMScan Ubiquitin Remnant Motif Kit (CST #5562). Lyophilized peptides were collected by centrifugation at 2,000 *g* for 5 minutes at RT and dissolved in 1.4 mL ice-cold Immunoaffinity Purification (IAP) buffer (50 mM MOPS pH 7.2, 10 mM disodium phosphate, 50 mM NaCl). The peptide solution was cleared by centrifugation at 10,000 *g* for 5 minutes at 4 °C. The peptide supernatant was added to a tube containing immunoaffinity beads pre-washed 4x with 1 mL of cold PBS. All centrifugation steps with antibody beads were done at 2,000 *g* for 30 seconds at 4 °C. Immunoprecipitations were performed using a predetermined ratio of 10 mg input protein per 10 µL of antibody bead slurry (Udeshi et al., 2013). Samples were rotated for 2 hours at 4 °C, and subsequently, peptide supernatant was removed from beads. Beads were washed twice with 1 mL ice-cold IAP buffer and 3 times with 1 mL ice-cold HPLC water. Peptides were eluted

from beads with two consecutive incubations of 55 µL and 50 µL 0.15% TFA for 10 minutes at RT with gentle agitation every 2-3 minutes. Eluants were desalted using Agilent OMIX C18 tips (A57003100), dried by vacuum concentration, and stored at -80 °C until analysis.

LC-MS/MS data acquisition (DDA)

One half of each sample was resuspended in 10 µL 0.1% FA or 10 µL 0.1% FA containing 2.5 nM eEF1A K385 standard peptide (SGK[diGly]KLEDGPK, with $^{13}C_6$,^{15}N-Leu). One quarter of each reconstituted sample (2.5 µL; 12.5% of total sample) was analyzed on an Orbitrap Fusion Lumos (Thermo Scientific) equipped with an ACQUITY M-Class UPLC (Waters) and an EASY-Spray C18 column (Thermo Scientific #ES800; 75 µm x 15 cm, 3 µm particle size, 100 Å pore size). Solvent A was 0.1% FA in water, and Solvent B was 0.1% FA in acetonitrile. Peptides were loaded onto the warmed column (45 ˚C), and equilibrated with 0% B for 13 min using a flow rate of 600 nL/min, followed by 0-30% B over 120 min at 300 nL/min, 30-80% B over 20 min, 80% B for 5 min, 80%-0% B over 2 min, and 0% B for 10 min with the flow rate changed back to 600 nL/min. The entire method ran for a total of 170 min. Mass spectra were acquired in data dependent mode. MS1 scans were collected in the orbitrap at a resolution of 120,000, a scan range of 375-1500 m/z, an automatic gain control (AGC) target of 4E5, and a maximum injection time of 50 ms. Ions with a peptide-like isotopic distribution (MIPS set to “peptide”) that exceeded an intensity threshold of 2E4 and contained a charge between 2 and 7 were selected for HCD fragmentation. MS2 spectra of HCD-fragmented peptides were collected using a 1.6 m/z isolation window and an HCD collision energy of 30%. Fragment ions were measured in the orbitrap at a resolution of 30,000 and were collected with an AGC target of 5E4 and a maximum injection time of 100 ms. Peptides selected for fragmentation were dynamically excluded for the following 30 seconds using a 10-ppm window. The maximum duty cycle was set to 3 s.

Mass spectrometric site identification and quantification

The raw data were searched against the human Uniprot database (73,651 entries) using MaxQuant (version 1.6.7.0) with a list of common laboratory contaminants added. 'Arg10' and 'Lys8' were selected as heavy labels. The digestion enzyme was set to trypsin, a maximum of three missed cleavages were allowed, and the minimum peptide length was set to 7. Cysteine carbamidomethylation was specified as a fixed modification, and N-terminal protein acetylation and methionine oxidation were set as variable modifications. Internal lysine diGlycine modifications, and lysine diGlycine modifications at the protein C-terminus were additionally set as variable modifications. The remainder of the search parameters were left at default settings. Peptide requantification was enabled for calculation of H/L SILAC ratios. DiGly site identifications and normalized SILAC ratios were obtained from the MaxQuant sites file. SILAC ratios were inverted for label swap experiments. Site values were averaged between biological replicates, $\log_2$-transformed, and reported in **Supplementary Table 2**.

Proximity-based ubiquitination assay

HEK293T cells were cultured in DMEM supplemented with 10% fetal bovine serum. The assay was based on Deshar et al., (2016), with some modifications. Cells were grown to 70% confluency in 10 cm dishes and were co-transfected with 0.88 µg AP-HA-Ub (pcDNA3.1) and 4.4 µg V5-BirA or V5-BirA-RNF14 (pHR) constructs using the manufacturer's protocol for Lipofectamine 2000. The next day, cells were treated with 50 µM biotin and with DMSO or 50 nM ternatin-4 for 2 h.

Following treatment, cells were washed once with ice-cold PBS and collected by scraping into PBS. Cells were centrifuged at 1000 *g* for 3 minutes at 4 °C, and cell pellets were frozen in liquid nitrogen and stored at -80 °C. Cells were lysed in lysis buffer (50 mM HEPES pH 7.4, 150 mM NaCl, 1% NP-40, 2x Roche EDTA-free protease inhibitors, and 50 mM chloroacetamide)

and lysate was cleared by centrifugation at 16,100 *g* for 10 minutes at 4 °C. SDS was added to supernatants to 1% final concentration, and samples were boiled for 10 minutes. Denatured lysates were quantified by the Bradford method, normalized, and diluted 10-fold in lysis buffer. Diluted lysates were filtered through 0.45 µm SFCA syringe filters (Thermo Scientific) and were added to tubes containing streptavidin magnetic beads (Pierce; 40 µL beads per 1 mg protein). Samples were rotated for 2 hours at 4 °C. Supernatants were removed from beads, and beads were washed twice with wash buffer 1 (50 mM HEPES pH 7.4, 150 mM NaCl, 1% NP-40, 0.1% SDS), and twice with wash buffer 2 (50 mM HEPES pH 7.4, 500 mM NaCl, 1% NP-40). Bound proteins were eluted by boiling beads for 10 minutes in elution buffer (50 mM HEPES pH 7.4, 150 mM NaCl, 1% NP-40, 5 mM biotin, and 1x SDS loading buffer). 10 µg of input protein (typically < 3% total input protein) and 40% of eluants were loaded on 7.5% gels and analyzed by immunoblotting.

K6-linked ubiquitin enrichment

HeLa RNF14 KO or rescue cells were grown to approximately 70% confluency in 15 cm dishes prior to treatment. Cells were harvested by scraping into ice-cold PBS and centrifuged at 1000 g for 3 minutes at 4 °C. Cells were lysed in lysis buffer (50 mM HEPES pH 7.4, 150 mM NaCl, 1% NP-40, 2x Roche EDTA-free protease inhibitors, 5 mM EDTA, and 50 mM chloroacetamide) and lysates were cleared by centrifugation at 16,100 g for 10 minutes at 4 °C. The K6-ubiquitin affimer (linked to GFP; Michel et al.), was added to lysates (1 µg affimer per 1 mg lysate) as indicated and rotated for 2 hours at 4 °C. GFP-Trap beads (ChromoTek; 5 µL per sample) were added to samples and rotated for an additional 2 hours at 4 °C. Supernatants were removed from beads, and beads were washed twice with wash buffer 1 (50 mM HEPES pH 7.4, 150 mM NaCl, 1% NP-40, 5 mM EDTA), and twice with wash buffer 2 (50 mM HEPES pH 7.4, 500 mM NaCl, 1% NP-40, 5 mM EDTA). Bound proteins were eluted by boiling beads for 10 minutes in elution buffer (50 mM HEPES pH 7.4, 150 mM NaCl, 1% NP-40, 5 mM EDTA, and 1x SDS

loading buffer). 10 µg of input protein (1-2% total input protein) and 33% of eluants were loaded on 4-12% Bis-Tris gradient gels (Invitrogen) gels and analyzed by immunoblotting.

References

Anand, N., Murthy, S., Amann, G., Wernick, M., Porter, L. a, Cukier, I.H., Collins, C., Gray, J.W., Diebold, J., Demetrick, D.J., et al. (2002). Protein elongation factor EEF1A2 is a putative oncogene in ovarian cancer. Nat. Genet. *31*, 301–305. http://www.ncbi.nlm.nih.gov/pubmed/12053177.

Bartok, O., Pataskar, A., Nagel, R., Laos, M., Goldfarb, E., Hayoun, D., Levy, R., Körner, P.R., Kreuger, I.Z.M., Champagne, J., et al. (2020). Anti-tumour immunity induces aberrant peptide presentation in melanoma. Nature.

Brandman, O., and Hegde, R.S. (2016). Ribosome-associated protein quality control. Nat. Struct. Mol. Biol. *23*, 7–15. http://www.ncbi.nlm.nih.gov/pubmed/26733220.

Brown, A., Shao, S., Murray, J., Hegde, R.S., and Ramakrishnan, V. (2015). Structural basis for stop codon recognition in eukaryotes. Nature *524*, 493–496. https://pubmed.ncbi.nlm.nih.gov/26245381/.

Budkevich, T., Giesebrecht, J., Altman, R.B., Munro, J.B., Mielke, T., Nierhaus, K.H., Blanchard, S.C., and Spahn, C.M.T. (2011). Structure and dynamics of the mammalian ribosomal pretranslocation complex. Mol. Cell *44*, 214–224. http://dx.doi.org/10.1016/j.molcel.2011.07.040.

Carelli, J.D., Sethofer, S.G., Smith, G.A., Miller, H.R., Simard, J.L., Merrick, W.C., Jain, R.K., Ross, N.T., and Taunton, J. (2015). Ternatin and improved synthetic variants kill cancer cells by targeting the elongation factor-1A ternary complex. Elife *4*. http://www.ncbi.nlm.nih.gov/pubmed/26651998.

Carvill, G.L., Helbig, K.L., Myers, C.T., Scala, M., Huether, R., Lewis, S., Kruer, T.N., Guida, B.S., Bakhtiari, S., Sebe, J., et al. (2020). Damaging de novo missense variants in EEF1A2 lead to a developmental and degenerative epileptic-dyskinetic encephalopathy. Hum. Mutat. *41*, 1263–1279.

Castilho, B.A., Shanmugam, R., Silva, R.C., Ramesh, R., Himme, B.M., and Sattlegger, E. (2014). Keeping the eIF2 alpha kinase Gcn2 in check. Biochim. Biophys. Acta *1843*,

1948–1968. https://pubmed.ncbi.nlm.nih.gov/24732012/.

Chen, J.J., Nathaniel, D.L., Raghavan, P., Nelson, M., Tian, R., Tse, E., Hong, J.Y., See, S.K., Mok, S.A., Hein, M.Y., et al. (2019). Compromised function of the ESCRT pathway promotes endolysosomal escape of tau seeds and propagation of tau aggregation. J. Biol. Chem. *294*, 18952–18966. https://pubmed.ncbi.nlm.nih.gov/31578281/.

Cotton, T.R., and Lechtenberg, B.C. (2020). Chain reactions: molecular mechanisms of RBR ubiquitin ligases. Biochem. Soc. Trans. *48*, 1737–1750. https://pubmed.ncbi.nlm.nih.gov/32677670/.

Cotton, T.R., Cobbold, S.A., Bernardini, J.P., Richardson, L.W., Wang, X.S., Lechtenberg, B.C., Cotton, T.R., Cobbold, S.A., Bernardini, J.P., Richardson, L.W., et al. (2022). Structural basis of K63-ubiquitin chain formation by the Gordon-Holmes syndrome RBR E3 ubiquitin ligase RNF216. Mol. Cell 1–18. https://doi.org/10.1016/j.molcel.2021.12.005.

Cox, J., and Mann, M. (2008). MaxQuant enables high peptide identification rates, individualized p.p.b.-range mass accuracies and proteome-wide protein quantification. Nat. Biotechnol. *26*, 1367–1372. https://www.nature.com/articles/nbt.1511.

Darnell, A.M., Subramaniam, A.R., and O'Shea, E.K. (2018). Translational Control through Differential Ribosome Pausing during Amino Acid Limitation in Mammalian Cells. Mol. Cell *71*, 229-243.e11. https://pubmed.ncbi.nlm.nih.gov/30029003/.

Daugeron, M.C., Prouteau, M., Lacroute, F., and Séraphin, B. (2011). The highly conserved eukaryotic DRG factors are required for efficient translation in a manner redundant with the putative RNA helicase Slh1. Nucleic Acids Res. *39*, 2221–2233.

Deshar, R., Moon, S., Yoo, W., Cho, E.B., Yoon, S.K., and Yoon, J.B. (2016). RNF167 targets Arl8B for degradation to regulate lysosome positioning and endocytic trafficking. FEBS J. *283*, 4583–4599. https://pubmed.ncbi.nlm.nih.gov/27808481/.

Deshar, R., Yoo, W., Cho, E.B., Kim, S., and Yoon, J.B. (2019). RNF8 mediates NONO degradation following UV-induced DNA damage to properly terminate ATR-CHK1

checkpoint signaling. Nucleic Acids Res. *47*, 762–778. https://pubmed.ncbi.nlm.nih.gov/30445466/.

Dever, T.E., and Green, R. (2012). The Elongation, Termination, and Recycling Phases of Translation in Eukaryotes. Cold Spring Harb. Perspect. Biol. *4*, a013706. https://pubmed.ncbi.nlm.nih.gov/22751155/.

Dever, T.E., Dinman, J.D., and Green, R. (2018). Translation Elongation and Recoding in Eukaryotes. Cold Spring Harb. Perspect. Biol. a032649. http://cshperspectives.cshlp.org/lookup/doi/10.1101/cshperspect.a032649.

Dmitriev, S.E., Vladimirov, D.O., and Lashkevich, K.A. (2020). A Quick Guide to Small-Molecule Inhibitors of Eukaryotic Protein Synthesis. Biochem. *85*, 1389–1421.

Doma, M.K., and Parker, R. (2006). Endonucleolytic cleavage of eukaryotic mRNAs with stalls in translation elongation. Nature *440*, 561–564. http://www.nature.com/doifinder/10.1038/nature04530.

Dove, K.K., and Klevit, R.E. (2017). RING-Between-RING E3 Ligases: Emerging Themes amid the Variations. J. Mol. Biol. *429*, 3363–3375. https://pubmed.ncbi.nlm.nih.gov/28827147/.

Elia, A.E.H., Boardman, A.P., Wang, D.C., Huttlin, E.L., Everley, R.A., Dephoure, N., Zhou, C., Koren, I., Gygi, S.P., and Elledge, S.J. (2015). Quantitative Proteomic Atlas of Ubiquitination and Acetylation in the DNA Damage Response. Mol. Cell *59*, 867–881. http://dx.doi.org/10.1016/j.molcel.2015.05.006.

Francis, S.M., Gas, M.E., Daugeron, M.C., Bravo, J., and Séraphin, B. (2012). Rbg1-Tma46 dimer structure reveals new functional domains and their role in polysome recruitment. Nucleic Acids Res. *40*, 11110–11114.

Fresno, M., Jiménez, A., and Vázquez, D. (1977). Inhibition of Translation in Eukaryotic Systems by Harringtonine. Eur. J. Biochem. *72*, 323–330. https://pubmed.ncbi.nlm.nih.gov/319998/.

Garcia-Barrio, M., Dong, J., Ufano, S., and Hinnebusch, A.G. (2000). Association of GCN1-

GCN20 regulatory complex with the N-terminus of eIF2alpha kinase GCN2 is required for GCN2 activation. EMBO J. *19*, 1887–1899. https://pubmed.ncbi.nlm.nih.gov/10775272/.

Garshott, D.M., An, H., Sundaramoorthy, E., Leonard, M., Vicary, A., Harper, J.W., and Bennet, E.J. (2021). iRQC, a surveillance pathway for 40S ribosomal quality control during mRNA translation initiation. Cell Rep. *36*, 109642. https://pubmed.ncbi.nlm.nih.gov/34469731/.

Garzia, A., Jafarnejad, S.M., Meyer, C., Chapat, C., Gogakos, T., Morozov, P., Amiri, M., Shapiro, M., Molina, H., Tuschl, T., et al. (2017). The E3 ubiquitin ligase and RNA-binding protein ZNF598 orchestrates ribosome quality control of premature polyadenylated mRNAs. Nat. Commun. *8*, 16056. https://pubmed.ncbi.nlm.nih.gov/28685749/.

Garzia, A., Meyer, C., and Tuschl, T. (2021). The E3 ubiquitin ligase RNF10 modifies 40S ribosomal subunits of ribosomes compromised in translation. Cell Rep. *36*, 109468. https://pubmed.ncbi.nlm.nih.gov/34348161/.

Gonzalez-Flores, J.N., Gupta, N., DeMong, L.W., and Copeland, P.R. (2012). The selenocysteine-specific elongation factor contains a novel and multi-functional domain. J. Biol. Chem. *287*, 38936–38945.

Gundogdu, M., Tadayon, R., Salzano, G., Shaw, G.S., and Walden, H. (2021). A mechanistic review of Parkin activation. BBA - Gen. Subj. *1865*, 129894. https://doi.org/10.1016/j.bbagen.2021.129894.

Hawer, H., Hammermeister, A., Ravichandran, K.E., Glatt, S., Schaffrath, R., and Klassen, R. (2019). Roles of elongator dependent tRNA modification pathways in neurodegeneration and cancer. Genes (Basel). *10*, 1–23. https://pubmed.ncbi.nlm.nih.gov/30597914/.

Heidelberger, J.B., Voigt, A., Borisova, M.E., Petrosino, G., Ruf, S., Wagner, S.A., and Beli, P. (2018). Proteomic profiling of VCP substrates links VCP to K6-linked ubiquitylation and c-Myc function. EMBO Rep. *19*, 1–20.

Hellen, C.U.T. (2018). Translation termination and ribosome recycling in eukaryotes. Cold Spring Harb. Perspect. Biol. *10*.

Hermand, D. (2020). Anticodon Wobble Uridine Modification by Elongator at the Crossroad of Cell Signaling, Differentiation, and Diseases. Epigenomes *4*. https://pubmed.ncbi.nlm.nih.gov/34968241/.

Horlbeck, M.A., Gilbert, L.A., Villalta, J.E., Adamson, B., Pak, R.A., Chen, Y., Fields, A.P., Park, C.Y., Corn, J.E., Kampmann, M., et al. (2016). Compact and highly active next-generation libraries for CRISPR-mediated gene repression and activation. Elife *5*, 1–20. https://pubmed.ncbi.nlm.nih.gov/27661255/.

Hundley, F. V., Delgado, N.S., Marin, H.C., Carr, K.L., Tian, R., and Toczyski, D.P. (2021). A comprehensive phenotypic CRISPR-Cas9 screen of the ubiquitin pathway uncovers roles of ubiquitin ligases in mitosis. Mol. Cell *81*, 1319–1336. https://pubmed.ncbi.nlm.nih.gov/33539788/.

Ikeuchi, K., Tesina, P., Matsuo, Y., Sugiyama, T., Cheng, J., Saeki, Y., Tanaka, K., Becker, T., Beckmann, R., and Inada, T. (2019). Collided ribosomes form a unique structural interface to induce Hel2-driven quality control pathways. EMBO J. *38*. https://pubmed.ncbi.nlm.nih.gov/30609991/.

Ishikawa, K., Azuma, S., Ikawa, S., Semba, K., and Inoue, J.I. (2005). Identification of DRG family regulatory proteins (DFRPs): Specific regulation of DRG1 and DRG2. Genes to Cells *10*, 139–150.

Ishimura, R., Nagy, G., Dotu, I., Zhou, H., Yang, X.L., Schimmel, P., Senju, S., Nishimura, Y., Chuang, J.H., and Ackerman, S.L. (2014). Ribosome stalling induced by mutation of a CNS-specific tRNA causes neurodegeneration. Science. *345*, 455–459. https://pubmed.ncbi.nlm.nih.gov/25061210/.

Itzhak, D.N., Tyanova, S., Cox, J., and Borner, G.H.H. (2016). Global, quantitative and dynamic mapping of protein subcellular localization. Elife e16950. https://pubmed.ncbi.nlm.nih.gov/27278775/.

Jackson, R.J., Hellen, C.U.T., and Pestova, T. V. (2010). The mechanism of eukaryotic

translation initiation and principles of its regulation. Nat. Rev. Mol. Cell Biol. *11*, 113–127. https://pubmed.ncbi.nlm.nih.gov/20094052/.

Juette, M.F., Carelli, J.D., Rundlet, E.J., Brown, A., Shao, S., Ferguson, A., Wasserman, M.R., Holm, M., Taunton, J., and Blanchard, S.C. (2022). Didemnin B and ternatin-4 inhibit conformational changes in eEF1A required for aminoacyl-tRNA accommodation into mammalian ribosomes. Elife *11*. https://elifesciences.org/articles/81608.

Juszkiewicz, S., and Hegde, R.S. (2017). Initiation of quality control during poly(A) translation requires site-specific ribosome ubiquitination. Mol. Cell *65*, 743–750. https://pubmed.ncbi.nlm.nih.gov/28065601/.

Juszkiewicz, S., Chandrasekaran, V., Lin, Z., Kraatz, S., Ramakrishnan, V., and Hegde, R.S. (2018). ZNF598 Is a Quality Control Sensor of Collided Ribosomes. Mol. Cell *72*, 469–481. https://pubmed.ncbi.nlm.nih.gov/30293783/.

Juszkiewicz, S., Speldewinde, S., Wan, L., Svejstrup, J.Q., and Hegde, R.S. (2020). The ASC-1 complex disassembles collided ribosomes. Mol. Cell *79*, 603–614. https://pubmed.ncbi.nlm.nih.gov/32579943/.

Kahns, S., Lund, A., Kristensen, P., Knudsen, C.R., Clark, B.F.C., Cavallius, J., and Merrick, W.C. (1998). The elongation factor 1 A-2 isoform from rabbit: Cloning of the cDNA and characterization of the protein. Nucleic Acids Res. *26*, 1884–1890.

Kampmann, M., Bassik, M.C., and Weissman, J.S. (2013). Integrated platform for genome-wide screening and construction of high-density genetic interaction maps in mammalian cells. Proc. Natl. Acad. Sci. *110*, 2317–2326. https://pubmed.ncbi.nlm.nih.gov/23739767/.

Kang, H.-Y., Yeh, S., Fujimoto, N., and Chang, C. (1999). Cloning and Characterization of Human Prostate Coactivator ARA54, a Novel Protein That Associates with the Androgen Receptor. J. Biol. Chem. *274*, 8570–8576. https://pubmed.ncbi.nlm.nih.gov/10085091/.

Khalyfa, A., Bourbeau, D., Chen, E., Petroulakis, E., Pan, J., Xu, S., and Wang, E. (2001). Characterization of Elongation Factor-1A (eEF1A-1) and eEF1A-2/S1 Protein Expression

in Normal and wasted Mice. J. Biol. Chem. *276*, 22915–22922. http://dx.doi.org/10.1074/jbc.M101011200.

Kim, K.Q., and Zaher, H.S. (2022). Canary in a coal mine: collided ribosomes as sensors of cellular conditions. Trends Biochem. Sci. *47*, 82–97. https://pubmed.ncbi.nlm.nih.gov/34607755/.

Kim, W., Bennett, E.J., Huttlin, E.L., Guo, A., Li, J., Possemato, A., Sowa, M.E., Rad, R., Rush, J., Comb, M.J., et al. (2011). Systematic and quantitative assessment of the ubiquitin-modified proteome. Mol. Cell *44*, 325–340. https://pubmed.ncbi.nlm.nih.gov/21906983/.

Knutsen, J.H.J., Rodland, G.E., Boe, C.A., Haland, T.W., Sunnerhagen, P., Grallert, B., and Boye, E. (2015). Stress-induced inhibition of translation independently of eIF2 phosphorylation. J. Cell Sci. *128*, 4420–4427. http://jcs.biologists.org/cgi/doi/10.1242/jcs.176545.

Krastel, P., Roggo, S., Schirle, M., Ross, N.T., Perruccio, F., Aspesi, Jr., P., Aust, T., Buntin, K., Estoppey, D., Liechty, B., et al. (2015). Nannocystin A: an Elongation Factor 1 Inhibitor from Myxobacteria with Differential Anti-Cancer Properties. Angew. Chemie *127*, 10287–10292. https://pubmed.ncbi.nlm.nih.gov/26179970/.

Kubota, H., Sakaki, Y., and Ito, T. (2000). GI domain-mediated association of the eukaryotic initiation factor 2alpha kinase GCN2 with its activator GCN1 is required for general amino acid control in budding yeast. J. Biol. Chem. *275*, 20243–20246. https://pubmed.ncbi.nlm.nih.gov/10801780/.

Kumar, S., Tomooka, Y., and Noda, M. (1992). Identification of a set of genes with developmentally down-regulated expression in the mouse brain. Biochem. Biophys. Res. Commun. *185*, 1155–1161.

Lam, W.W.K., Millichap, J.J., Soares, D.C., Chin, R., McLellan, A., Fitzpatrick, D.R., Elmslie, F., Lees, M.M., Schaefer, G.B., and Abbott, C.M. (2016). Novel de novo EEF1A2 missense mutations causing epilepsy and intellectual disability. Mol. Genet. Genomic Med. *4*, 465–

474.

Lechtenberg, B.C., Rajput, A., Sanishvili, R., Dobaczewska, M.K., Ware, C.F., Mace, P.D., and Riedl, S.J. (2016). Structure of a HOIP/E2~ubiquitin complex reveals RBR E3 ligase mechanism and regulation. Nature *529*, 546–550. http://dx.doi.org/10.1038/nature16511.

Leipe, D.D., Wolf, Y.I., Koonin, E. V., and Aravind, L. (2002). Classification and evolution of P-loop GTPases and related ATPases. J. Mol. Biol. *317*, 41–72.

Liu, B., Han, Y., and Qian, S.B. (2013). Cotranslational Response to Proteotoxic Stress by Elongation Pausing of Ribosomes. Mol. Cell *49*, 453–463. http://dx.doi.org/10.1016/j.molcel.2012.12.001.

Liu, J., Xu, Y., Stoleru, D., and Salic, A. (2012). Imaging protein synthesis in cells and tissues with an alkyne analog of puromycin. Proc. Natl. Acad. Sci. *109*, 413–418. https://pubmed.ncbi.nlm.nih.gov/22160674/.

Liu, S., Hausmann, S., Carlson, S.M., Fuentes, M.E., Francis, J.W., Pillai, R., Lofgren, S.M., Hulea, L., Tandoc, K., Lu, J., et al. (2019). METTL13 Methylation of eEF1A Increases Translational Output to Promote Tumorigenesis. Cell *176*, 491-504.e21. https://doi.org/10.1016/j.cell.2018.11.038.

Lorick, K.L., Jensen, J.P., Fang, S., Ong, a M., Hatakeyama, S., and Weissman, A.M. (1999). RING fingers mediate ubiquitin-conjugating enzyme (E2)-dependent ubiquitination. Proc. Natl. Acad. Sci. *96*, 11364–11369. https://pubmed.ncbi.nlm.nih.gov/10500182/.

MacLean, B., Tomazela, D.M., Shulman, N., Chambers, M., Finney, G.L., Frewen, B., Kern, R., Tabb, D.L., Liebler, D.C., and MacCoss, M.J. (2010). Skyline: an open source document editor for creating and analyzing targeted proteomics experiments. Bioinformatics *26*, 966–968. https://academic.oup.com/bioinformatics/article/26/7/966/212410.

Marton, M.J., Crouch, D., and Hinnebusch, A.G. (1993). GCN1, a translational activator of GCN4 in Saccharomyces cerevisiae, is required for phosphorylation of eukaryotic translation initiation factor 2 by protein kinase GCN2. Mol. Cell. Biol. *13*, 3541–3556.

https://pubmed.ncbi.nlm.nih.gov/8497269/.

Matsuo, Y., Ikeuchi, K., Saeki, Y., Iwasaki, S., Schmidt, C., Udagawa, T., Sato, F., Tsuchiya, H., Becker, T., Tanaka, K., et al. (2017). Ubiquitination of stalled ribosome triggers ribosome-associated quality control. Nat. Commun. *8*, 159. https://pubmed.ncbi.nlm.nih.gov/28757607/.

Matsuo, Y., Tesina, P., Nakajima, S., Mizuno, M., Endo, A., Buschauer, R., Cheng, J., Shounai, O., Ikeuchi, K., Saeki, Y., et al. (2020). RQT complex dissociates ribosomes collided on endogenous RQC substrate SDD1. Nat. Struct. Mol. Biol. *27*, 323–332. https://pubmed.ncbi.nlm.nih.gov/32203490/.

Matyskiela, M.E., Lu, G., Ito, T., Pagarigan, B., Lu, C.C., Miller, K., Fang, W., Wang, N.Y., Nguyen, D., Houston, J., et al. (2016). A novel cereblon modulator recruits GSPT1 to the CRL4 CRBN ubiquitin ligase. Nature *535*, 252–257. http://dx.doi.org/10.1038/nature18611.

Meydan, S., and Guydosh, N.R. (2020). Disome and Trisome Profiling Reveal Genome-wide Targets of Ribosome Quality Control. Mol. Cell *79*, 588–602. https://pubmed.ncbi.nlm.nih.gov/32615089/.

Meydan, S., and Guydosh, N.R. (2021). A cellular handbook for collided ribosomes: surveillance pathways and collision types. Curr. Genet. *67*, 19–26. https://doi.org/10.1007/s00294-020-01111-w.

Michel, M.A., Swatek, K.N., Hospenthal, M.K., and Komander, D. (2017). Ubiquitin Linkage-Specific Affimers Reveal Insights into K6-Linked Ubiquitin Signaling. Mol. Cell *68*, 233–246. https://doi.org/10.1016/j.molcel.2017.08.020.

Montellese, C., van den Heuvel, J., Ashiono, C., Dörner, K., Melnik, A., Jonas, S., Zemp, I., Picotti, P., Gillet, L.C., and Kutay, U. (2020). USP16 counteracts mono-ubiquitination of RPS27a and promotes maturation of the 40S ribosomal subunit. Elife *9*. https://pubmed.ncbi.nlm.nih.gov/32129764/.

Moon, S.L., Morisaki, T., Stasevich, T.J., and Parker, R. (2020). Coupling of translation quality

control and mRNA targeting to stress granules. J. Cell Biol. *219*.

Parmeggiani, A., Krab, I.M., Okamura, S., Nielsen, R.C., Nyborg, J., and Nissen, P. (2006). Structural basis of the action of pulvomycin and GE2270 A on elongation factor Tu. Biochemistry *45*, 6846–6857.

Piette, B.L., Alerasool, N., Lin, Z., Lacoste, J., Hiu, M.H.Y., Qian, W.W., Tran, S., Larsen, B., Campos, E., Peng, J., et al. (2021). Comprehensive interactome profiling of the human Hsp70 network highlights functional differentiation of J domains. Mol. Cell *81*, 1–17. 10.1016/j.molcel.2021.04.012.

Pochopien, A.A., Beckert, B., Kasvandik, S., Berninghausen, O., Beckmann, R., Tenson, T., and Wilson, D.N. (2021). Structure of Gcn1 bound to stalled and colliding 80S ribosomes. Proc. Natl. Acad. Sci. *118*, e2022756118. https://pubmed.ncbi.nlm.nih.gov/33790014/.

Ran, F., Hsu, P., Wright, J., and Agarwala, V. (2013). Genome engineering using the CRISPR-Cas9 system. Nat. Protoc. *8*, 2281–2308. https://pubmed.ncbi.nlm.nih.gov/24157548/.

Richter, J.D., and Coller, J. (2015). Pausing on Polyribosomes: Make Way for Elongation in Translational Control. Cell *163*, 292–300. http://dx.doi.org/10.1016/j.cell.2015.09.041.

Sattlegger, E., and Hinnebusch, A.G. (2000). Separate domains in GCN1 for binding protein kinase GCN2 and ribosomes are required for GCN2 activation in amino acid-starved cells. EMBO J. *19*, 6622–6633. https://pubmed.ncbi.nlm.nih.gov/11101534/.

Sattlegger, E., and Hinnebusch, A.G. (2005). Polyribosome binding by GCN1 is required for full activation of eukaryotic translation initiation factor 2α kinase GCN2 during amino acid starvation. J. Biol. Chem. *280*, 16514–16521. https://pubmed.ncbi.nlm.nih.gov/15722345/.

Sattlegger, E., Swanson, M.J., Ashcraft, E.A., Jennings, J.L., Fekete, R.A., Link, A.J., and Hinnebusch, A.G. (2004). YIH1 Is an Actin-binding Protein That Inhibits Protein Kinase GCN2 and Impairs General Amino Acid Control When Overexpressed. J. Biol. Chem. *279*, 29952–29962. http://dx.doi.org/10.1074/jbc.M404009200.

Sazuka, T., Kinoshita, M., Tomooka, Y., Ikawa, Y., Noda, M., and Kumar, S. (1992). Expression

of DRG during murine embryonic development. Biochem. Biophys. Res. Commun. *189*, 371–377.

Schuller, A.P., and Green, R. (2018). Roadblocks and resolutions in eukaryotic translation. Nat. Rev. Mol. Cell Biol. *8*, 526–541. https://pubmed.ncbi.nlm.nih.gov/29760421/.

Shalgi, R., Hurt, J.A., Krykbaeva, I., Taipale, M., Lindquist, S., and Burge, C.B. (2013). Widespread Regulation of Translation by Elongation Pausing in Heat Shock. Mol. Cell *49*, 439–452. http://dx.doi.org/10.1016/j.molcel.2012.11.028.

Shao, S., Murray, J., Brown, A., Taunton, J., Ramakrishnan, V., and Hegde, R.S. (2016). Decoding Mammalian Ribosome-mRNA States by Translational GTPase Complexes. Cell *167*, 1229–1240. http://dx.doi.org/10.1016/j.cell.2016.10.046.

Shao, Y., Molestak, E., Su, W., Stankevič, M., and Tchórzewski, M. (2022). Sordarin— An anti-fungal antibiotic with a unique modus operandi. Br. J. Pharmacol. *179*, 1125–1145.

Sharma, J., Du, M., Wong, E., Mutyam, V., Li, Y., Chen, J., Wangen, J., Thrasher, K., Fu, L., Peng, N., et al. (2021). A small molecule that induces translational readthrough of CFTR nonsense mutations by eRF1 depletion. Nat. Commun. 1–16. http://dx.doi.org/10.1038/s41467-021-24575-x.

Shenton, D., Smirnova, J.B., Selley, J.N., Carroll, K., Hubbard, S.J., Pavitt, G.D., Ashe, M.P., and Grant, C.M. (2006). Global translational responses to oxidative stress impact upon multiple levels of protein synthesis. J. Biol. Chem. *281*, 29011–29021.

Shi, Z., Fujii, K., Kovary, K.M., Genuth, N.R., Röst, H.L., Teruel, M.N., and Barna, M. (2017). Heterogeneous Ribosomes Preferentially Translate Distinct Subpools of mRNAs Genome-wide. Mol. Cell *67*, 71–83. https://pubmed.ncbi.nlm.nih.gov/28625553/.

Shoemaker, C.J., Eyler, D.E., and Green, R. (2010). Dom34:Hbs1 Promotes Subunit Dissociation and Peptidyl-tRNA Drop-Off to Initiate No-Go Decay. Science. *330*, 369–372. https://pubmed.ncbi.nlm.nih.gov/20947765/.

Simms, C.L., Yan, L.L., Zaher, H.S., Simms, C.L., Yan, L.L., and Zaher, H.S. (2017). Ribosome

Collision Is Critical for Quality Control during No-Go Decay. Mol. Cell *68*, 1–13. https://pubmed.ncbi.nlm.nih.gov/28943311/.

Simonović, M., and Puppala, A.K. (2018). On elongation factor eEFSec, its role and mechanism during selenium incorporation into nascent selenoproteins. Biochim. Biophys. Acta - Gen. Subj. *1862*, 2463–2472.

Sinha, N.K., Ordureau, A., Best, K.M., Saba, J.A., Zinshteyn, B., Sundaramoorthy, E., Fulzele, A., Garshott, D.M., Denk, T., Thoms, M., et al. (2020). EDF1 coordinates cellular responses to ribosome collisions. Elife *9*. https://pubmed.ncbi.nlm.nih.gov/32744497/.

Sonenberg, N., and Hinnebusch, A.G. (2009). Regulation of Translation Initiation in Eukaryotes: Mechanisms and Biological Targets. Cell *136*, 731–745. https://pubmed.ncbi.nlm.nih.gov/19239892/.

Spahn, C.M.T., Gomez-Lorenzo, M.G., Grassucci, R.A., Jørgensen, R., Andersen, G.R., Beckmann, R., Penczek, P.A., Ballesta, J.P.G., and Frank, J. (2004). Domain movements of elongation factor eEF2 and the eukaryotic 80S ribosome facilitate tRNA translocation. EMBO J. *23*, 1008–1019.

Spandidos, A., Wang, X., Wang, H., and Seed, B. (2010). PrimerBank: a resource of human and mouse PCR primer pairs for gene expression detection and quantification. Nucleic Acids Res. *38*, 792–799.

Stein, K.C., and Frydman, J. (2019). The stop-and-go traffic regulating protein biogenesis: How translation kinetics controls proteostasis. J. Biol. Chem. *294*, 2076–2084. https://pubmed.ncbi.nlm.nih.gov/30504455/.

Stickel, S.A., Gomes, N.P., Frederick, B., Raben, D., and Su, T.T. (2015). Bouvardin is a Radiation Modulator with a Novel Mechanism of Action. Radiat. Res. *184*, 392–403.

Sundaramoorthy, E., Leonard, M., Mak, R., Liao, J., Fulzele, A., and Bennett, E.J. (2017). ZNF598 and RACK1 Regulate Mammalian Ribosome-Associated Quality Control Function by Mediating Regulatory 40S Ribosomal Ubiquitylation. Mol. Cell *65*, 751–760.

https://pubmed.ncbi.nlm.nih.gov/28132843/.

Surka, C., Jin, L., Mbong, N., Lu, C.C., Jang, I.S., Rychak, E., Mendy, D., Clayton, T., Tindall, E., Hsu, C., et al. (2021). CC-90009, a novel cereblon E3 ligase modulator, targets acute myeloid leukemia blasts and leukemia stem cells. Blood *137*, 661–677.

Tian, R., Gachechiladze, M.A., Ludwig, C.H., Ward, M.E., Tian, R., Gachechiladze, M.A., Ludwig, C.H., Laurie, M.T., and Hong, J.Y. (2019). CRISPR Interference-Based Platform for Multimodal Genetic Screens in Human iPSC-Derived Neurons. Neuron *104*, 239-255.e12. https://doi.org/10.1016/j.neuron.2019.07.014.

Udeshi, N.D., Svinkina, T., Mertins, P., Kuhn, E., Mani, D.R., Qiao, J.W., and Carr, S.A. (2013). Refined Preparation and Use of Anti-diglycine Remnant (K-ε-GG) Antibody Enables Routine Quantification of 10,000s of Ubiquitination Sites in Single Proteomics Experiments. Mol. Cell. Proteomics *12*, 825–831. https://pubmed.ncbi.nlm.nih.gov/23266961/.

Urakov, V.N., Valouev, I.A., Lewitin, E.I., Paushkin, S. V, Kosorukov, V.S., Kushnirov, V. V, Smirnov, V.N., and Ter-Avanesyan, M.D. (2001). Itt1p, a novel protein inhibiting translation termination in Saccharomyces cerevisiae. BMC Mol. Biol. *2*. https://pubmed.ncbi.nlm.nih.gov/11570975/.

Wainberg, M., Kamber, R.A., Balsubramani, A., Meyers, R.M., Sinnott-Armstrong, N., Hornburg, D., Jiang, L., Chan, J., Jian, R., Gu, M., et al. (2021). A genome-wide atlas of co-essential modules assigns function to uncharacterized genes. Nat. Genet. *53*, 638–649. https://pubmed.ncbi.nlm.nih.gov/33859415/.

Walden, H., and Rittinger, K. (2018). RBR ligase-mediated ubiquitin transfer: A tale with many twists and turns. Nat. Struct. Mol. Biol. *25*, 440–445. http://dx.doi.org/10.1038/s41594-018-0063-3.

Wang, H.-Y., Yang, H., Holm, M., Tom, H., Oltion, K., Al-Khdhairawi, A.A.Q., Weber, J.-F.F., Blanchard, S.C., Ruggero, D., and Taunton, J. (2022). Synthesis and single-molecule

imaging reveal stereospecific enhancement of binding kinetics by the antitumor eEF1A antagonist SR-A3. Nat. Chem. 1–20. https://doi.org/10.1038/s41557-022-01039-3.

Wang, J., Johnson, A.G., Lapointe, C.P., Choi, J., Prabhakar, A., Chen, D.H., Petrov, A.N., and Puglisi, J.D. (2019). eIF5B gates the transition from translation initiation to elongation. Nature *573*, 605–608. http://dx.doi.org/10.1038/s41586-019-1561-0.

Wauer, T., Simicek, M., Schubert, A., and Komander, D. (2015). Mechanism of phospho-ubiquitin-induced.

Westrip, C., Paul, F., Al-Murshedi, F., Qaitoon, H., Cham, B., Fletcher, S., Hendrix, E., Boora, U., Ng, A.Y.J., Bonnard, C., et al. (2022). Inactivation of DRG1, encoding a translation factor GTPase, causes a Recessive Neurodevelopmental Disorder. Medrxiv Prepr.

Westrip, C.A.E., Zhuang, Q., Hall, C., Eaton, C.D., and Coleman, M.L. (2021). Developmentally regulated GTPases: structure, function and roles in disease. Cell. Mol. Life Sci. *78*, 7219–7235. https://doi.org/10.1007/s00018-021-03961-0.

Wout, P.K., Sattlegger, E., Sullivan, S.M., and Maddock, J.R. (2009). Saccharomyces cerevisiae Rbg1 protein and its binding partner gir2 interact on polyribosomes with Gcn1. Eukaryot. Cell *8*, 1061–1071. https://pubmed.ncbi.nlm.nih.gov/19448108/.

Wu, C.C., Peterson, A., Zinshteyn, B., Regot, S., and Green, R. (2020). Ribosome Collisions Trigger General Stress Responses to Regulate Cell Fate. Cell *182*, 404-416.e14. https://doi.org/10.1016/j.cell.2020.06.006.

Wu, C.C.C., Zinshteyn, B., Wehner, K.A., and Green, R. (2019). High-Resolution Ribosome Profiling Defines Discrete Ribosome Elongation States and Translational Regulation during Cellular Stress. Mol. Cell *73*, 959-970.e5. https://doi.org/10.1016/j.molcel.2018.12.009.

Yamazaki, H., Kasai, S., Mimura, J., Ye, P., Inose-Maruyama, A., Tanji, K., Wakabayashi, K., Mizuno, S., Sugiyama, F., Takahashi, S., et al. (2020). Ribosome binding protein GCN1 regulates the cell cycle and cell proliferation and is essential for the embryonic

development of mice. PLoS Genet. *16*, 1–23. http://dx.doi.org/10.1371/journal.pgen.1008693.

Yan, L.L., and Zaher, H.S. (2021). Ribosome quality control antagonizes the activation of the integrated stress response on colliding ribosomes. Mol. Cell *81*, 614-628.e4. https://doi.org/10.1016/j.molcel.2020.11.033.

Yan, L.L., Simms, C.L., McLoughlin, F., Vierstra, R.D., and Zaher, H.S. (2019). Oxidation and alkylation stresses activate ribosome-quality control. Nat. Commun. *10*, 5611. http://dx.doi.org/10.1038/s41467-019-13579-3.

Yip, M.C.J., and Shao, S. (2021). Detecting and Rescuing Stalled Ribosomes. Trends Biochem. Sci. *46*, 731–743. http://www.ncbi.nlm.nih.gov/pubmed/33966939.

Yoo, W., Cho, E.B., Kim, S., and Yoon, J.B. (2019). The E3 ubiquitin ligase MARCH2 regulates ERGIC3-dependent trafficking of secretory proteins. J. Biol. Chem. *294*, 10900–10912. https://pubmed.ncbi.nlm.nih.gov/31142615/.

Zecha, J., Meng, C., Zolg, D.P., Samaras, P., Wilhelm, M., and Kuster, B. (2018). Peptide Level Turnover Measurements Enable the Study of Proteoform Dynamics. Mol. Cell. Proteomics *17*, 974–992. https://pubmed.ncbi.nlm.nih.gov/29414762/.

Zeng, F., Li, X., Pires-Alves, M., Chen, X., Hawk, C.W., and Jin, H. (2021). Conserved heterodimeric GTPase Rbg1/Tma46 promotes efficient translation in eukaryotic cells. Cell Rep. *37*, 109877. https://doi.org/10.1016/j.celrep.2021.109877.

Zhang, P., McGrath, B.C., Reinert, J., Olsen, D.S., Lei, L.L., Gill, S., Wek, S.A., Vattem, K.M., Wek, R.C., Kimball, S.R., et al. (2002). The GCN2 eIF2 Kinase Is Required for Adaptation to Amino Acid Deprivation in Mice. Mol. Cell. Biol. *22*, 6681–6688. https://pubmed.ncbi.nlm.nih.gov/12215525/.

Zhou, Y., Kastritis, P.L., Dougherty, S.E., Bouvette, J., Hsu, A.L., Burbaum, L., Mosalaganti, S., Pfeffer, S., Hagen, W.J.H., Förster, F., et al. (2020). Structural impact of K63 ubiquitin on yeast translocating ribosomes under oxidative stress. Proc. Natl. Acad. Sci. *117*, 22157–

22166. https://pubmed.ncbi.nlm.nih.gov/32855298/.

Zinoviev, A., Goyal, A., Jindal, S., Lacava, J., Komar, A.A., Rodnina, M. V., Hellen, C.U.T., and Pestova, T. V. (2018). Functions of unconventional mammalian translational GTPases GTPBP1 and GTPBP2. Genes Dev. *32*, 1226–1241.

Publishing Agreement

It is the policy of the University to encourage open access and broad distribution of all theses, dissertations, and manuscripts. The Graduate Division will facilitate the distribution of UCSF theses, dissertations, and manuscripts to the UCSF Library for open access and distribution. UCSF will make such theses, dissertations, and manuscripts accessible to the public and will take reasonable steps to preserve these works in perpetuity.

I hereby grant the non-exclusive, perpetual right to The Regents of the University of California to reproduce, publicly display, distribute, preserve, and publish copies of my thesis, dissertation, or manuscript in any form or media, now existing or later derived, including access online for teaching, research, and public service purposes.

DocuSigned by:
Keely Oltion
5A42222B61214BE...
Author Signature

12/13/2022
Date